國立臺灣大學工學院環境工程學研究所

博士論文

Graduate Institute of Environmental Engineering

College of Engineering

National Taiwan University

Doctoral Dissertation

全氟辛烷磺酸與全氟辛酸於使用氧化石墨烯二氧化鈦電極的光電化學系統之降解機制及競爭抑制行為

PFOS and PFOA degradation mechanisms and their associated competitive inhibition via photoelectrochemical system using GOTiO_2 photoelectrodes

楊政憲

Jheng-Sian Yang

指導教授：林郁真 博士

Advisor: Angela Yu-Chen Lin, Ph.D.

中華民國 111 年 6 月

June, 2022

doi:10.6342/NTU202201196

國立臺灣大學博士學位論文
口試委員會審定書

全氟辛烷磺酸與全氟辛酸於使用氧化石墨烯二氧化鈦電極的光電化學系統之降解機制及競爭抑制行為

PFOS and PFOA degradation mechanisms and their associated competitive inhibition via photoelectrochemical system using $GOTiO_2$ photoelectrodes

本論文係楊政憲君(學號 D02541006)在國立臺灣大學環境工程學研究所完成之博士學位論文，於民國 111 年 6 月 16 日承下列考試委員審查通過及口試及格，特此證明

論文審查委員：

林逸彬博士
國立台灣大學環境工程學研究所教授

侯嘉洪博士
國立台灣大學環境工程學研究所教授

陳建易博士
國立中正大學地球與環境科學系
專任教授兼理學院院長

駱尚廉博士
國立台灣大學環境工程學研究所特聘教授

賴威博博士
東海大學環境工程與工程學系助理教授

林郁真博士
國立台灣大學環境工程學研究所特聘教授

指導教授：林郁真

所　　長：

致謝

感謝博士班期間林郁真老師在研究上的啟發及鼓勵，在研究上給予學生很多自由發揮的空間，讓我可以自由的依照自己的想法做研究，又能適時給予建議。除了在研究領域外，在我的人生中也扮演著導師的角色，除了讓我更有耐心，脾氣變得更好之外，看待事情的角度也變得比較多元、做決定的時候也會想得比較長遠。老師也像我的好友一般常常與我分享許多寶貴的經驗，聆聽我的想法及關心我。十年樹木，百年樹人!感謝老師花這麼多時間培育學生，今後也將會帶著這些寶貴的經驗向未來邁進。

感謝擔任我學位考試的口試委員：台大環工所林正芳教授、林逸彬教授、侯嘉洪教授、駱尚廉教授、中正地環系的陳建易教授、美國猶他大學的康佩群教授及東海大學的賴威博教授，從資格考、40%、70%及學位口試不吝給予學生創新及寶貴的建議，造就豐富且具有深度的研究成果：如動力模式的探討、讓學生更了解實驗的原理及機制；對於論文嚴謹的態度讓學生對論文的細節更加重視；對於材料的建議讓學生對於材料分析的內容有更完善的探討；對於理論的指教，讓學生發現更多沒有發現的面向。

在實驗室的這段期間，感謝實驗室團隊的成員實驗室大總管彥妗學姐在研究及生活上給予我很多協助；煇翔學長把我帶進電化學的領域；Sri 教授的神來一筆讓我的目標汙染物變成全氟化合物。威博學長給我的鼓勵及經驗的分享到現在依然覺得非常受用，在兩篇期刊及論文的撰寫也給我很多的幫助！明皓學長幫我調整實驗設計，不厭其煩的與我討論實驗的結果。世偉學長三不五時就問我要畢業了沒？婉寧學姊在撰寫論文的期間給我很多很好的建議。還有與我一起奮戰的同學明季及怡如在就學期間互相鼓勵。有文學氣質又學識淵博的宥翔在降解機制方面給我很多很好的意見。感謝碩士班的學弟妹：常常都在讚美人的佳蓉、易聰、佳佩、很大愛的詠恩、冠文、先洋、坤霖、昱蓉、有練身體的酒仙昆圃、神鵰俠侶的女主角俐君、冠宇、很有效率的松娟及內向的怡瑄、想法特別的欣瑜、

doi:10.6342/NTU202201196

做事迅速的同鄉姿伃、能言善道的俊宇、至演、給我很多鼓勵及支持的植夫、很聰明的慧如、很隨興的正軒及給我很多幫助又很帥的書頡以及在我口試期間給我很多協助的學弟妹們：台大及成大羽球霸主世杰、排球舉球手奕宣、同間中學又半個同鄉的連恩、很有自己想法的庭州、為鳴、有好聽南美口音的雅文，因為你們，繽紛了我博士生涯的色彩。

最後感謝我的家人，在我的博士生涯期間給我很多體諒及支持，終於為楊家添加榮耀。希望往後可以貢獻自己的所學，回饋給我的故鄉，能為大家帶來幸福及幫助。

楊政憲　謹誌於

臺灣大學環境工程研究所

二〇二二年六月三十日

doi:10.6342/NTU202201196

中文摘要

全氟烷基酸 (Perfluorinated alkyl acids, PFAAs) 為一廣泛分布於全球各環境中的持久性有機污染物，其中的全氟辛烷磺酸 (perfluorooctane sulfonic acid, PFOS) 和全氟辛酸 (perfluorooctanoic acid, PFOA) 因其在環境中流佈廣泛且濃度較高，為當今國際間所重視的重要環境議題之一。儘管目前有許多研究致力於 PFOS 及 PFOA 的去除及降解後副產物的鑑定，然而至今仍僅發現由 PFOA 降解後所生成部分的全氟羧酸 (Perfluorinated carboxylic acid, PFCAs) 副產物。此外，亦有研究發現，PFAAs 在高級氧化處理系統中，所產生之副產物在水中存在不同基質影響下，不會僅產生簡單的短鏈 PFAAs。本研究之結果不僅重新定義 PFOS 和 PFOA 的降解機制與途徑、鑑定新的副產物、更深入探討混合 PFAAs 於系統中降解可能受到之影響。

本研究成功製造出應用於光電化學系統中降解 PFOS 及 PFOA 的氧化石墨烯二氧化鈦光電極。研究結果發現 5 wt. %的氧化石墨烯二氧化鈦光電極具有最佳的光電化學效能：能隙為 2.42 eV；比表面積為 72.6 $m^2 g^{-1}$；比電容為 4.63 mF cm^{-2}。在應用此光電極的光電化學系統中，PFOS 及 PFOA 可以在 4 小時內於各最佳化條件下（包含電流密度，電極距離，溶液 pH 值，PFOS 與 PFOA 初始濃度及電解質濃度）達去除率 98.2 及 100 %，其擬一級速率常數分別為 0.80 及 0.74 $hour^{-1}$。在光電化學系統中造成 PFOS 與 PFOA 降解的主要原因為經電子轉移，以及與羥基自由基、超氧自由基和活性氯物種反應。另外，在使用氯化鈉做為電解質的光電化學系統中，氯化副產物的發現可以證明系統中所產生的活性氯物種參與了 PFOS 與 PFOA 的降解。

本研究共鑑定出 30 種 PFOS 降解之副產物，並定義其在系統中的降解途徑，亦首次發現全氟烷烴磺酸鹽、全氟醛類及氫氟碳化物的產生。PFOS 在系統中降解的第一步為脫磺化，然後氧化接著脫氟、脫羧、脫羰、磺化、脫氟和羥基化。另外，PFOA 的降解途徑可能有以下四種：脫羧後氧化、脫氟、羥基化和氯原子取代。此

doi:10.6342/NTU202201196

外，本研究發現 PFAAs 的反應性與其碳鏈長度有關，例如較短鏈的 PFAAs 降解速率較長鏈的 PFAAs 為慢。在混合不同碳長度 PFAAs 於系統中之降解情況發現，較短鏈的 PFAAs 與較長鏈的 PFAAs 相比，降解速率下降較不明顯，其結果表示較短鏈的 PFAAs 在處理過程中具有更強的競爭抑制作用和更強的環境抵抗力，此結果有助於了解實際廢水處理過程中所存在之混合 PFAAs 的降解宿命。

關鍵字：光電化學系統，全氟辛烷磺酸，全氟辛酸，活性氧物質，活性氯物質，副產物和反應途徑，競爭抑制作用

doi:10.6342/NTU202201196

ABSTRACT

The global distribution and environmental persistence of perfluoroalkyl acids (PFAAs) has been considered a critical environmental concern. Although many efforts have been made to identify perfluorooctane sulfonate (PFOS) and perfluorooctanoic acid (PFOA) degradation byproducts, previous studies have only reported byproducts that are related to perfluorinated carboxylic acids (PFCAs). In addition, in the case of combinatorial advanced oxidation processes (AOPs), the decomposition products may not just be simple short-chain PFAAs, especially under the influence of a matrix. This is the first study to elucidate the new PFOS and PFOA degradation pathway and byproducts. This study further systematically explores how PFAA degradation may be affected in the mixture system.

In this work, a graphene oxide-titanium dioxide ($GOTiO_2$) photoelectrode was successfully fabricated for PFOS and PFOA degradation in a photoelectrochemical (PEC) system. The results reveal that a 5 wt. % $GOTiO_2$ anode possesses the optimal PEC performance, with a band gap (E_g) of 2.42 eV, surface area (S_{BET}) of 72.6 $m^2\ g^{-1}$ and specific capacitance (C_s) of 4.63 mF cm^{-2}. In the PEC system, the process parameters, including current density, electrode distance, solution pH, PFOS and PFOA concentration and electrolytes concentration were optimized. PFOA was significantly reduced in 4 h (98.2 % removal); PFOS can be efficiently removed within 4 h of reaction time, with a

doi:10.6342/NTU202201196

pseudo-first-order rate constant of 0.80 and 0.74 hour^{-1}. The transfer of electrons, hydroxyl radicals and superoxide radicals are all responsible for PFOS and PFOA decomposition/transformation using chloride anion (Cl^-) as an electrolyte; the presence of chlorinated byproducts in PEC system using Cl^- as electrolyte indicated that reactive chlorine species contributed to PFOS and PFOA degradation.

New degradation pathways were identified; a total of 30 PFOS byproducts are reported in this work; perfluoroalkane sulfonates (PFSAs), perfluorinated aldehydes (PFALs) and hydrofluorocarbons (HFCs) were identified for the first time. PFOS degradation involves the desulfonation pathway as the first step, followed by oxidation and subsequent defluorination, decarboxylation, decarbonylation, sulfonation, defluorination and hydroxylation. Four possible routes of PFOA decomposition, namely, decarboxylation followed by oxidation, defluorination, hydroxylation and Cl atom substitution, were determined in PEC system using Cl^- as electrolyte. The results from this work also show that the reactivity of PFAAs is related to their carbon chain length, with shorter-chain PFAAs exhibiting a lower degradation rate. In a PFAA mixture, a decline in the degradation rate was observed for the shorter-chain-length PFAAs, suggesting stronger competitive inhibition and indicating stronger environmental recalcitrance during the treatment process. The results acquired in this study aid in

doi:10.6342/NTU202201196

comprehensively understanding the degradation and fate of PFAA cocktails during wastewater treatment.

Keywords: Photoelectrochemical, PFOS, PFOA, Reactive oxygen species, Reactive chlorine species, Byproducts and reaction pathways, Competitive inhibition

doi:10.6342/NTU202201196

CONTENT

doi:10.6342/NTU202201196

doi:10.6342/NTU202201196

LIST OF TABLES

doi:10.6342/NTU202201196

LIST OF FIGURES

doi:10.6342/NTU202201196

doi:10.6342/NTU202201196

doi:10.6342/NTU202201196

doi:10.6342/NTU202201196

1. Introduction

1.1. Background

Our environment, particularly water, is contaminated by various perfluoroalkyl acids (PFAAs), and this contamination has become a global concern. Among PFAAs, perfluorooctane sulfonate (PFOS) and perfluorooctanoic acid (PFOA) are of interest because of their widespread use, persistence and toxicity (Ahrens, 2011; Conder et al., 2008; Post et al., 2012). PFOS and PFOA have been detected in drinking water around the world and have the potential to accumulate in human red blood cells; consequently, these two compounds have been detected and measured in humans (Richardson and Ternes, 2018; U.S.EPA., 2016b). Based on human health considerations, the US Environmental Protection Agency (EPA) announced in 2016 that the lifetime drinking water health advisory for both PFOS and PFOA in drinking water is 70 ng L^{-1} (U.S.EPA., 2016a; c), and this decision was preceded by phasing out the use of PFOA in 2015. The European Union restricts the use of PFOS and PFOA (EC., 2006; 2017), and the Stockholm Convention listed these two compounds as persistent organic pollutants (POPs) (UNEP., 2004). In the US EPA's third Unregulated Contaminant Monitoring Rule (UCMR3) database, the concentration of PFAAs in drinking water has been detected in the range of 103−351 ng L^{-1} (U.S.EPA., 2016b). Even if PFOS and PFOA have been regulated and restricted in a country, they can still be detected in the aquatic environments

doi:10.6342/NTU202201196

of that country due to their persistent nature. Previous studies have indicated that the major sources of PFOS and PFOA are industrial effluents (Hansen et al., 2002; Lin et al., 2009; Xiao et al., 2015). These PFOS and PFOA residues in aquatic environments can impact the ecological environment and humans.

Traditional physical, chemical and biological processes cannot achieve complete PFOS degradation due to the strength of carbon–fluorine bonds (C–F, 530 kJ mol^{-1}) (Key et al., 1997). Electrochemical (EC) methods provide a strongly oxidizing environment, fast reaction rate, easy operation and environmental compatibility and are automation friendly with low-volume application (Zhuo et al., 2011). A few studies have reported the PFOA or PFOS degradation efficiency for EC processes (Carter and Farrell, 2008; Urtiaga et al., 2015). Titanium dioxide (TiO_2) is a popular semiconductor that is used as a photocatalyst. Graphene oxide (GO) serves as a versatile support and electrocatalyst due to its high surface area, high electrical conductivity, and good thermal stability (Liu et al., 2012; Panchangam et al., 2018). Recent studies have also applied photoirradiation in the EC process; the combination of photochemical and EC oxidation processes (namely, the PEC process) has been reported to facilitate synergistic effects and can efficiently decompose various contaminants (Koo et al., 2017; Olvera-Rodríguez et al., 2019; Peng et al., 2017; Xie et al., 2016).

doi:10.6342/NTU202201196

Very limited research is available on application of the PEC treatment for PFOS and PFOA removal until now, the associated degradation mechanism also requires in-depth elucidation. During PEC treatment, PFOS and PFOA decomposes/transforms into various byproducts. The formation of short-chain-length perfluorinated carboxylic acids (PFCAs) via PFOS and PFOA decomposition has been previously reported (Duan et al., 2020; Zhang et al., 2013); however, owing to the complex mechanism and reactive species involvement via advanced oxidation processes, the transformation byproducts may be more than simple short-chain PFCAs and warrant further exploration. For instance, the abundance of chloride anion (Cl^-) in wastewater (e.g., wastewater effluents and brackish groundwater) will lead to the formation of perchlorates during the electrochemical process (Schaefer et al., 2015). Chloride anions in water matrices could also be involved in the (photo)electrochemical reaction and thus produce reactive chlorine species (RCSs, e.g., HOCl/OCl^- and •Cl), affecting the rate of the pollutant degradation as well as the associated degradation mechanism and pathways (Cho and Hoffmann, 2015; Cho et al., 2014; Rubí-Juárez et al., 2016). In addition, in actual aquatic environments, in addition to PFOS and PFOA, other PFAAs also exist; the coexistence of these PFAAs could possibly lead to their competitive inhibition in the treatment system. However, most of the existing literature has focused on the removal of a single PFAA, and only a very few studies have investigated the degradation and competition behavior of a PFAA mixture.

doi:10.6342/NTU202201196

A recent study conducted by Wang et al. (2020) explored the simultaneous EC treatment of eight PFAAs, noting that the competitive inhibition behavior of each PFAA may be related to its carbon chain length. Overall, information regarding the competitive inhibition between different PFAAs, including perfluoroalkane sulfonates (PFSAs) and PFCAs in a mixture system, is still lacking.

To date, no information has been reported regarding the generation of transformation byproducts containing sulfonate groups, aldehyde groups and hydrofluorocarbon compounds during PFOS and PFOA decomposition. To the authors' knowledge, this study is the first to provide an in-depth understanding of the PFOS and PFOA transformation byproducts, pathways and competitive inhibition behaviors among PFAAs with different chain lengths by utilizing fabricated GOTiO_2 as a photoelectrode. The PFOS and PFOA degradation kinetics, participation of reactive species such as •OH, •O_2^-, RCSs and electron transfer in the PEC system were investigated, as were the associated changes in toxicity. This work is the first to reveal that PFOS and PFOA byproducts include not only PFCAs but also PFSAs, perfluorinated aldehydes (PFALs) and hydrofluorocarbons (HFCs). The reactivities of PFAAs with different chain lengths in the mixture system were also thoroughly elucidated. The results acquired in this study aid in comprehensively understanding the degradation and fate of PFAA cocktails during wastewater treatment.

doi:10.6342/NTU202201196

1.2. Hypotheses

Hypothesis 1:

The presence of GO led to the decrease of the optical band gap, increases the surface area and electrical conductivity, and will enhance the electrochemical performance.

Hypothesis 2:

With the presence of chloride in the system and the involvement of other reactive species via advanced oxidation processes, the transformation byproducts may be more complicated than the formation of simple short-chain PFCAs.

Hypothesis 3:

With the presence of chloride in the PEC system, the generated RCSs will result in different degradation mechanisms and transformation byproducts compared to that in other advanced oxidation processes.

Hypothesis 4:

The shorter-chain-length PFAAs is likely to experienced stronger competitive inhibition between different PFAAs due to the fact that PFAAs with shorter chain lengths possess less molecular volumes; they might have less opportunities to contact the GOTiO_2 photoelectrode and undergo further degradation.

doi:10.6342/NTU202201196

1.3. Aims of this study

The overall objective of this study was to investigate the PFOS and PFOA transformation pathways and the competitive inhibition with the presence of other perfluoroalkyl acids (PFAAs) via PEC processes using $GOTiO_2$ film photoelectrodes. The specific objectives of this thesis are summarized below:

I. To optimized the electrochemical performance of $GOTiO_2$ material with different various amounts of GO addition (0 to 5 wt. %).

II. To evaluate the PEC degradation mechanisms, including byproduct identification and transformation pathways, and the associated change of toxicity.

III. To examining the participation of the reactive species and electron transfer. The scavenger experiments (by adding benzoic acid, *p*-benzoquinone, potassium iodide nitrobenzene and tert-butanol) were performed to elucidate the participation of reactive species (e.g., •OH, $•O_2^-$, RCSs and electron transfer)).

IV. To examine and compare the change in byproduct pathway and the associated change of toxicity using different electrolytes (Cl^- and ClO_4^-).

V. To verify the competitive inhibition behaviors. Nine PFAAs (PFOS, PFHxS, PFBS, PFOA, PFHpA, PFHxA, PFPeA, PFBA and PFPrA) were used to examine the competitive inhibition between each of PFAAs in PEC system.

doi:10.6342/NTU202201196

1.4. Research framework of this study

Figure 1-1 shows the research framework of this study. Firstly, $GOTiO_2$ photoelectrode was fabricated, and fully determined for its physicochemical and electrochemical properties. The electrochemical performance of $GOTiO_2$ photoelectrode was optimized by the addition amount of GO. In addition, this study investigated PEC degradation mechanism of PFOS and PFOA by optimizing the operation parameters, examining the participation of the reactive species and electron transfer in the PEC system, defining transformation byproducts, predicting degradation pathway and its associated acute toxicity. The reactivity and competitive inhibition behavior of among PFAAs also investigated to determine effect of carbon chain length via PEC process in the mixture system. In addition to PFOS and PFOA, the relationship between the carbon chain length and degradation efficiency ratio for different PFAAs in the individual solution and in the mixture solution was also compared. Finally, based on these results and observations in this study, the conclusions and suggestions regarding the degradation of PFAAs by PEC degradation in aqueous environments were provided.

doi:10.6342/NTU202201196

1.5. Dissertation Overview

This dissertation is presented in seven chapters. **Chapter 1** introduction of this thesis providing the background, motivation, hypotheses and framework. **Chapter 2** is the literature review of this work. **Chapter 3** describes the experimental methods, and lists the required chemicals/materials. **Chapter 4** gives the experimental results and discussion of this study. **Chapter 5** summarizes the major results of this dissertation in conclusion section, and shows the environmental implications and suggestions. The references supporting this work are located in **Chapter 6**.

The content of this dissertation has been publishing in Journal of hazardous materials (2020) 391, 122247 under the title of "Photoelectrochemical degradation of perfluorooctanoic acid (PFOA) with GOP25/FTO anodes: Intermediates and reaction pathways" and Water Research (2021) 207, 117805 under the title of "New insight into PFOS transformation pathways and the associated competitive inhibition with other perfluoroalkyl acids via photoelectrochemical processes using GOTiO_2 film photoelectrodes."

doi:10.6342/NTU202201196

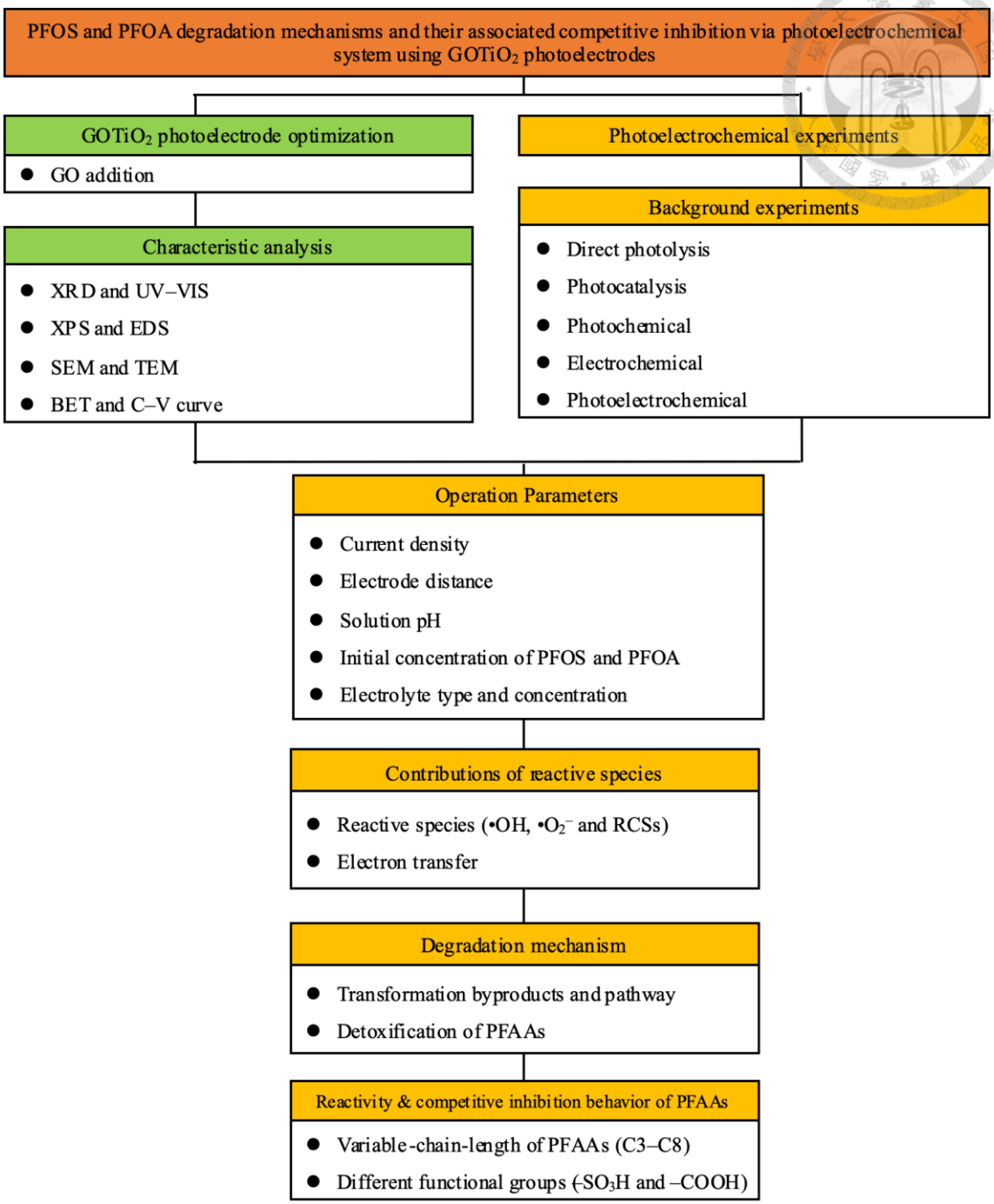

Figure 1-1. Research framework of this study.

doi:10.6342/NTU202201196

2. Literature review

2.1. PFOS and PFOA: usage, environmental occurrence and regulation

Since the 1950s, PFOS and PFOA are the commonly used perfluoroalkyl acids (PFAAs) with different properties and chemical structures (shown in **Table 2-1**), and have been broadly used as firefighting foams, industrial surfactants, surface coating agents, additives, and other products due to their special physicochemical properties, such as chemical and thermal stability, water and lipid repellence and high surface activity (Lehmler, 2005; Zhang et al., 2013). Despite offering many advantages, PFAAs possess the characteristics of widespread occurrence, environmental persistence and toxicity, making them a critical environmental issue worldwide (Hu et al., 2016b). Perfluorooctane sulfonate (PFOS) is one of the commonly used PFAAs, and was listed as a persistent organic pollutant (POP) at the Stockholm Convention in 2009 (Wang et al., 2009). In the Unregulated Contaminant Monitoring Rule (UCMR3) database established by the United States Environmental Protection Agency (USEPA), the lifetime health advisory for combined PFOS and another frequently used PFAA, perfluorooctanoic acid (PFOA) in drinking water is 70 ng L^{-1} (Hu et al., 2016b; Hurley et al., 2016).

Even if PFOS and PFOA have been regulated and restricted in many places, they can still be detected in the aquatic environments due to their persistent nature. The

doi:10.6342/NTU202201196

conventional wastewater treatment process cannot efficiently remove PFOS and PFOA, which results in its ubiquitous occurrence in aquatic environments in countries worldwide. For instance, In various countries such as Vietnam, Taiwan, Japan, the UK and Spain, the maximum detected concentrations of PFOS and PFOA in wastewater treatment plant (WWTP) effluent, industrial wastewater and rivers were 8200, 24000 and 125 ng L^{-1}, respectively (Becker et al., 2008; Duong et al., 2015; Hansen et al., 2002; Lai et al., 2016; Lin et al., 2009; Murakami et al., 2009a). Even in the surface water, the detected concentration of PFOS and PFOA in surface water were in the range of 0.09–3704 and 4.6–2709 ng L^{-1} in China, Japan, India, Spain and Germany (Llorca et al., 2012; Yao et al., 2014; Yeung et al., 2009; Zushi et al., 2011). PFOS and PFOA have also been monitored in groundwater at concentrations of 0.1–40.3 and 0.19–18000 ng L^{-1} in Taiwan, the USA and Europe (Bräunig et al., 2017; Lin et al., 2015; Loos et al., 2010). Furthermore, PFOS and PFOA residues have been observed in tap water in numerous countries, with a maximum concentration of 35 and 258 ng L^{-1} (Harada et al., 2003; Llorca et al., 2012; Mak et al., 2009; Rostkowski et al., 2008). The detail data of the occurrence of PFOS and PFOA were shown in **Table 2-2** and **Table 2-3**. The widespread distribution and persistent nature of PFOS and PFOA prompt us to develop efficient treatment technology for removing PFOS and PFOA.

doi:10.6342/NTU202201196

Table 2-1.Physicochemical properties and molecular structures of PFOS and PFOA.

	Molecular formula	M. W. (g mol^{-1})	pKa	Structure
PFOS	$C_8F_{17}SO_3H$	500	−3.27	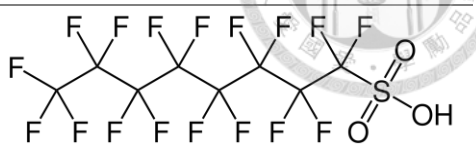
PFOA	$C_8F_{15}COOH$	414	2.8	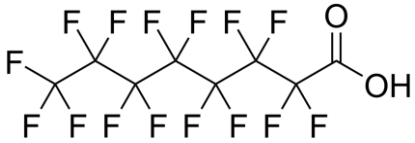

doi:10.6342/NTU202201196

Table 2-2. Environmental occurrence of PFOS in various water matrices.

Compound	Country	WWTP influents (ng L^{-1})	Surface waters (ng L^{-1})	Groundwaters (ng L^{-1})	Tap waters (ng L^{-1})	Reference
PFOS	Germany	80-8200				(Becker et al., 2008)
			<0.04-4.6		<0.04-0.4	(Llorca et al., 2012)
	Spain	<0.22-501	<0.04-2709		<0.04-258	(Llorca et al., 2012)
	Vietnam		0.18-5.3	0.19-8.2		(Duong et al., 2015)
	Japan	14-336	<0.1-191	0.28-133		(Murakami et al., 2009b)
			0.11-99.4			(Zushi et al., 2011)
					0.1-4	(Harada et al., 2003)
	USA		13.8-598			(Hansen et al., 2002)
	Taiwan	5.6-20.8	1.8-5.9			(Lai et al., 2016)
			48.9-5440			(Lin et al., 2009)
				1.1-76.8		(Lin et al., 2015)
	Europe			0.4-135		(Loos et al., 2010)
	India		n.d.-3.91			(Yeung et al., 2009)
	Australia			170-18000		(Bräunig et al., 2017)
	China		0.621-8.44			(Yao et al., 2014)
					10.6	(Mak et al., 2009)

doi:10.6342/NTU202201196

Table 2-3. Environmental occurrence of PFOA in various water matrices.

Compound	Country	WWTP influents (ng L^{-1})	Surface waters (ng L^{-1})	Groundwaters (ng L^{-1})	Tap waters (ng L^{-1})	Reference
PFOA	Germany	<0.04-1.8	<0.16-6.5		<0.16-1.9	(Llorca et al., 2012)
	Spain	<0.04-17	<0.16-68		<0.16-35	(Llorca et al., 2012)
	Vietnam		0.09-18	0.14-4.5		(Duong et al., 2015)
	Japan	14-41	0.1-1.5	<0.1-1.3		(Murakami et al., 2009b)
			0.08-3704			(Zushi et al., 2011)
	USA		<25-507			(Hansen et al., 2002)
	Taiwan	9.3-24.7	11.8-16.8			(Lai et al., 2016)
			10.9-310			(Lin et al., 2009)
				0.1-40.3		(Lin et al., 2015)
	India		n.d.-23.1			(Yeung et al., 2009)
	Europe			0.4-39		(Loos et al., 2010)
	China		8.58-25.9			(Yao et al., 2014)

doi:10.6342/NTU202201196

2.2. PFOS and PFOA degradation via photo-assisted oxidation processes

The recalcitrance and persistence of PFAAs are results of the bond between carbon and fluorine being the strongest known bond in chemistry. Because conventional WWTP processes are inefficient at removing these chemicals (Cheng et al., 2014; Dhangar and Kumar, 2021; Lin et al., 2010; Santos et al., 2016), the abatement of PFOS and PFOA is challenging. Photo-assisted oxidation may occur by direct photodegradation and indirect photodegradation. In direct photodegradation mechanism, organic pollutants absorb photons directly going through bond breaking process and resulted in their transformation byproducts. Direct photodegradation of PFOS and PFOA were reported with the half-life of 5.3 and 1 days, respectively (Hori et al., 2004; Yamamoto et al., 2007). Indirect photodegradation includes homogeneous and heterogeneous.

In homogeneous photodegradation, UV/H_2O_2 and UV/persulfate advanced oxidation processes are the popular treatment techniques for the destruction of PFOS and PFOA owing to their great oxidative capability and efficiency (Leung et al., 2022; Lu et al., 2020; Yang et al., 2020; Zhang et al., 2018). For example, •OH and $•O_2^-$ can be generated via UV/H_2O_2 or UV/persulfate systems, and sulfate radicals ($•SO_4^-$) and •OH could be produced by the UV/persulfate system (Aleboyeh et al., 2005; Tan et al., 2013; Zhang et al., 2018). These radicals can directly degrade PFOS and PFOA into shorter-

doi:10.6342/NTU202201196

chain PFCAs and CO_2. PFOS and PFOA degradations via UV/H_2O_2 and UV/persulfate processes was reported by Kim et al. (2019), Santos et al. (2016) and Yin et al. (2016).

In addition to homogeneous photodegradation processes, heterogeneous photodegradation processes are also widely used on degrading micropollutants. Photocatalysis, one of the heterogeneous photodegradation processes, absorbs light under a threshold wavelength λ, the fundamental absorption edge, which corresponding to the band-gap energy via **Equation (2-1)**. If photons with energy equal to or greater than band gap energy (E_g), photon-induced ionization occurred, the electrons are excited from valence band to conduction band after illumination. The mechanism of photocatalysis is shown in **Figure 2-1**: the electrons are excited and the electron-hole formed migrates to the surface to proceed catalytic reaction (**Equation (2-2)**). Then the excited electrons and holes react with oxygen (O_2) and water on the catalyst surface and form super oxide radical ($\bullet O_2^-$), hydrogen ion (H^+) and •OH (**Equations (2-3)** and **(2-4)**), the high active free radicals show strong redox abilities to remove the pollutant (Hoffmann et al., 1995). PFOS and PFOA degradation was reported by Jin et al. (2014), Park et al. (2018), de S. Furtado et al. (2021) and Panchangam et al. (2018) examined photocatalytic oxidation kinetics and degradation byproducts.

PEC process is a one of the popular heterogeneous photodegradation procedure, which has attracted a major attention in the water treatment arena because of its high

doi:10.6342/NTU202201196

energy efficiency, easy operation environmental compatibility and operation under mild conditions. PEC has been used to remove PFAAs in recent year and the results are promising. Further introduction on the PEC degradation of PFOS and PFOA will be reviewed in **Section 2.3**.

doi:10.6342/NTU202201196

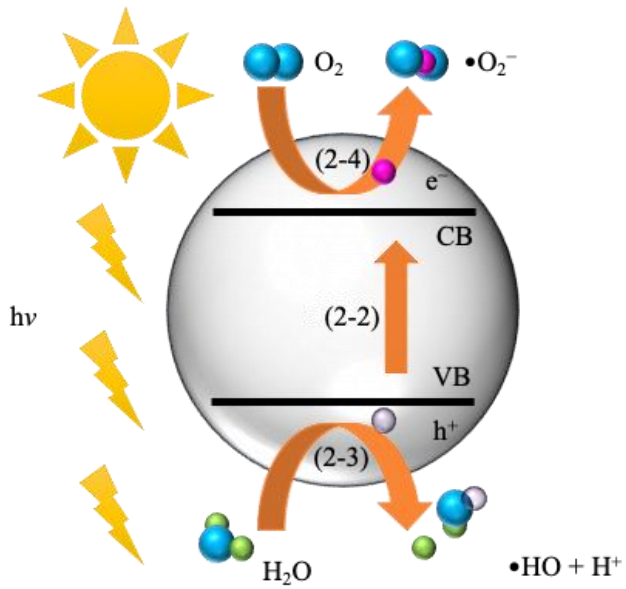

Figure 2-1. Mechanism of photocatalysis (PC).

$$E_g = h\nu = \frac{hc}{\lambda} = \frac{1240}{\lambda}(\text{eV}) \quad (2\text{-}1)$$

$$PC + h\nu \rightarrow e^- + PC\,(h^+) \quad (2\text{-}2)$$

$$PC\,(h^+) + H_2O \rightarrow PC + H^+ + \bullet OH \quad (2\text{-}3)$$

$$O_2 + e^- \rightarrow \bullet O_2^- \quad (2\text{-}4)$$

doi:10.6342/NTU202201196

2.3. PFOS and PFOA degradation mechanism and reactive species in the PEC process

PEC processes have been a promising technology for the decomposition of obsessive and complex wastewater. This process involves the electron transfer from H_2O on photoelectrode surface, multiple radical chain reactions occurred, and several reactive oxygen species (ROSs) were generated as follows (Liu et al., 2019; Muruganandham and Swaminathan, 2004):

$$OH^- \rightarrow \bullet OH + e^- \quad (2\text{-}5)$$

$$H_2O \rightarrow \bullet OH + H^+ + e^- \quad (2\text{-}6)$$

$$2\bullet OH \rightarrow H_2O_2 \quad (2\text{-}7)$$

$$H_2O_2 + h\nu \rightarrow 2\bullet OH \quad (2\text{-}8)$$

$$H_2O_2 \rightarrow O_2 + 2H^+ + 2e^- \quad (2\text{-}9)$$

$$O_2 + e^- \rightarrow \bullet O_2^- \quad (2\text{-}10)$$

The hydroxyl radical (•OH) generated on the surface of the photoelectrode through an electron transfer reaction (**Equations (2-5)** and **(2-6)**). Then the production of hydrogen peroxide (H_2O_2) from the •OH self-recombination reaction, and further simultaneously transformed to •OH by absorbing UV light (**Equations (2-7) and (2-8)**). In addition, H_2O_2 will be oxidized into O_2, which further reacts with electrons to generate superoxide radical anions ($\bullet O_2^-$) (**Equations (2-9)** and **(2-10)**). The mechanism of PEC

doi:10.6342/NTU202201196

process is shown in **Figure 2-2**. Sodium perchlorate ($NaClO_4$) was selected as the electrolyte because the perchlorate ion exhibits stable physicochemical properties in aqueous solutions and is inert even under strong oxidation–reduction conditions (Brown and Gu, 2006; Láng et al., 2008; Rusanova et al., 2006).

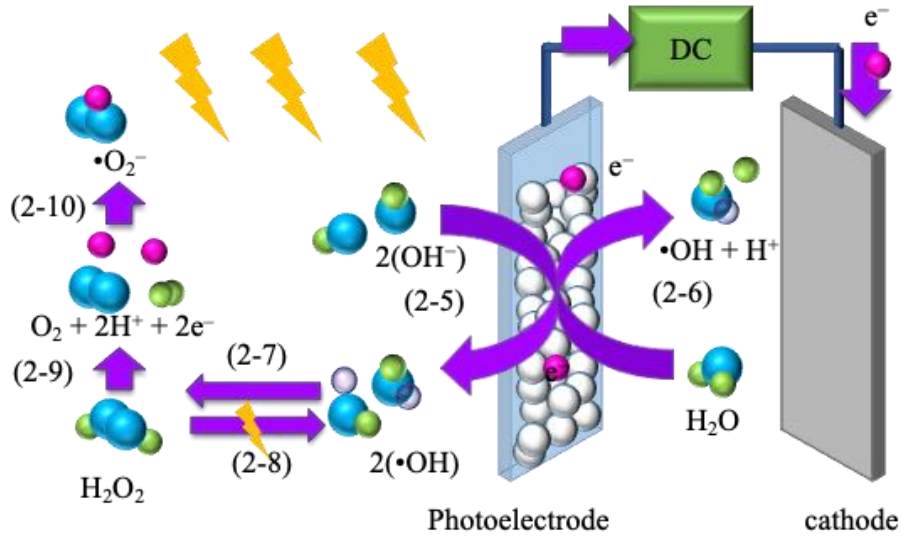

Figure 2-2. Mechanism of photoelectrochemical process.

doi:10.6342/NTU202201196

On the other hand, owing to the abundance of Cl^- in wastewater, the Cl^- as an electrolyte was studied in order to observe the PFAAs degradation during the PEC process in wastewater. Besides •OH, several inorganic radicals such as RCSs are produced and have potential to degrade organic compounds with the use of Cl^-. The produced RCSs was also produced in the electrochemical (EC) system alone while using indirect oxidation mediated by active chlorine, which was demonstrated to participate in pollutant degradation while treating urea and real textile wastewaters (Aquino et al., 2014; Cho and Hoffmann, 2014).

The predominant reactions in the EC system (**Equations (2-11)**–**(2-15)**) and PEC system (**Equations (2-11)**–**(2-17)**) with Cl^- electrolyte are as follows (Cho and Hoffmann, 2014; Cho et al., 2014; Cotillas et al., 2016; Liu et al., 2019).

$$OH^- \rightarrow \bullet OH + e^- \quad (2\text{-}11)$$

$$\bullet OH + Cl^- \rightarrow OH^- + \bullet Cl \quad (2\text{-}12)$$

$$\bullet Cl + Cl^- \rightarrow \bullet Cl_2^- \quad (2\text{-}13)$$

$$\bullet OH + Cl^- \rightarrow HOCl + e^- \quad (2\text{-}14)$$

$$HOCl \rightarrow OCl^- + H^+ \quad pK_a = 7.5 \quad (2\text{-}15)$$

$$HOCl + h\nu \rightarrow \bullet OH + \bullet Cl \quad (2\text{-}16)$$

$$OCl^- + h\nu \rightarrow \bullet O^- + \bullet Cl \quad (2\text{-}17)$$

doi:10.6342/NTU202201196

Equation (2-11) shows the generation of •OH by electron transfer on the surface of the TiO_2 anode. **Equations (2-12)**–**(2-15)** show the production of •Cl and $HOCl/OCl^-$ through the reaction between •OH and Cl^-; •Cl can also react with Cl^- to generate $•Cl_2^-$. In the PEC system, in the presence of UV irradiation, $HOCl/OCl^-$ can be transformed into $•OH/•O^-$ and •Cl (**Equations (2-16)** and **(2-17)**). The mechanism of PEC process with Cl^- electrolyte is shown in **Figure 2-3**.

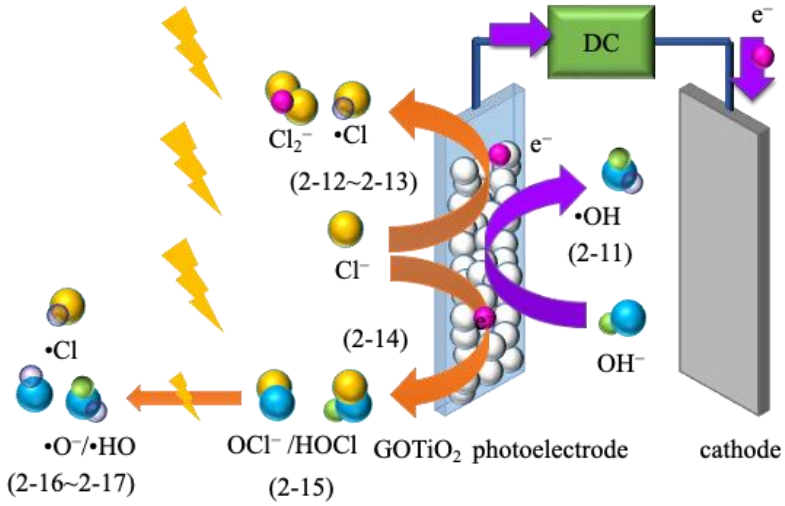

Figure 2-3. Mechanism of PEC process with chloride anion electrolyte.

Based on the fundamental concept of PEC system, five different configurations can be illustrated and discussed as **Figure 2-4**: (a) Photolysis: The system was irradiated only by UVC light; (b) Photocatalysis: TiO_2 powder was coated onto the fluorine-doped tin oxide (FTO) matrix and put in water; then, the system was irradiated by the UVC light; (c) photochemical system: In water, TiO_2 powder was coated onto the FTO anode and

doi:10.6342/NTU202201196

connected to the stainless-steel (SS) cathode via an external circuit; then, the system was irradiated by the UVC light; (d) EC system: The TiO_2 anode and connected SS cathode in water was then powered by the DC power supply. (e) PEC system: The TiO_2 anode and connected SS cathode in water was then powered by the DC power supply in the presence of UVC light irradiation.

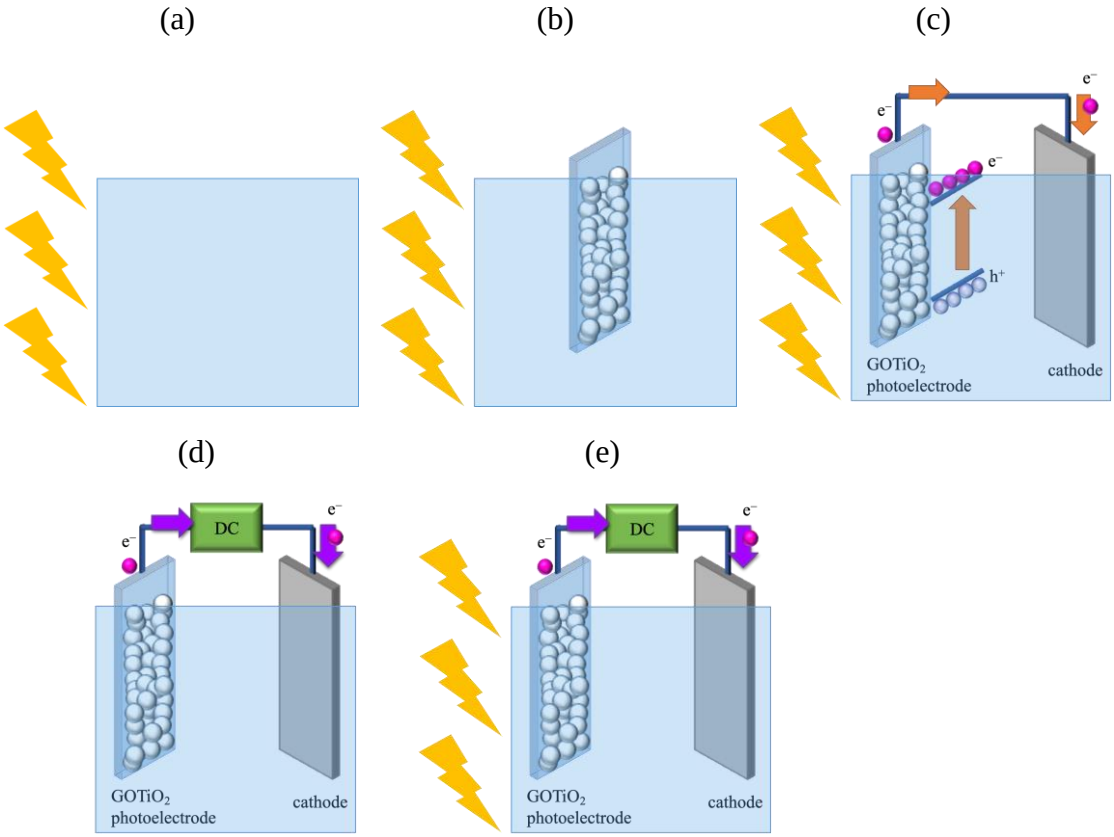

Figure 2-4. The illustration of (a) direct photolysis, (b) photocatalysis, (c) photochemical, (d) electrochemical and (e) photoelectrochemical systems.

doi:10.6342/NTU202201196

2.3.1. GOTiO_2 photoelectrode material

Several studies have reported that PFOS or PFOA can be efficiently degraded in the EC or PEC systems by using different anodes, such as boron-doped diamond electrodes (Carter and Farrell, 2008; Urtiaga et al., 2015), a Ce-doped modified PbO_2 electrode (Niu et al., 2012), Yb-doped Ti/SnO_2-Sb/PbO_2 anodes (Ma et al., 2015) and a Ti/RuO_2 anode (Schaefer et al., 2015). In general, oxidation of the contaminants is predominantly determined by the properties of the anodes used in the either EC or PEC system.

In recent years, the development of photocatalysis oxidation has been the focus of considerable attention since the electrochemical water splitting breakthrough on a TiO_2 electrode reported in 1972 (Fujishima and Honda, 1972). TiO_2 has being used in a variety of material across a broad range of research areas, including specifically energy and environmental fields due to its environmental friendly, nontoxicity, hydrophilicity, physical and chemical stability, long durability, relatively low cost and high photooxidative ability. It has three commonly known polymorphs in nature: anatase, bookie and rutile. Among them, the crystal structure of anatase and rutile have a tetragonal structure, anatase and brookite phases can transformed to the rutile structure, the photocatalyst activity of the rutile structure is very poor. The band gaps of anatase, brookite and rutile phases are 3.23, 3.14 and 3.02 eV, respectively (Brillas and Martínez-Huitle, 2015; Garcia-Segura and Brillas, 2017; Georgieva et al., 2012). TiO_2

doi:10.6342/NTU202201196

photocatalytic property is derived from the formation of photogenerated electrons and holes which occurs on ultraviolet light absorption corresponding to the band gap. In the valence band, the holes diffuse to the TiO_2 surface and react with adsorbed hydroxyl ions to produce •OH; in the conduction band, the electrons react with oxygen molecular, forming $•O_2^-$ (Fujishima et al., 2008). TiO_2 photocatalytic oxidation is one of the most effective advanced oxidation processes (AOPs) (Hassan et al., 2016; Hoffmann et al., 1995), which has been studied for decomposing phenol, dyes, pharmaceuticals and PFAAs. Although TiO_2 has been shown to be an effective alternative for PFAAs decomposition (Li et al., 2016; Panchangam et al., 2009; Sansotera et al., 2014), its high electron-hole pair recombination rate is a potential drawback. Several studies have been performed to enhance the TiO_2 photocatalytic oxidation efficiency by metal or nonmetal element doping (Devi and Kavitha, 2013; Zhang et al., 2011), surface modification (Wooh et al., 2015; Zhang et al., 2017) and dye sensitization (Hagfeldt et al., 2010; O'Regan and Grätzel, 1991).

The thinnest and strongest nanomaterial, graphene is one of the advanced carbon nano-materials, separated graphene through a process of scotch tape peeling in 2004 (Novoselov et al., 2004). It is a 2-dimensional single sheet of carbonaceous material arranged in a hexagonal honeycomb crystal structure, which expresses excellent mechanical flexibility, exhibit outstanding surface areas, high electron mobility, physical

doi:10.6342/NTU202201196

and chemical stability, optical properties and transparency. However, graphene has certain limitations, greatly limit the application of graphene, such as easy agglomeration, weak electrochemical activity and difficult processing.

Compared with graphene, GO serves as a versatile support and electrocatalyst due to it has abundant oxygen-containing functional groups such as hydroxyl and epoxy groups, and the sheet edges are formed carbonyl and carboxyl groups (Liu et al., 2012; Panchangam et al., 2018). The existence of oxygen-containing functional groups endue GO with many interesting physicochemical properties include thermal, optical, mechanical, electronic, electrochemical and chemical reactivity (Compton et al., 2012; Saxena et al., 2011). Significantly, GO and its derivative composites with the great structural diversity and properties, and studied in versatile applications of electrochemical system, including capacitors, fuel cells, dye-sensitized solar cell and PEC oxidation process. The advantage of it is easy processing, low production cost and large-scale production. Combining the advantages of TiO_2 and GO, synthesized $GOTiO_2$ composites material can serve as a photoelectrode with stable and high photocatalytic activity in PEC system (Hunge et al., 2020; Qi et al., 2019; Ribao et al., 2018).

doi:10.6342/NTU202201196

2.3.2. PFOS and PFOA degradation byproducts via PEC processes

PEC degradation has also shown to remove PFOS and PFOA through electron transfer and reactive oxygen species (ROSs) (Li et al., 2011; Lin et al., 2012; Peng et al., 2017). The oxidation process is generally initiated by photoanodes. The PFOS degradation mechanism by photoanodes is described in the following reactions (Li et al., 2017; Peng et al., 2017). PFOS ($F(CF_2)_nSO_3^-$) was converted to PFOS radical through the electron transfer from the head group to the photoanode to formed $\bullet F(CF_2)_n$ (**Equations (2-18)** and **(2-19)**). Then, $\bullet F(CF_2)_n$ would combine with •OH to form the unstable alcohol $F(CF_2)_nOH$, then $F(CF_2)_nOH$ rapidly decomposed into $F(CF_2)_{n-1}COF$ with F^- release (**Equations (2-20)** and **(2-21)**). After that, $F(CF_2)_{n-1}COF$ undergoes hydrolysis and subsequently generated PFOA ($F(CF_2)_{n-1}COO^-$) with another F^- release **Equation (2-22)**. Similarly, PFOA ($F(CF_2)_{n-1}COO^-$) was converted to $\bullet F(CF_2)_{n-1}COO$ through the electron transfer and decarboxylated to form $\bullet F(CF_2)_{n-1}$ on photoanode surface (**Equations (2-23)** and **(2-24)**). After decarboxylation, $\bullet F(CF_2)_{n-1}$ could react with •OH and hydrolysis to generate shorter chain PFCAs (**Equations (2-25)−(2-27)**). In summary, PFSAs and PFCAs can be converted to shorter chain PFCAs via PEC oxidation process. However, owing to the complex degradation mechanism and abundant reactive species involvement in the PEC system, byproducts formed may be more than these of

doi:10.6342/NTU202201196

PFCAs. In addition, information regarding the competitive inhibition between different PFSAs and PFCAs in the mixture is very limited. This work is the first to show that PFCAs are not the only byproducts of PFOS and PFOA. The reactivity of PFAAs with different chain lengths in mixture were also studied.

$$F(CF_2)_nSO_3^- \rightarrow \bullet F(CF_2)_nSO_3 + e^- \quad (2\text{-}18)$$

$$\bullet F(CF_2)_nSO_3 \rightarrow \bullet F(CF_2)_n + SO_3 \quad (2\text{-}19)$$

$$\bullet F(CF_2)_n + \bullet OH \rightarrow F(CF_2)_nOH \quad (2\text{-}20)$$

$$F(CF_2)_nOH \rightarrow F(CF_2)_{n-1}COF + H^+ + F^- \quad (2\text{-}21)$$

$$F(CF_2)_{n-1}COF + H_2O \rightarrow F(CF_2)_{n-1}COO^- + 2H^+ + F^- \quad (2\text{-}22)$$

$$F(CF_2)_{n-1}COO^- \rightarrow \bullet F(CF_2)_{n-1}COO \quad (2\text{-}23)$$

$$\bullet F(CF_2)_{n-1}COO \rightarrow \bullet F(CF_2)_{n-1} + CO_2 \quad (2\text{-}24)$$

$$\bullet F(CF_2)_{n-1} + \bullet OH \rightarrow F(CF_2)_{n-1}OH \quad (2\text{-}25)$$

$$\bullet F(CF_2)_{n-1}OH \rightarrow F(CF_2)_{n-2}COF + H^+ + F^- \quad (2\text{-}26)$$

$$F(CF_2)_{n-2}COF + H_2O \rightarrow F(CF_2)_{n-2}COO^- + 2H^+ + F^- \quad (2\text{-}27)$$

doi:10.6342/NTU202201196

3. Materials and methods

3.1. Chemicals

Perfluorooctanoic acid (PFOA, C8), perfluoroheptanoic acid (PFHpA, C7), perfluorohexanoic acid (PFHxA, C6), perfluoropentanoic acid (PFPeA, C5), perfluorobutanoic acid (PFBA, C4), pentafluoropropopionic acid (PFPrA, C3), ammonium acetate solution, p-benzoquinone, ethanol, hydrochloric acid, hydroquinone, nitrobenzene, potassium iodide, sodium bicarbonate, sodium carbonate, sodium fluoride, sodium hydroxide, *tert*-butyl alcohol (*t*-BuOH) and Tween 80 were purchased from Sigma Aldrich (St. Louis, MO, USA). Perfluorooctane sulfonate (PFOS, C8), tridecafluorohexane-1-sulfonic acid potassium salt (PFHxS, C6), and perfluorobutane sulfonate (PFBS, C4) were purchased from Fluka (Buchs, Switzerland). Ammonium hydroxide, benzoic acid (BA) and sodium sulfate were purchased from JT Baker (Phillipsburg, NJ, USA). LC–MS-grade acetonitrile, methanol, hydrogen peroxide, Sodium chloride and sodium perchlorate were purchased from Merck (Billerica, MA, USA). GO and TiO_2 powder (Degussa P25) were purchased from UniRegion Bio-Tech (Taiwan). All chemical standards were reagent grade or analytical grade and were used without further purification. The PFAA stock solutions were placed in amber polypropylene centrifuge tubes and stored at −20 °C under dark conditions until use.

doi:10.6342/NTU202201196

Milli−Q water (conductivity < 18.2 MΩ cm; Millipore Co., MA, US) was used in all experiments.

3.2. Preparation of $GOTiO_2$ photoelectrode

$GOTiO_2$ was synthesized by a sol-gel method and is shown in **Figure 3-1**. Briefly, 10 mL ethanol and 5 g L^{-1} commercial GO (0–5 mL) were mixed, adjusted to 15 mL with Milli−Q water, and then uniformly dispersed by ultrasonication for 1 hour. Later, 0.5 g of TiO_2 (P25) was added, and the mixture was stirred for 2 h and then sonicated for 1 h. Next, 5 g Tween 80 surfactant was added, and the solution was stirred again for 0.5 hours and then sonicated for 1 hour to form a gel. The gel was coated onto clean fluorine-doped tin oxide (FTO) glass by the doctor blade technique, and the $GOTiO_2$ photoelectrode was dried at 200 °C for 6 h in an oven. FTO-coated glass was first cleaned with alkaline liquid (ammonium hydroxide (28–30 %):hydrogen peroxide (30 %) = 1:1) at 80 °C for 2 h, washed in methanol and Milli-Q water by ultrasonic washing twice for 15 min, and dried in an oven at 80 °C for 30 min.

doi:10.6342/NTU202201196

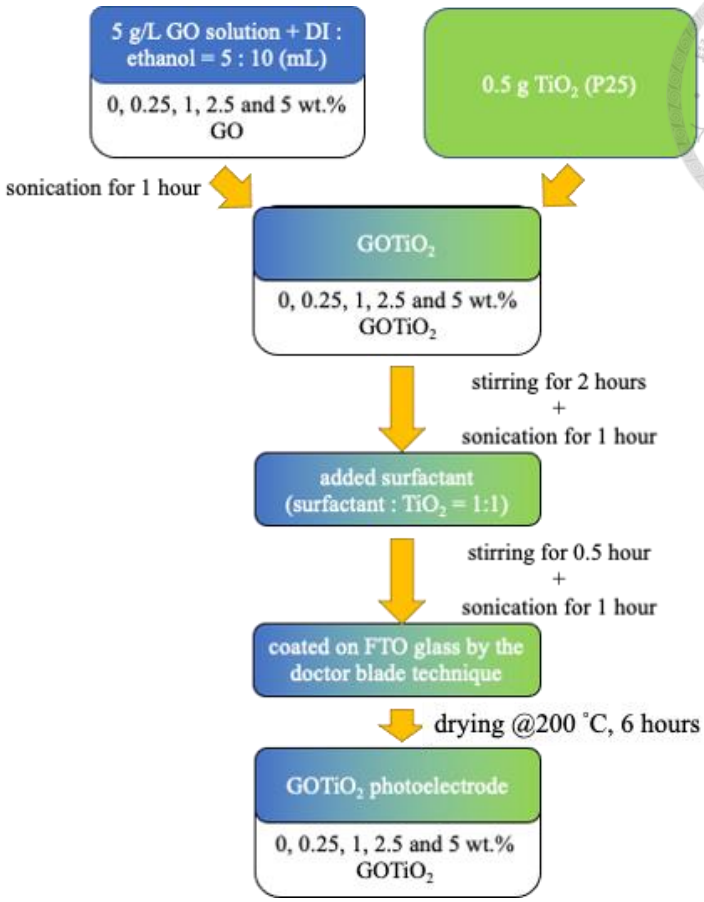

Figure 3-1. Fabrication of the TiO_2 (P25) and $GOTiO_2$ photoelectrodes.

3.3. Physicochemical characterization and electrochemical measurements

The crystal structures of GO, TiO_2 and $GOTiO_2$ were probed by X-ray powder diffraction (XRD, Rigaku Miniflex, Japan with Cu-Kα radiation) (**Figure 3-2 (a)**). Field-emission scanning electron microscopy (SEM; Hitachi S-4800, Japan) (**Figure 3-2 (b)**) and transmission electron microscopy (TEM; FEI Tecnai™ G2 F-20 S-TWIN microscope, USA) (**Figure 3-2 (c)**) were used to observe the morphologies, microstructures and dispersibility. Energy dispersive spectroscopy (EDS, QUANTAX Annular XFlash® QUAD FQ5060, Germany) was used to analyze the compositions of GO, TiO_2 and

doi:10.6342/NTU202201196

$GOTiO_2$. Furthermore, X-ray photoelectron spectroscopy (XPS, Hermoelectricity Instruments, UK) (**Figure 3-2 (d)**) was used to measure the binding energies for the survey and high-resolution spectra of C 1s, O 1s and Ti 2p. The surface area, pore size, particle size and pore volume were calculated by the Brunauer-Emmett-Teller (BET, Micromeritics ASAP 2020M, USA) (**Figure 3-2 (e)**) method based on the nitrogen adsorption-desorption isotherm. The absorption wavelengths of GO, TiO_2 and $GOTiO_2$ were analyzed using a UV–vis spectrophotometer (JASCO V755, Japan) (**Figure 3-2 (f)**). Cyclic voltammetry (C−V) was measured with a CH Instruments (CHI 627D, USA) (**Figure 3-2 (g)**) potentiostat in 50 mM $NaClO_4$ and NaCl solution under 16 W UVC irradiation.

3.4. Photoelectrochemical degradation experiments

All experiments were performed in a 60 mL single-cell cylindrical quartz batch reactor under irradiation by a UV−C lamp (16 W, 254 nm, Phillips, Poland) inserted in a quartz tube; the light intensity was 2.4 W m^{-2}, which was measured by an UV radiant power meter (Apogee Instruments, Inc.) (**Figure 3-2 (h)**). Before the experiment, the UV−C lamp was allowed to stabilize for 30 min. The electrolyte was 10–100 mM sodium perchlorate. The photoelectrode (2 cm × 3 cm) was $GOTiO_2$, and the counter electrode (2 cm × 3 cm) was Hastelloy C-22 nickel-based alloy stainless steel (USA). The electrode distance was set at 5–20 mm. The current density (in the range of 2–20 mA cm^{-2}) was

doi:10.6342/NTU202201196

applied to the electrodes with a DC power supply (GWINSTEK GPD-3043S, Taiwan) (**Figure 3-2 (i)**). Direct photolysis, photocatalysis, photochemical and EC experiments were performed as control experiments. The temperature was maintained at 25 °C by using a thermostat circulating water bath and a stirring speed of 1000 rpm for uniform mixing solution. $NaClO_4$ was selected as the electrolyte because the perchlorate ion exhibits stable physicochemical properties in aqueous solutions and is inert even under strong oxidation–reduction conditions (Brown and Gu, 2006; Láng et al., 2008; Rusanova et al., 2006). Five sets of PFOS degradation experiments were conducted to evaluate the effects of variables including the current density, electrode distance, solution pH, initial PFOS concentration and $NaClO_4$ electrolyte concentration (detailed information on the optimized variable conditions is presented in **Table 3-1**). Briefly, the current density of 20 mA cm^{-2} was applied in all experiments, with the exception of the control factors used to study the effect of the current density, which were in the range of 2–20 mA cm^{-2}. An electrode distance of 5 mm was used in all experiments, with the exception of the control factors used to study the effect of the electrode distance, which were in the range of 5–20 mm. The solution pH was 5.64 in all experiments, with the exception of the control factors used to study the effect of pH, which included pH values in the range of 3–11. The initial PFOS concentration of 0.5 μM was used in all experiments, with the exception of the control factors used to study the effect of the initial PFOS concentration, which were in

doi:10.6342/NTU202201196

the range of 0.5–10 μM. The $NaClO_4$ electrolyte concentration of 50 mM was used in all experiments, with the exception of the control factors used to study the effect of the $NaClO_4$ electrolyte, which were in the range of 10–100 mM. In the experiments studying the pH effect, sodium hydroxide (0.1 N) or hydrochloric acid (0.1 N) were used to adjust the solution pH. In the experiments studying the Cl^- electrolyte, the electrolyte was 50 mM sodium chloride. Aliquots were collected at specified intervals and then centrifuged at 13,000 rpm before analysis.

doi:10.6342/NTU202201196

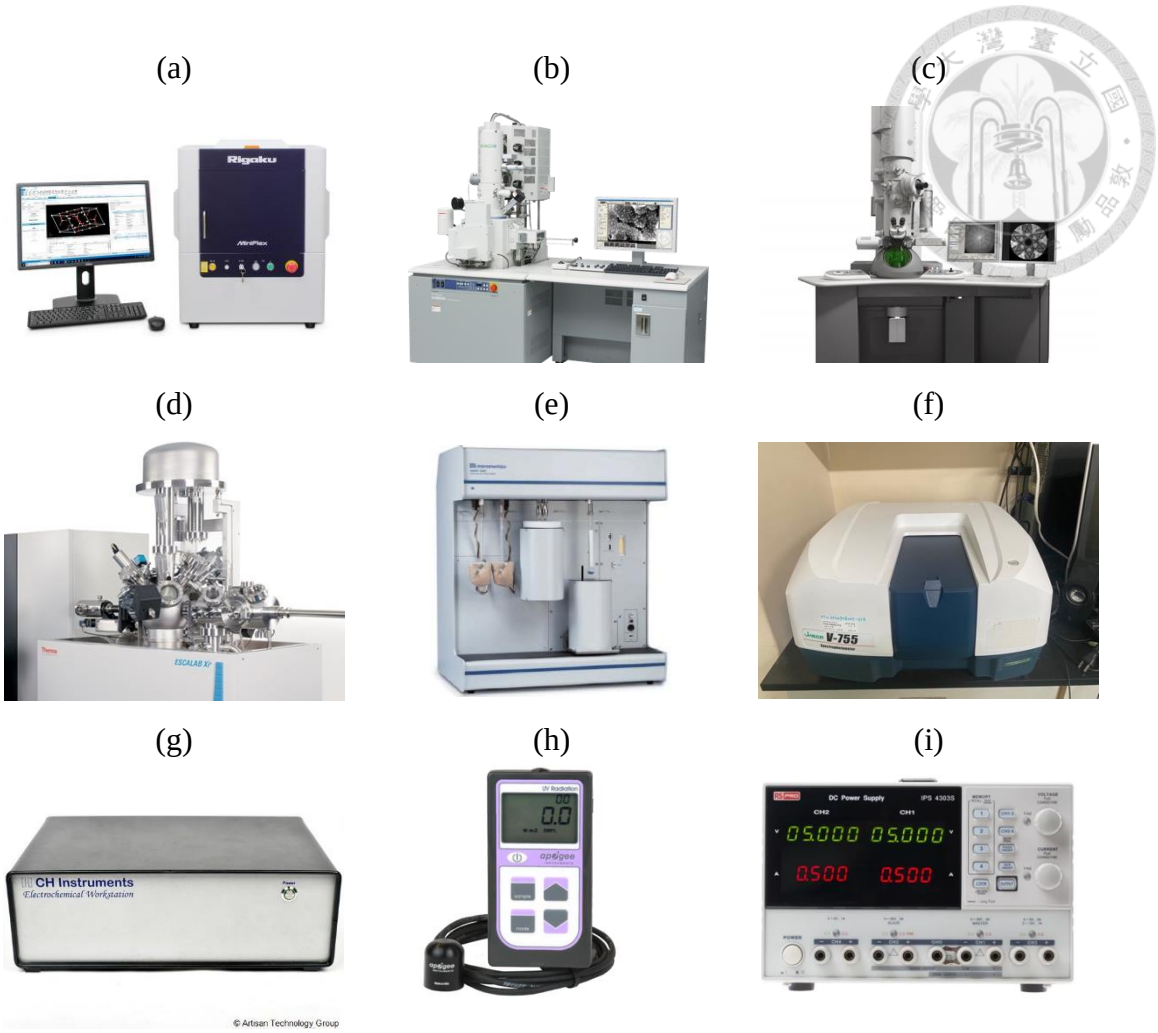

Figure 3-2. (a) X-ray powder diffractometer, (b) scanning electron microscope, (c) transmission electron microscope, (d) X-ray photoelectron spectroscope, (e) high resolution surface area and porosimetry analyzer, (f) UV–vis spectrophotometer (g) ch instruments potentiostat, (h) UV Radiant power meter, (i) DC power supply.

doi:10.6342/NTU202201196

Table 3-1. Summary of PFOS degradation in direct photolysis, photocatalysis, photochemical, electrochemical and photoelectrochemical systems.

Degradation process	Initial PFOS concentration (μM)	Initial pH	Electrode distance (mm)	Electrolyte concentration (mM)	Current density (mA cm^{-2})	Degradation efficiency (η, %)	Pseudo-first-order rate constant (k, $hour^{-1}$)	R^2 value
Direct photolysis	0.5	5.64	-	50	0	0	-	-
Photocatalysis	0.5	5.64	-	50	0	0	-	-
Photochemical	0.5	5.64	5	50	0	0	-	-
Electrochemical	0.5	5.64	5	50	20	75.00 %	0.39 ± 0.04	0.9979
Photoelectrochemical	0.5	5.64	5	50	20	94.83 %	0.74 ± 0.05	0.9985
Effect of the current density								
Photoelectrochemical	0.5	5.64	5	50	**2**	7.23 %	0.02 ± 0.00	0.9899
Photoelectrochemical	0.5	5.64	5	50	**5**	33.43 %	0.10 ± 0.01	0.9989
Photoelectrochemical	0.5	5.64	5	50	**10**	81.26 %	0.41 ± 0.01	0.9980
Photoelectrochemical	0.5	5.64	5	50	**15**	87.97 %	0.53 ± 0.02	0.9993
Photoelectrochemical	0.5	5.64	5	50	**20**	94.83 %	0.74 ± 0.05	0.9985
Effect of the electrode distance								
Photoelectrochemical	0.5	5.64	**5**	50	20	94.83 %	0.74 ± 0.05	0.9985
Photoelectrochemical	0.5	5.64	**10**	50	20	85.33 %	0.49 ± 0.02	0.9986
Photoelectrochemical	0.5	5.64	**15**	50	20	66.72 %	0.27 ± 0.01	0.9965
Photoelectrochemical	0.5	5.64	**20**	50	20	47.54 %	0.17 ± 0.01	0.9944

doi:10.6342/NTU202201196

Effect of pH								
Photoelectrochemical	0.5	**3**	5	50	20	98.77 %	1.12 ± 0.02	0.9998
Photoelectrochemical	0.5	**5**	5	50	20	95.19 %	0.75 ± 0.02	0.9977
Photoelectrochemical	0.5	**7**	5	50	20	78.71 %	0.40 ± 0.03	0.9987
Photoelectrochemical	0.5	**9**	5	50	20	73.25 %	0.34 ± 0.01	0.9986
Photoelectrochemical	0.5	**11**	5	50	20	54.49 %	0.20 ± 0.01	0.9988
Effect of the electrolyte concentration								
Photoelectrochemical	0.5	5.64	5	**10**	20	52.58 %	0.19 ± 0.01	0.9943
Photoelectrochemical	0.5	5.64	5	**25**	20	77.65 %	0.37 ± 0.01	0.9986
Photoelectrochemical	0.5	5.64	5	**50**	20	94.83 %	0.74 ± 0.05	0.9985
Photoelectrochemical	0.5	5.64	5	**100**	20	95.16 %	0.76 ± 0.08	0.9989
Effect of the PFOS concentration								
Photoelectrochemical	**0.5**	5.64	5	100	20	95.16 %	0.76 ± 0.08	0.9989
Photoelectrochemical	**1**	5.64	5	50	20	82.02 %	0.44 ± 0.06	0.9984
Photoelectrochemical	**2.5**	5.65	5	50	20	72.38 %	0.32 ± 0.01	0.9991
Photoelectrochemical	**5**	5.66	5	50	20	57.43 %	0.22 ± 0.02	0.9991
Photoelectrochemical	**10**	5.68	5	50	20	38.77 %	0.13 ± 0.01	0.9943

doi:10.6342/NTU202201196

3.5. Analysis

3.5.1. Analysis of compounds

PFOS, PFHxS, PFBS, PFOA, PFHpA, PFHxA, PFPeA, PFBA and PFPrA were qualified and quantified by high-performance liquid chromatography coupled with tandem mass spectrometer (HPLC–MS/MS). The HPLC–MS/MS system used in this study was an Agilent 1200 module (Agilent, Palo Alto, CA, USA), and mass spectrometric measurements were carried out on an Applied Biosystems Sciex API 4000 spectrometer (AB SCIEX, Foster City, CA, USA) (**Figure 3-3 (a)**) equipped with an electrospray ionization interface in negative ion mode. Mobile phase A was 1 mM ammonium acetate in DI water, and mobile phase B was 1 mM ammonium acetate in methanol. The detailed LC gradients and mass spectrometry conditions of all the analyzed compounds are described in **Table 3-2** and **Table 3-3**. A binary gradient with a flow rate of 1.0 ml min^{-1} was used. The autosampler was operated at room temperature. Data acquisition and analyses were performed using Sciex SCIEX OS version 1.6.1 software.

doi:10.6342/NTU202201196

Table 3-2. LC gradient conditions used in negative mode for MRM analysis.

ESI: Negative mode

Mobile phases	A: 1 mM ammonium acetate in DI water B: 1 mM ammonium acetate in MeOH		
Time (min)	Flow rate ($\mu L\ min^{-1}$)	Mobile A (%)	Mobile B (%)
0.0	1000	63	37
0.4	1000	50	50
0.8	1000	20	80
4.8	1000	5	95
5.5	1000	5	95
6.0	1000	63	37
8.0	1000	63	37

Table 3-3. Mass spectroscopy parameters for PFCs in this study.

Compounds	**MSMS parameters**							
			Quantitation			Confirmation		
	Precursor ion (m/z)	DP (V)	Product ion (m/z)*	CE (V)	CXP (V)	Product ion (m/z)*	CE (V)	CXP (V)
PFOS	499	-60.0	99	-46.2	-8.0	80	-51.3	-4.8
PFHxS	399	-42.2	119	-75.9	-18.3	80	-48.6	-3.0
PFBS	299	-61.2	99	-60.4	-5.8	80	-48.1	-4.9
PFOA	413	-25.0	369	-15.0	-7.0	169	-28.5	-9.1
PFHpA	363	-20.3	169	-34.2	-6.1	119	-35.2	-11.8
PFHxA	313	-28.4	269	-35.0	-8.6	119	-24.0	-4.8
PFPeA	263	-29.0	269	-24.6	-7.8	119	-15.6	-9.1
PFBA	213	-28.8	169	-14.9	-7.4	69	-31.2	-8.2
PFPrA	163	-28.3	69	-12.5	-8.6	119	-34.2	-9.6

doi:10.6342/NTU202201196

3.5.2. Competition kinetic experiment

Nitrobenzene and hydroquinone were quantified by high-performance liquid chromatography with a diode-array detector (HPLC–DAD) (**Figure 3-3 (b)**). The HPLC–DAD system used in this study was an Agilent 1200 module (Agilent, Palo Alto, CA, USA). The mobile phase was a mixture of DI water and acetonitrile. The gradient is shown in **Table 3-4**, and a ZORBAX Extend-C18 column (150 × 4.6 mm, 5 μm) was used. The DI water mobile phase was filtered through a 0.2-mm cellulose acetate membrane before analysis by liquid chromatography. The optimum column temperature was found to be 40 ℃. The injection volume was 100 μL. The detection wavelengths for nitrobenzene and hydroquinone were 265 and 295 nm, respectively (reference wavelength: 360 nm).

Table 3-4. LC gradient conditions for probes used in DAD analysis.

Mobile phases	A: DI water B: ACN		
Time (min)	Flow rate (μL min^{-1})	Mobile A (%)	Mobile B (%)
0	1000	95	5
0.5	1000	95	5
2	1000	5	95
2.5	1000	5	95
4	1000	95	5
5.0	1000	95	5

doi:10.6342/NTU202201196

3.5.3. Anion and free chlorine analysis

Fluoride ions and sulfate ions were quantified by ion chromatography (IC). The IC system used in this study was a Metrohm Eco-925 Ion Chromatography (IC) system coupled with a 863 compact autosampler (**Figure 3-3 (c)**) and equipped with Metrohm A Supp 5–250/4.0 IC analytical column, and the mobile phase was a mixture of 1 mM sodium bicarbonate and 3.2 mM sodium carbonate dissolved in DI water with a flow rate of 0.7 mL min^{-1}. The free chlorine concentration was analyzed with preprogrammed methods on a DR 6000™ (Hach Lange Led., Germany) in a 10-mL quartz cell with an N,N-diethyl-1,4-phenylenediamine sulfate (DPD) reaction kit (Loveland, CO, USA).

3.5.4. Toxicity measurements

To understand the changes in toxicity during the PEC degradation of PFOS, a toxicity assessment was performed using a Microtox® Model 500 acute toxicity analyzer (Microbics Corp., Carlsbad, CA, USA) (**Figure 3-3 (d)**), which functions based on the measurement of the reduction in luminescence emitted by the marine microorganism *Vibrio fischeri*. Samples were collected out from the PEC reactor after specific time intervals and were adjusted to pH 7.0 prior to the toxicity test. Subsequently, the samples were subjected to appropriate treatments including dilution and salinity adjustment and were then spiked into a *Vibrio fischeri* bacterial suspension (the prepared solutions for

doi:10.6342/NTU202201196

toxicity measurement contained 1 % NaCl, 1 % bacterial, and samples at 5.63, 11.25, 22.5 and 45 %). The changes in luminescence intensity emitted by *Vibrio fischeri* in the as-prepared solutions were recorded after 5 and 15 min of exposure and compared with those of the toxin-free control. All toxicity tests were conducted at a temperature of 15 °C. The toxicity value is expressed as toxicity units (TU, where TU = $100/EC_{50}$).

3.5.5. Byproducts analysis and identification

For the byproduct study, PFOS, PFHxS, PFBS, PFOA, PFHpA, PFHxA, PFPeA, PFBA and PFPrA were quantified and qualified by authentication standards using ultrahigh-performance liquid chromatography with a Sciex TripleTOF® 5600+ quadrupole time-of-flight mass spectrometer (UHPLC–QTOFMS, Sciex ExionLC AC system, AB SCIEX, Concord, ON, Canada) (**Figure 3-3 (e)**), which was equipped with a DuoSpray™ ion source to allow MRM^{HS} analysis (the QTOFMS parameters and detection limits (limits of detection and limits of quantification) of these nine compounds are shown in **Table 3-6**). Other byproducts were identified by $SWATH^{HR}$ analysis. For byproducts without standards, the signal peak area acquired by UHPLC–QTOFMS analysis was used to express their evolution. Data acquisition and analyses were performed using Sciex SCIEX OS version 1.6.1 software. Detailed information about the UHPLC–QTOFMS conditions is presented as follow:

doi:10.6342/NTU202201196

I. Identification of PFOS and PFOS transformation byproducts in negative mode by MRMHS analysis.

PFOS, PFHxS, PFBS, PFOA, PFHpA, PFHxA, PFPeA, PFBA and PFPrA were identified using UHPLC–QTOFMS with negative electrospray ionization (ESI) by MRM^{HS} analysis. The mobile phase was a mixture of eluent A (DI water) and eluent B (methanol), both containing 1 mM ammonium acetate, with the gradient shown in **Table 3-5**, and a ZORBAX Eclipse XDB-C_{18} column (150 × 4.6 mm, 5 μm) was used. The DI water mobile phase was filtered through a 0.2-mm cellulose acetate membrane before analysis by liquid chromatography. The injection volume was 100 μL. The QTOFMS conditions were as follows: ion source gas 1 (GS1): 50 L h^{-1}; ion source gas 2 (GS2): 50 L h^{-1}; curtain gas (CUR): 25 L h^{-1}; temperature (TEM): 500 °C; and ion spray voltage floating (ISVF): –4500 V. The detailed QTOFMS conditions of all the analyzed compounds are described in **Table 3-6**.

doi:10.6342/NTU202201196

(a) (b) (c)



(d) (e) (f)

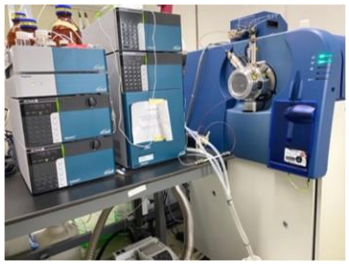

Figure 3-3. (a) High-performance liquid chromatography coupled with tandem mass spectrometer, (b) high-performance liquid chromatography with a diode-array detector., (c) ion chromatography system coupled with autosampler, (d) toxicity analyzer, (e) ultrahigh-performance liquid chromatography with quadrupole time-of-flight mass spectrometer.

Table 3-5. LC gradient conditions used in negative mode for MRM^{HS} analysis.

ESI: Negative mode

Mobile phases	A: 1 mM ammonium acetate in DI water B: 1 mM ammonium acetate in MeOH		
Time (min)	Flow rate ($\mu L\ min^{-1}$)	Mobile A (%)	Mobile B (%)
0.0	1000	63	37
0.4	1000	50	50
0.8	1000	20	80
4.8	1000	5	95
5.5	1000	5	95
6.0	1000	63	37
8.0	1000	63	37

doi:10.6342/NTU202201196

Table 3-6. QTOFMS parameters, limits of detection (LODs) and limits of quantification (LOQs) of PFOS and the PFOS transformation byproducts.

Compounds	QTOFMS parameters								Detection limit	
	Quantitation					Confirmation			LOD ($\mu g\ L^{-1}$)	LOQ ($\mu g\ L^{-1}$)
	Precursor ion (m/z)	DP (V)	Product ion (m/z)*	CE (V)	CES (V)	Product ion (m/z)*	CE (V)	CES (V)		
PFOS	498.93022	-60.0	98.9538	-46.2	0	79.9558	-51.3	0	0.1	0.2
PFHxS	398.93661	-42.2	118.9897	-75.9	0	79.9558	-48.6	0	0.1	0.2
PFBS	298.94299	-61.2	98.9538	-60.4	0	79.9558	-48.1	0	0.1	0.2
PFOA	412.96643	-25.0	368.9764	-15.0	0	168.9897	-28.5	0	0.1	0.5
PFHpA	362.96962	-20.3	168.9897	-34.2	0	118.9897	-35.2	0	0.2	0.5
PFHxA	312.97281	-28.4	268.9832	-35.0	0	118.9897	-24.0	0	0.5	1.0
PFPeA	262.97601	-29.0	268.9832	-24.6	0	118.9897	-15.6	0	0.5	2.0
PFBA	212.9792	-28.8	168.9897	-14.9	0	68.9959	-31.2	0	2.0	5.0
PFPrA	162.98239	-28.3	68.9959	-12.5	0	118.9897	-34.2	0	2.0	5.0

* Product ions (m/z) were extracted with Sciex SCIEX OS software.

doi:10.6342/NTU202201196

II. Identification of PFOS transformation byproducts in negative mode by SWATH^{HR} analysis.

The transformation byproducts were identified using UHPLC–QTOFMS with negative electrospray ionization (ESI) by SWATH^{HR} analysis. The mobile phase was a mixture of eluent A (DI water) and eluent B (methanol), both containing 1 mM ammonium acetate. The DI water mobile phase was filtered through a 0.2-mm cellulose acetate membrane before analysis by liquid chromatography. The gradient is shown in **Table 3-7**, and a ZORBAX Eclipse XDB-C_{18} column (150 × 4.6 mm, 5 μm) was used. The injection volume was 100 μL. The QTOFMS conditions were as follows: ion source gas 1 (GS1): 50 L h^{-1}; ion source gas 2 (GS2): 50 L h^{-1}; curtain gas (CUR): 25 L h^{-1}; temperature (TEM): 500 °C; ion spray voltage floating (ISVF): –4500 V. The declustering potential (DP) was –60 V, and the collision energy (CE) was –10 V in TOFMS (–). Full-scan high-resolution mass spectrometry data were acquired within an m/z range of 30–600, DP = –40 V; CE = –35 V, and CES (collision energy spread) = 15 V.

doi:10.6342/NTU202201196

Table 3-7. LC gradient conditions used in negative mode for SWATH^{HR} analysis.

ESI: Negative mode			
Mobile phases	A: 1 mM ammonium acetate in DI water B: 1 mM ammonium acetate in MeOH		
Time (min)	Flow rate (μL min^{-1})	Mobile A (%)	Mobile B (%)
0.0	1000	95	5
0.4	1000	50	50
0.8	1000	20	80
4.8	1000	5	95
5.5	1000	5	95
6.0	1000	95	5
8.0	1000	95	5

doi:10.6342/NTU202201196

4. Results and discussion

4.1. Characterization and electrochemical performance

Prior to the PFOS degradation experiments, the fabricated $GOTiO_2$ material was comprehensively characterized to fully determine its physicochemical and electrochemical properties. The addition of GO on TiO_2 material (0−5 wt. %) were examining.

4.1.1. $GOTiO_2$ material under 200 °C calcination

Morphology and chemical structure

To further optimize the $GOTiO_2$ material, the Tween 80 was used as the surfactant, and the $GOTiO_2$ material was calcined under 200 °C. XRD was utilized to identify the crystal structure and phase formation of the synthesized material. **Figure 4-1** (**a)** shows the XRD patterns of GO, TiO_2 and $GOTiO_2$ nanocomposites obtained with various amounts of added GO; the weight ratios of GO are 0–5 wt. %. The GO samples show an XRD peak of 2θ at 10°, confirming the reflection of the (0 0 2) peak of GO. The TiO_2 component (P25) was anatase and rutile. The tetragonal anatase phase of TiO_2 shows an XRD pattern of 2θ at 25°, 38° and 48°, which can be indexed to the (1 0 1), (0 0 4) and (2 0 0) planes, respectively; the tetragonal rutile phase peak of 2θ at 27° can be indexed to the (1 1 0) plane. In addition, the typical diffraction peak of GO was not observed in

doi:10.6342/NTU202201196

the $GOTiO_2$ patterns, which was probably because of poor ordering in the stacked sheets (Khannam et al., 2016) or the addition of small amounts of GO. On the other hand, the elemental composition of $GOTiO_2$ was determined by energy dispersive spectroscopy (EDS) and is presented in **Figure 4-1 (b)**. The results confirmed the presence of the elements carbon, oxygen and titanium in the $GOTiO_2$ nanocomposites, with the carbon content increasing from 9.77 to 13.28 % by the addition of 5 wt. % GO.

doi:10.6342/NTU202201196

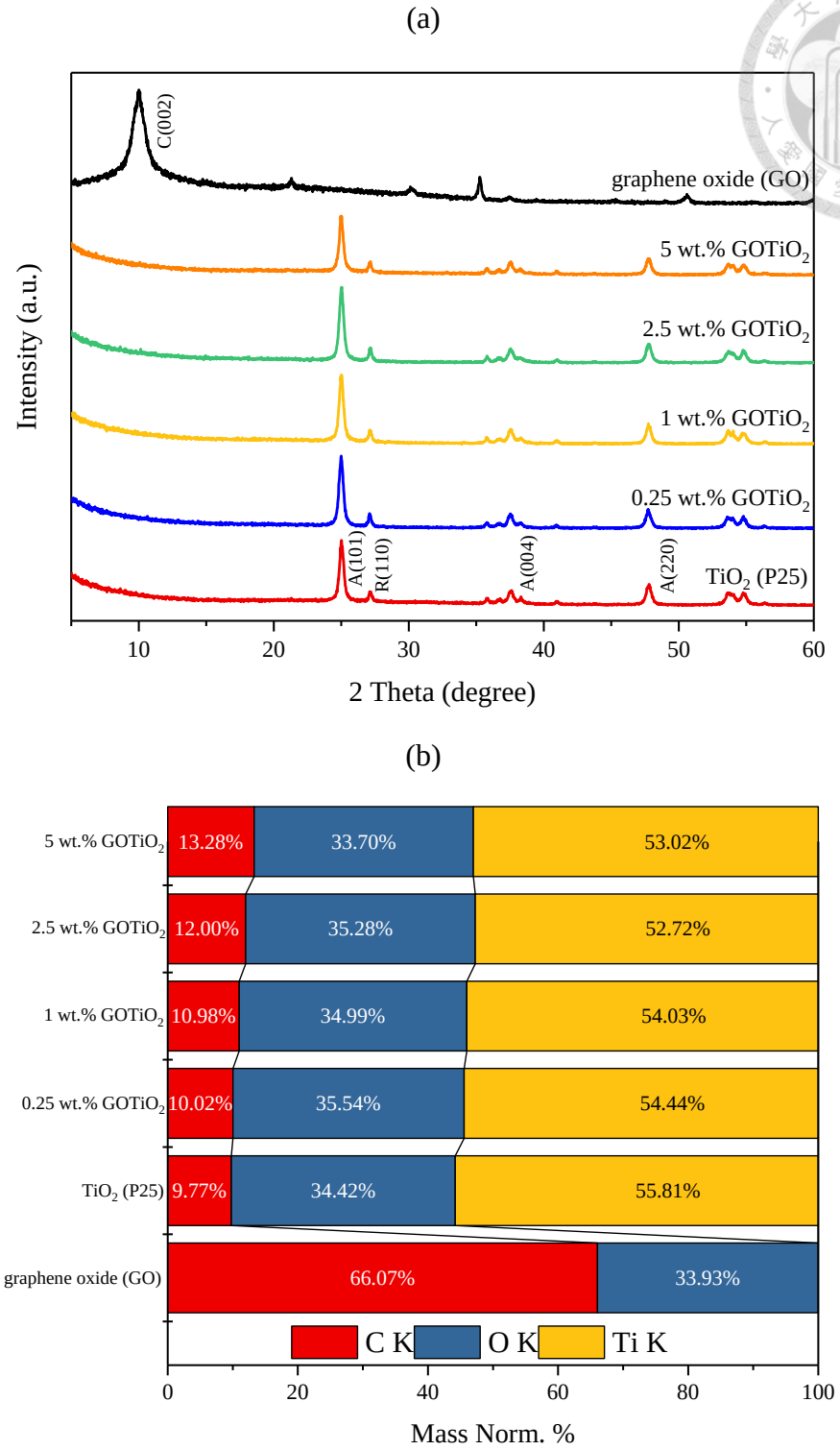

Figure 4-1. (a) XRD analysis, (b) EDS spectra of GO, TiO_2 (P25) and $GOTiO_2$ with various amounts of GO added under 200 °C calcination.

doi:10.6342/NTU202201196

XPS analyses were conducted to identify the functional groups and chemical composition in GO, TiO_2 and $GOTiO_2$. **Figure 4-2 (a)** shows the full-scale XPS survey spectrum; it indicates peaks with binding energies of 295–280 eV, 472–447 eV and 545–525 eV, which refer to the C 1s, Ti 2p and O 1s orbitals. **Figure 4-2 (c)** shows the C 1s spectrum, in which four peaks are observed at 284.8 eV, 286.4 eV, 288.8 eV and 287 eV, which represent the C–C bond, C–O–C bond, O–C=O bond and C=O bond, respectively; this is consistent with the results of Hunge et al. (2020). Regarding the O 1 s orbital in the XPS pattern (**Figure 4-2 (d)**), only one peak appears at 533.8 eV, which can be ascribed to the O–C bond, while the O–Ti bond, O–H bond and O–C bond appeared in TiO_2 and the $GOTiO_2$ composite, with binding energies of 530 eV, 532.2 eV and 533.8 eV, respectively. Additionally, the Ti 2p spectrum is shown in **Figure 4-2 (b)**. Binding energies of 458.3 eV and 464 eV are observed and are attributed to Ti $2P_{3/2}$ and Ti $2p_{1/2}$ in the anatase phase of TiO_2, respectively, showing that Ti is mainly present as Ti^{4+} in TiO_2 and $GOTiO_2$ (Tian et al., 2013).

doi:10.6342/NTU202201196

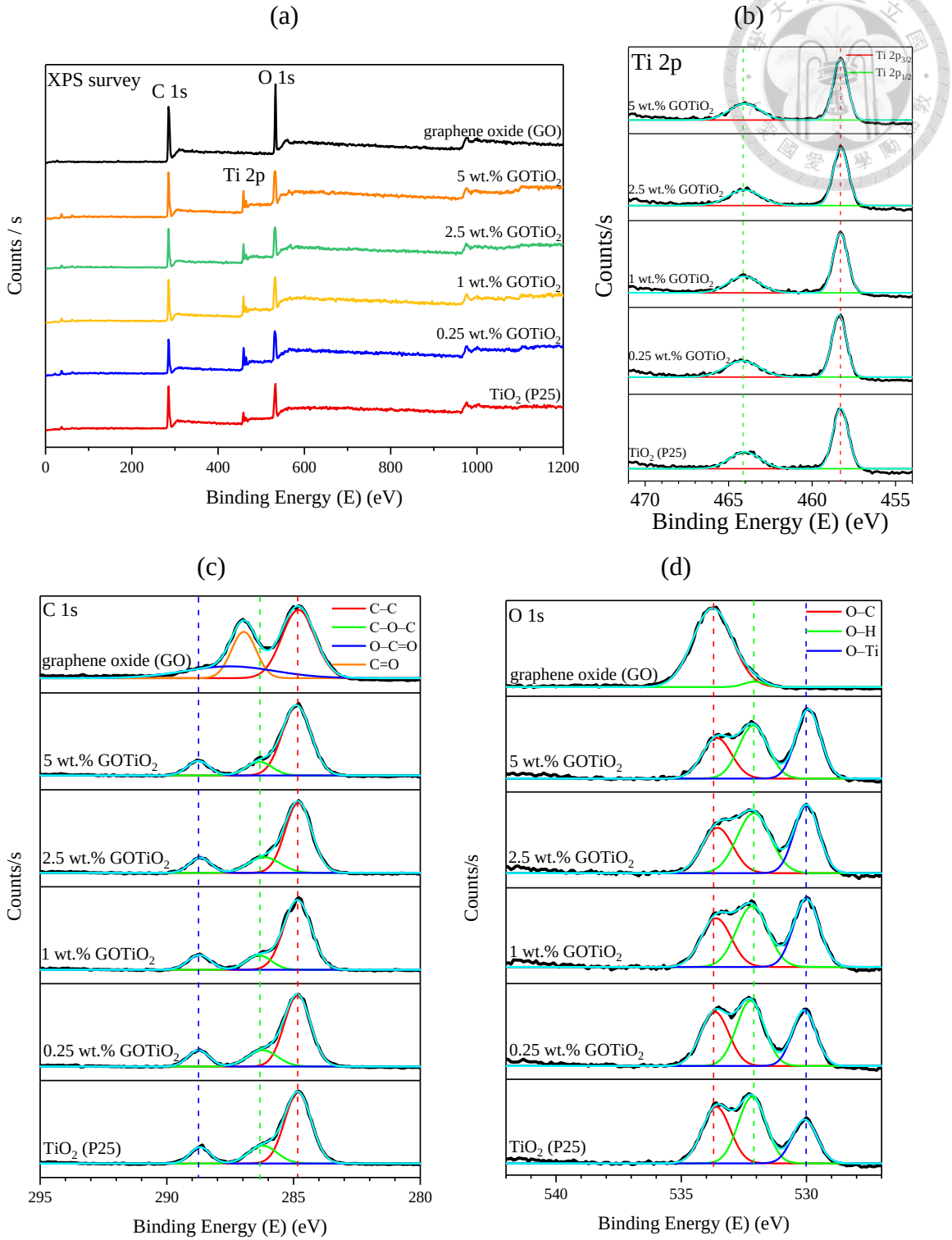

Figure 4-2. XPS spectra of (a) the full survey, (b) Ti 2p orbital, (c) C 1s orbital and (d) O 1s orbital of GO, TiO_2 and $GOTiO_2$ with various amounts of GO added under 200 °C calcination.

doi:10.6342/NTU202201196

The morphology and crystallinity of $GOTiO_2$ were investigated by SEM and TEM analysis. The micrograph of the GO is presented in **Figure 4-3 (a)** and **(g)**, in which a single layer of GO rugose sheets is easily visible. In the TiO_2 images (**Figure 4-3 (b)** and **(h)**), we can observe the typical spherical shape of TiO_2 nanoparticle aggregates. On the other hand, the images of $GOTiO_2$ are shown in **Figure 4-3 (c)**–**(f)** and **(i)**–**(l)** (0.25, 1, 2.5 and 5 wt. % $GOTiO_2$). When only 0.25 wt. % GO was added, only a small piece of the GO rugose sheets covered the surface of the TiO_2 nanoparticles due to insufficient GO addition, while most TiO_2 nanoparticles were present as agglomerates on GO sheets. However, when the addition amount of GO increased to 1, 2.5 and 5 wt. %, TiO_2 nanoparticles were more homogeneously dispersed on the GO layers. This homogeneous dispersion may be the reason behind the increased electrochemical performance of the $GOTiO_2$ photoelectrode.

(a) (g)

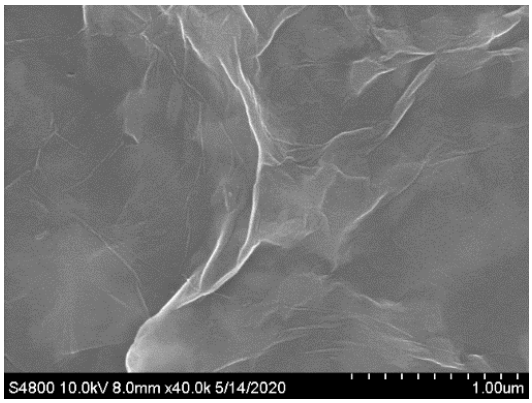

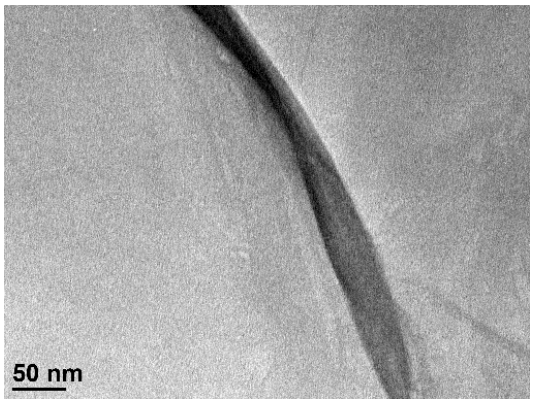

doi:10.6342/NTU202201196

(b)

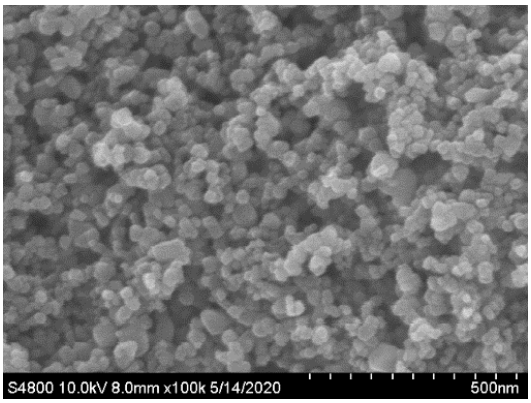

(h)

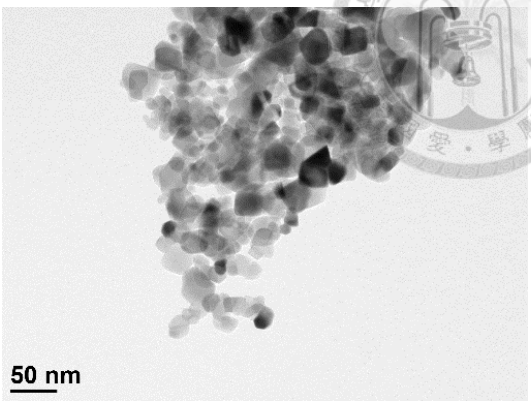

(c)

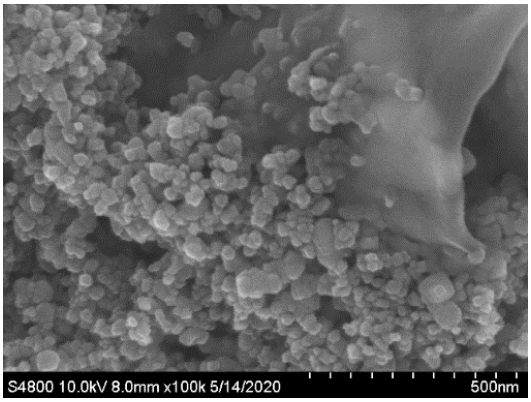

(i)

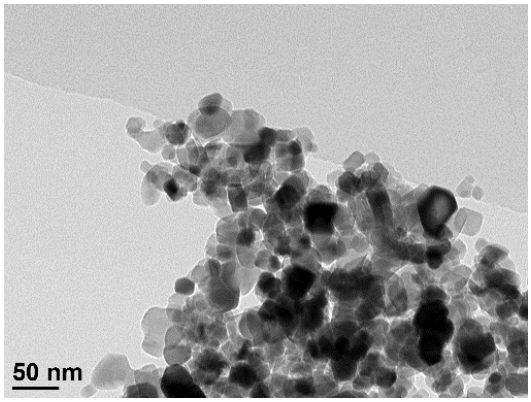

(d)

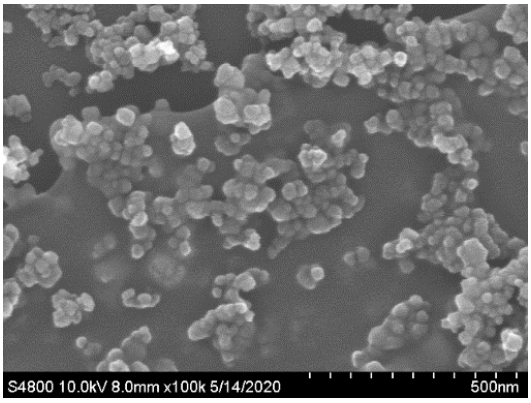

(j)

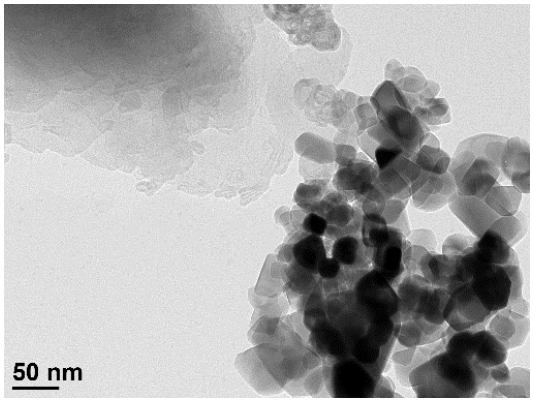

doi:10.6342/NTU202201196

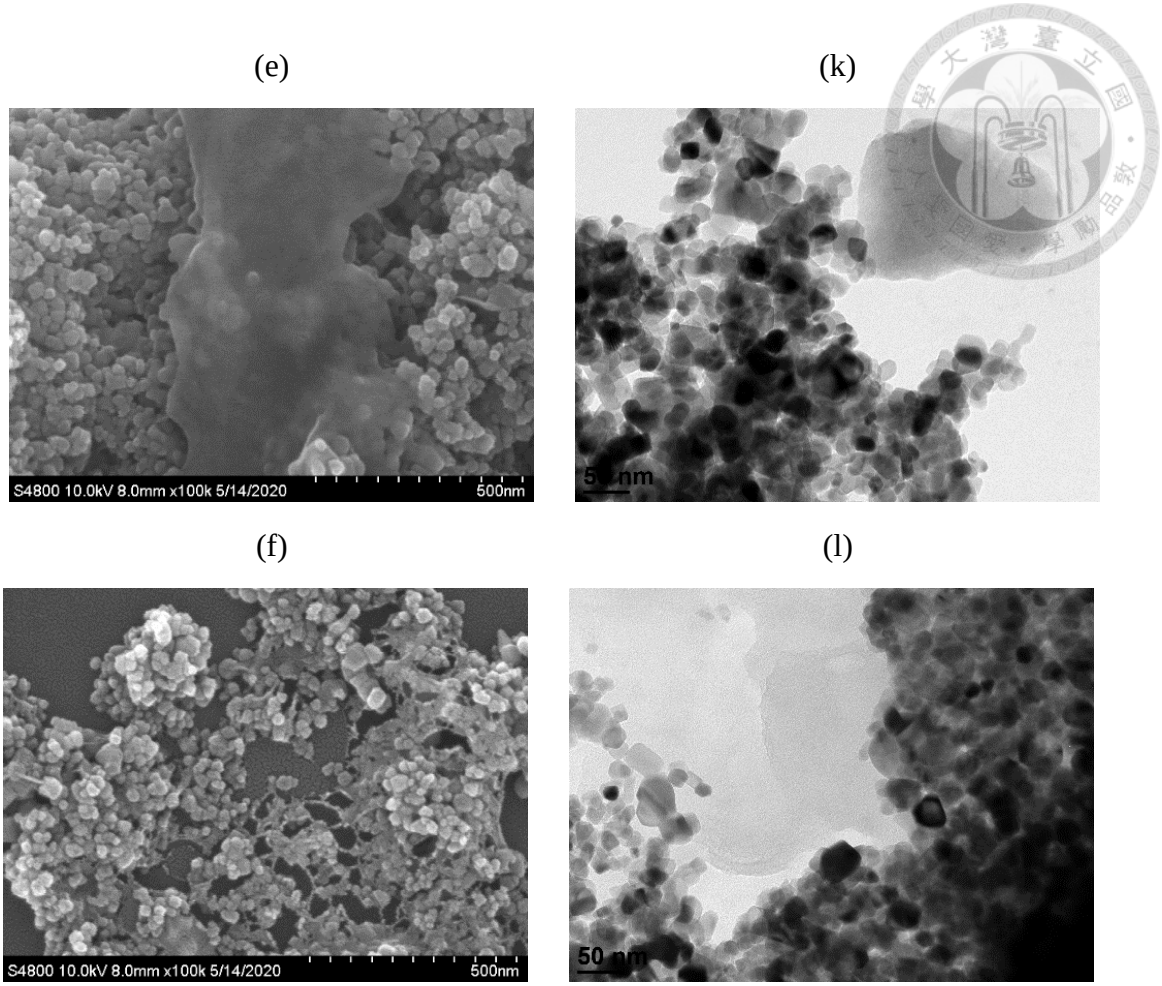

Figure 4-3. SEM images of (a) GO, (b) TiO_2, (c) 0.25 wt. % $GOTiO_2$, (d) 1 wt. % $GOTiO_2$, (e) 2.5 wt. % $GOTiO_2$, (f) 5 wt. % $GOTiO_2$ and TEM images of (g) GO, (h) TiO_2, (i) 0.25 wt. % $GOTiO_2$, (j) 1 wt. % $GOTiO_2$, (k) 2.5 wt. % $GOTiO_2$, (l) 5 wt. % $GOTiO_2$ under 200 °C calcination.

doi:10.6342/NTU202201196

The UV–vis spectroscopy results of the synthesized $GOTiO_2$ are provided in **Figure 4-4 (a)**. The results show that the absorption edge of $GOTiO_2$ redshifts towards higher wavelengths in the absorption region with varying amounts of GO addition. By using the photon energy equation (**Equation (4-2)**), the optical band gap (E_g) was calculated from the absorption edge, as shown in **Figure 4-4 (b)**. A tendency was observed that the band gap energy of $GOTiO_2$ decreased with increasing GO addition. The increase in the GO amount would also enhance the conductivity by reducing the recombination rate of electron-hole pairs (Lv et al., 2019; Zhao et al., 2019; Zhu et al., 2010), which would contribute to better catalytic activity.

To explore the surface characteristics of $GOTiO_2$, the S_{BET} was investigated by BET isotherm measurements; the results of S_{BET}, pore volume, pore size and particle size are presented in **Figure 4-5** and **Table 4-1**. By analysis, the S_{BET} and pore volume of $GOTiO_2$ obviously increased from 51.1 to 72.6 $m^2\ g^{-1}$ and from 0.35 to 0.41 $cm^3\ g^{-1}$ with increasing GO addition, respectively; simultaneously, the pore size and the particle size decreased. This results in the better electrochemical capacitance of the $GOTiO_2$ photoelectrode (Liu et al., 2018).

doi:10.6342/NTU202201196

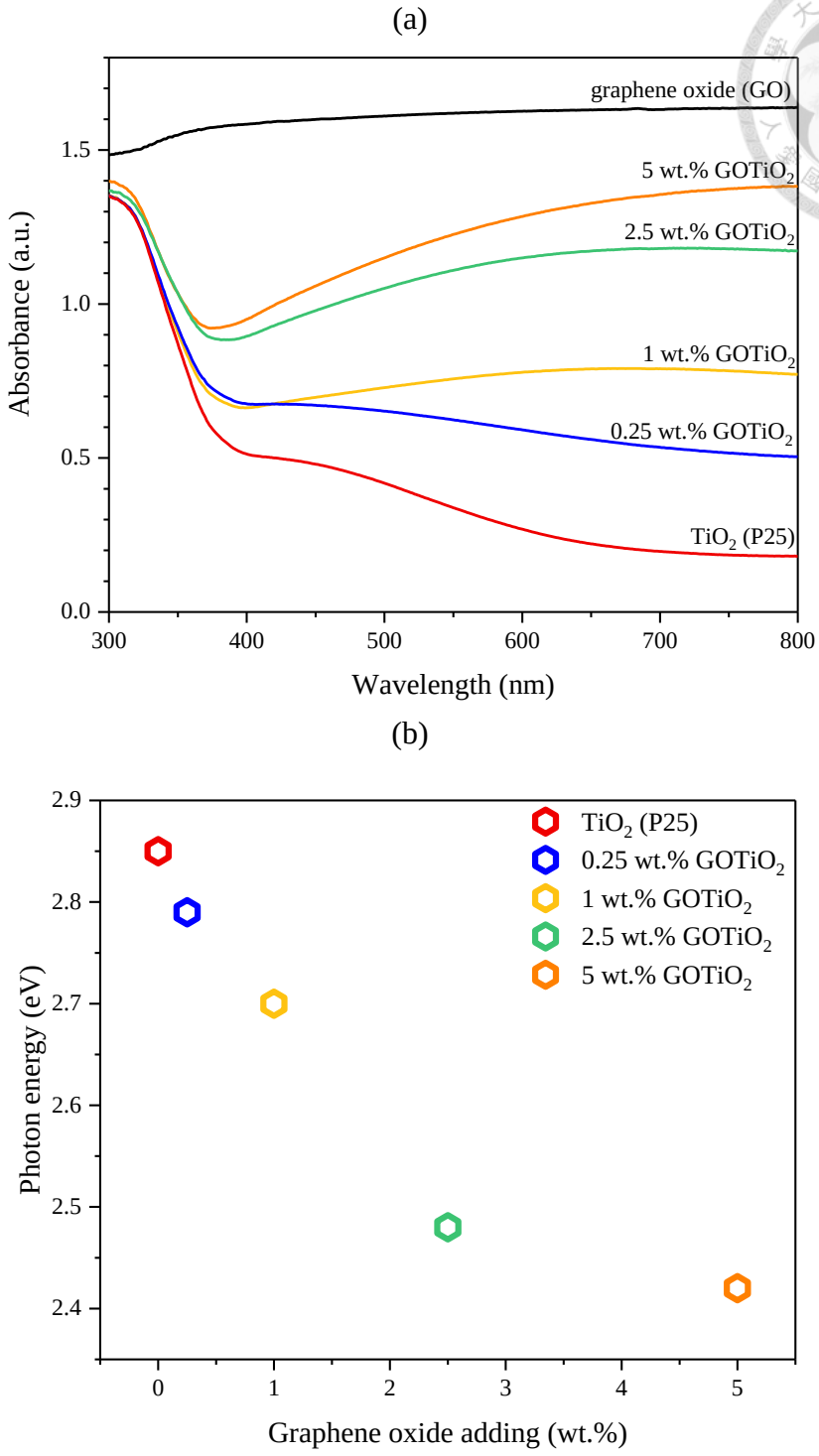

Figure 4-4. (a) UV–vis spectra, (b) bandgap energy of GO, TiO_2 and $GOTiO_2$ with various amounts of GO added under 200 °C calcination.

doi:10.6342/NTU202201196

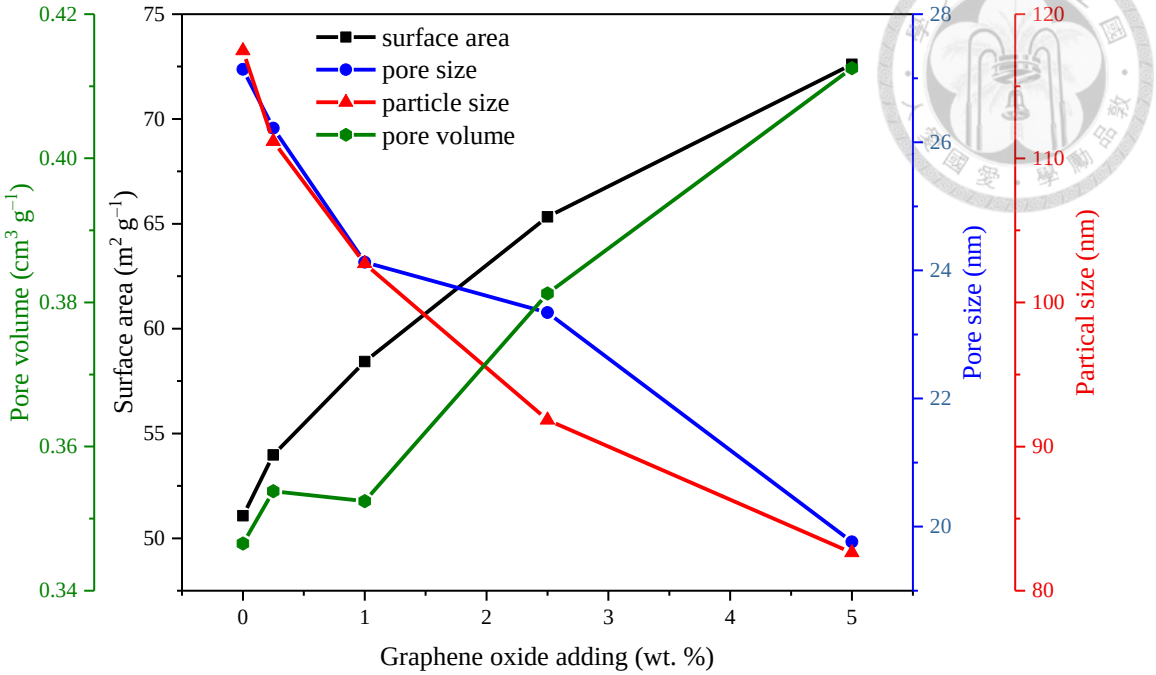

Figure 4-5. Surface area, pore volume, pore size and particle size of GO, TiO_2 and $GOTiO_2$ with various amounts of GO added under 200 °C calcination.

Table 4-1. Surface area, pore volume, pore size, particle size and capacitance of TiO_2 and $GOTiO_2$ obtained with various amounts of GO added.

Sample	Surface Area ($m^2 g^{-1}$)	Pore Volume ($cm^3 g^{-1}$)	Pore Size (nm)	Particle Size (nm)	Capacitance (mF cm^{-2})
5 wt. % $GOTiO_2$	72.604	0.413	19.762	82.639	4.629
2.5 wt. % $GOTiO_2$	65.330	0.381	23.342	91.840	3.703
1 wt. % $GOTiO_2$	58.427	0.352	24.128	102.692	1.925
0.25 wt. % $GOTiO_2$	53.973	0.354	26.221	111.168	0.250
TiO_2 (P25)	51.077	0.347	27.138	117.469	0.159

doi:10.6342/NTU202201196

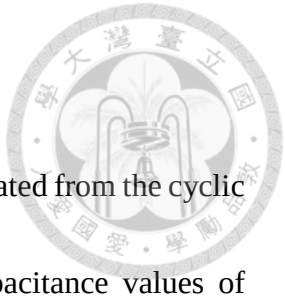

Electrochemical performance

The specific capacitance (Cs) of the photoelectrode can be calculated from the cyclic voltammetry curves according to **Equation (4-4)**, the specific capacitance values of $GOTiO_2$ photoelectrodes are obtained. **Figure 4-6 (a)** shows the C–V characteristic curves of $GOTiO_2$ obtained with various amounts of GO addition under UV irradiation. The results show that when GO addition was increased from 0 to 5 wt. %, the specific capacitance increased from 0.159 to 4.63 mF cm^{-2} (**Table 4-1**), indicating that a higher GO amount in the $GOTiO_2$ electrode contributed to better electrochemical characteristics. Furthermore, **Figure 4-6 (b)** shows the C–V characteristic curves of the 5 wt. % $GOTiO_2$ photoelectrode under UV irradiation at various scan rates. All of the cyclic voltammetry curves were rectangular in shape, indicating ideal capacitive properties, and the current intensity of this photoelectrode was independent of the potential energy. The specific capacitance of the $GOTiO_2$ photoelectrode has a close relationship with the surface area, namely, the surface area plays a major role in determining the specific capacitance.

Summarizing the above analytical results from XRD, XPS, SEM, TEM, UV–vis, BET and Cs, $GOTiO_2$ was successfully fabricated. Its improved properties result in the enhanced PEC performance of 5 wt. % $GOTiO_2$ photoelectrode under 200 °C calcination.

doi:10.6342/NTU202201196

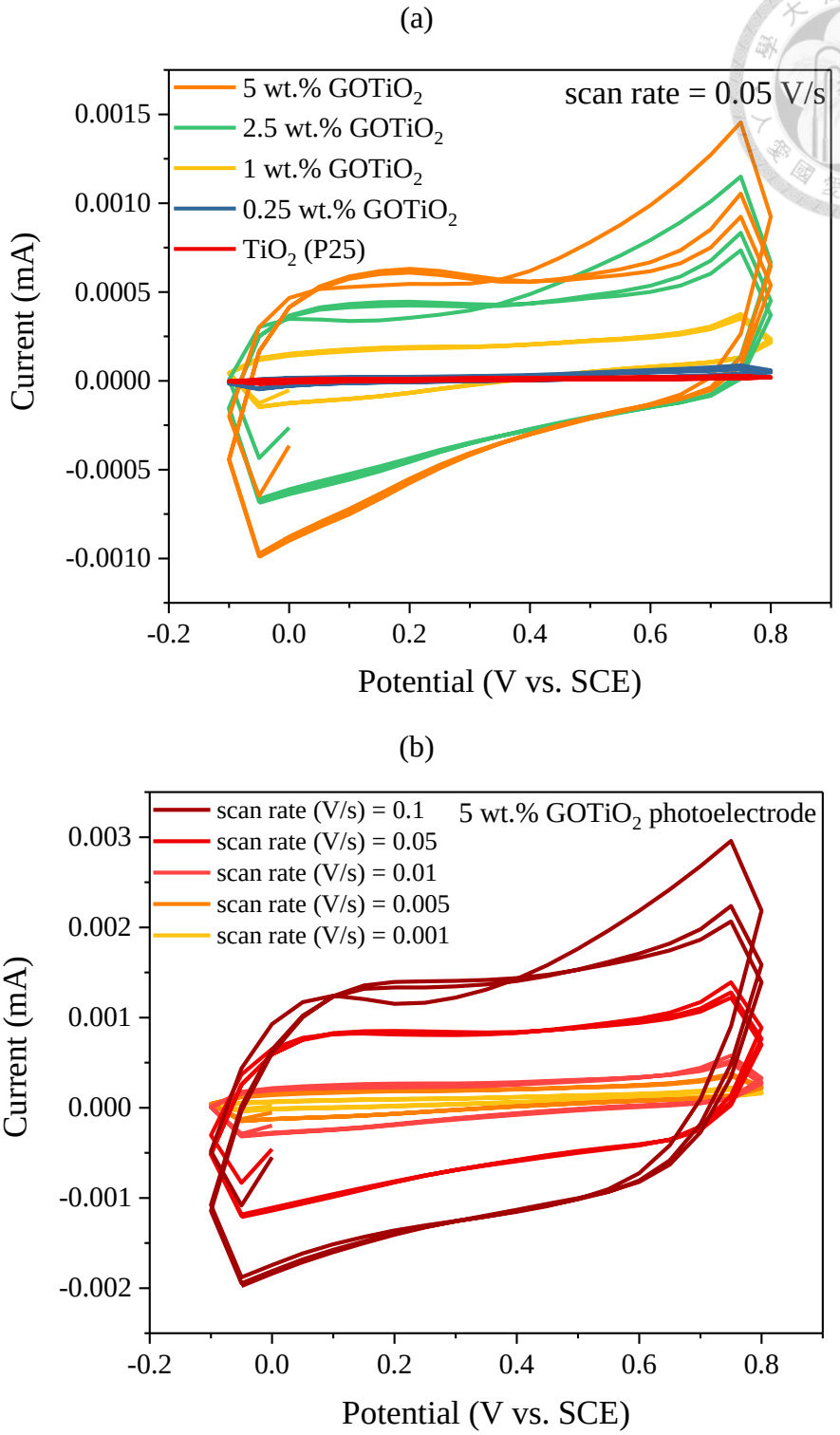

Figure 4-6. C–V curves of (a) GO, TiO_2 and $GOTiO_2$ with various amounts of GO added and (b) the 5 wt. % $GOTiO_2$ at different scan rates from 0.001 to 0.1 V s^{-1} under 200 °C calcination.

doi:10.6342/NTU202201196

4.2. Photoelectrochemical degradation

Before conducting the PEC and EC experiments, background tests, including direct photolysis (without the $GOTiO_2$ electrode), photocatalysis and photochemical degradation, were first conducted. No PFOS or PFOA degradation was observed in 4 h under these three conditions (**Figure 4-7**). EC experiments under low voltage (0.5 V) were also conducted to understand the adsorption behavior of PFOS and PFOA on the anode; the results showed that the PFOS and PFOA removals were both negligible (**Figure 4-7**), suggesting that electroadsorption of these two compounds on the anode can be neglected.

doi:10.6342/NTU202201196

(a)

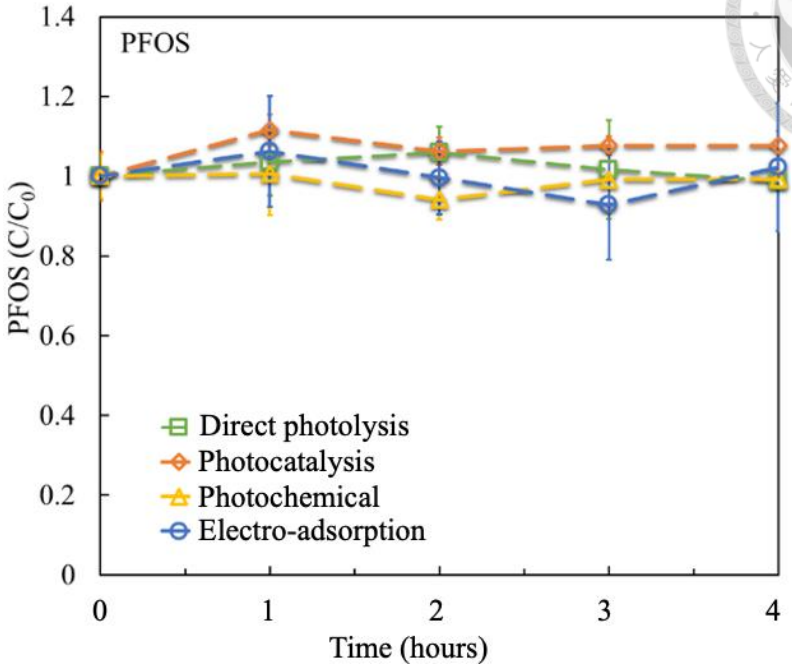

(b)

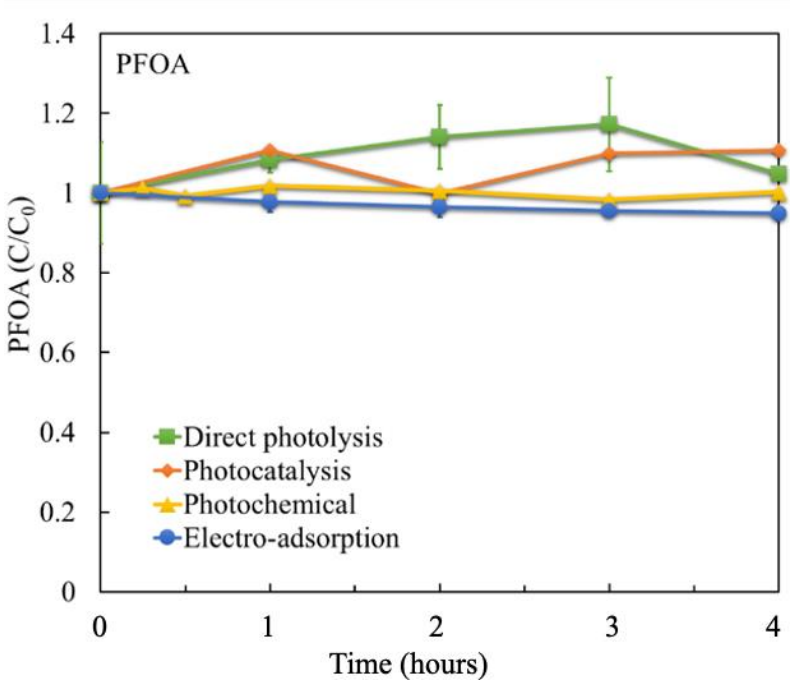

Figure 4-7. Direct photolysis, photocatalysis, photochemical degradation and electroadsorption test of (a) PFOS and (b) PFOA using chloride anion as electrolyte ($[PFOA]_0$ = 12 μM, $[PFOS]_0$ = 10 μM, [NaCl] = 50 mM, initial solution pH = 5.3; 16 W UVC lamp for direct photolysis, photocatalysis and photochemical reactions).

doi:10.6342/NTU202201196

4.2.1. Parametric study of the PEC system

Influences of operational factors on PFOS removal

PFOS was selected as a representative PFAAs, and the PEC performance of the $GOTiO_2$ electrode was evaluated by the degradation of PFOS under five treatment processes, namely, direct photolysis, photocatalysis, photochemical, EC and PEC processes, and the results are shown in **Figure 4-8** (detailed information on the PFOS degradation efficiencies (η) and rate constants (k) is presented in **Table 3-1**). Among all five processes, the PEC treatment possessed the best degradation efficiency in PFOS degradation, while no PFOS degradation was observed in the background experiments (i.e., direct photolysis, photocatalysis and photochemical processes). The results showed that the degradation of PFOS followed pseudo-first-order kinetics in the PEC and EC processes. The PFOS removal reached 94.83 and 75 % in the PEC and EC processes, respectively, within 4 hours of reaction time; the associated k values were 0.74 and 0.39 $hour^{-1}$, respectively. Our results revealed a synergistic effect on the photoassisted EC degradation of PFOS (a detailed explanation of the synergistic mechanism of the enhancement of PFOS degradation is provided in **Section 4.2.3**). Similar phenomena were observed in other studies. Xu et al. (2020), Peng et al. (2017) and Zhao et al. (2009) investigated the degradation of 2,4-dichlorophenoxyacetic acid, PFOA, and ibuprofen

doi:10.6342/NTU202201196

and found that the removal efficiency in the PEC process was higher than that in the EC process.

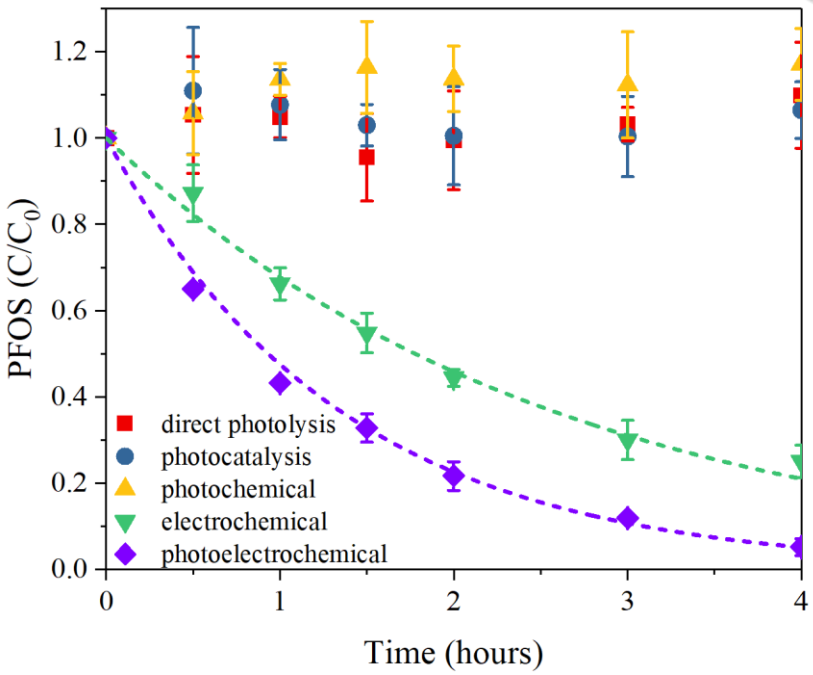

Figure 4-8. PFOS degradation by direct photolysis, photocatalysis, photochemical, electrochemical and photoelectrochemical processes on PFOS degradation in the PEC system.

doi:10.6342/NTU202201196

Figure 4-9 shows the influences of various operational factors, including current density, electrode distance, solution pH, PFOS concentration and electrolyte concentration, on the PFOS removal efficiency by the PEC process. The applied potential voltage plays an important role in the PEC process. The red line in **Figure 4-9** shows that the increase in current density from 2 to 20 mA cm^{-2} was associated with an increase in the ***k*** value from 0.02 to 0.74 $hour^{-1}$. The enhancement of the applied potential could result in a decrease in recombination between holes and electrons and thus enhance the electrochemical performance (Peng et al., 2017; Zhao and Zhu, 2006).

The alteration in electrode distance has an impact on the electron transport behavior and electric resistance and thus affects the current efficiency. In our results (blue line in **Figure 4-9**), the best PFOS degradation occurred with an electrode distance of 5 mm; an increase in the electrode distance from 5 to 20 mm led to a decrease in PFOS degradation efficiency (the ***k*** values decreased from 0.74 to 0.17 $hour^{-1}$). A higher electrode distance led to a reduction in the electron diffusion efficiency, thereby decreasing the PFOS degradation efficiency (Duan et al., 2018; Hu et al., 2016a; Ma et al., 2015). Accordingly, in the following experiments, 5 mm was selected as the optimal electrode distance.

The solution pH was also a significant factor in the PEC process. The optimal PFOS degradation rate occurred under acidic solution pH conditions (i.e., pH = 3), as shown in **Figure 4-9** (yellow line). Because PFOS has a pKa value of −3.27 (Brooke et al., 2004),

doi:10.6342/NTU202201196

at the pH values studied in this work (pH = 3–11), PFOS mainly exists in its anionic form ($F(CF_2)_8SO_3^-$). Hence, negatively charged PFOS will have favorable affinity for the photoanode, subsequently leading to its degradation. However, at alkaline pH values, the PFOS degradation rate was reduced. With increasing pH, the concentration of OH^- increased, which led to competition between the PFOS anion and OH^- for the sorption sites on the anode (Zhuo et al., 2020), thereby leading to the lowest PFOS removal at pH 11. Zhuo et al. (2020) investigated the EC treatment of F-53B, which is a PFOS substitute, and observed that a lower compound degradation rate occurred under alkaline pH conditions.

Since PFOS exists in a wide range of concentrations in aquatic environments (Lin et al., 2010; Lin et al., 2009), it is meaningful to investigate the influence of the initial PFOS concentration on the degradation efficiency in the PEC system. The result (the green line in **Figure 4-9**) shows that a lower initial PFOS concentration facilitates its degradation; when the PFOS concentration decreases from 10 to 0.5 μM, the ***k*** values increase from 0.13 to 0.74 $hour^{-1}$. Since the amount of PFOS treatment per unit time was constant under the conditions of the PEC system, an increase in the initial concentration of PFOS led to a reduction in the PFOS degradation efficiency (Duan et al., 2018).

The electrolyte concentration was varied to study its effects on PFOS degradation. As shown in **Figure 4-9** (purple line), the PFOS degradation ***k*** values increase from 0.19

doi:10.6342/NTU202201196

to 0.74 hour^{-1} with increasing electrolyte concentration from 10 to 50 mM; however, for increasing electrolyte concentrations from 50 to 100 mM, no influence of electrolyte concentration on the rate of PFOS removal was observed. During the PEC process, enough ions in the system were required to promote electron transfer and facilitate the PEC reaction, while at lower electrolyte concentrations, the abundance of ions was insufficient, thereby leading to a reduction in the PFOS degradation rate. This phenomenon was consistent with the literature (Li et al., 2009; Song et al., 2010). Thus, a 50 mM electrolyte (sodium perchlorate) was used in this study.

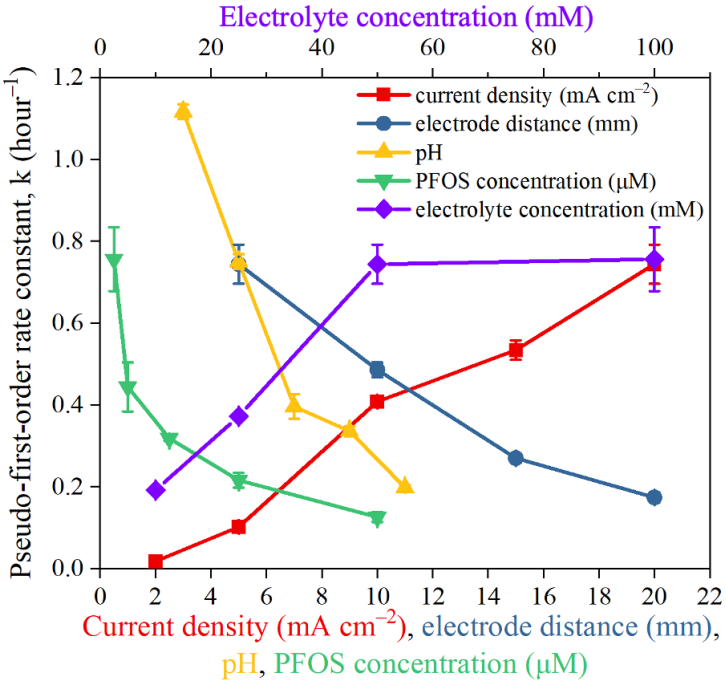

Figure 4-9. Effects of the current density, electrode distance, pH, electrolyte concentration and PFOS concentration on PFOS degradation in the PEC system.

doi:10.6342/NTU202201196

Influences of operational factors on PFOA removal with chloride anion electrolyte

It is meaningful to study the influence of different type of electrolytes, the electrolyte was the significant factor in PEC process. Sodium chloride (NaCl) was selected as an electrolyte, and using PFOA as the model compound of PFAAs. The degradation of PFOS and PFOA by $GOTiO_2$ and TiO_2 in the PEC and EC systems under different experimental conditions is examined, as shown in **Table 4-2**. Several operational parameters (the initial compound concentration, electrode potential, solution pH, (photo)electrochemical conditions and anodic material) were investigated, and an applied current density (J) of 16.7 mA cm^{-2} was used in all investigations except those of the electrode potential. The initial pollutant concentration will affect the degradation rate. **Figure 4-10** shows that a low PFOA concentration resulted in a high degradation efficiency under the PEC conditions with the $GOTiO_2$ electrode. As the PFOA concentration increased from 0.5 to 5 mg L^{-1}, the PFOA degradation efficiency decreased from 98.2–76 % with a 4 hour reaction time. Garcia-Segura et al. (2013) investigated Acid Orange 7 degradation in a PEC system and observed similar phenomena.

doi:10.6342/NTU202201196

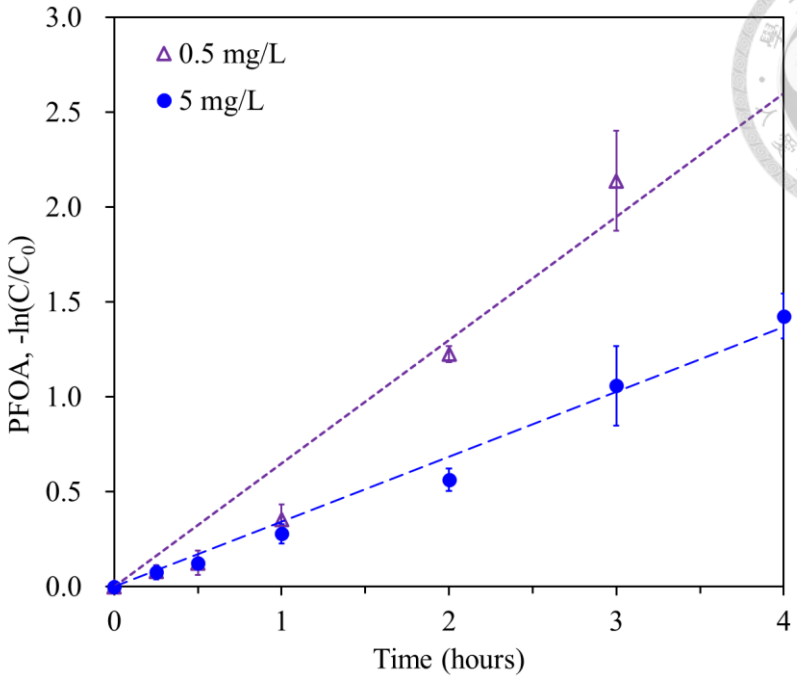

Figure 4-10. Effect of the PFOA concentration on PEC degradation with the $GOTiO_2$ electrode on PFOA degradation in the PEC and EC systems ([NaCl] = 50 mM, initial solution pH = 5.3).

doi:10.6342/NTU202201196

Table 4-2. Summary of PFOA and PFOS degradation in PEC and EC systems using chloride anion as an electrolyte with $GOTiO_2$ and TiO_2 anodes.

No.	Degradation process	Anode	Target compound	Initial compound concentration (mg L^{-1})	Degradation efficiency (%)	Half-life (Hour)	Pseudo-first-order rate constant (hr^{-1})	R^2 Value
1	PEC	$GOTiO_2$	PFOA	0.5	98.2	0.72 ± 0.01	0.96 ± 0.10	0.9785
2	PEC	$GOTiO_2$	PFOA	5	76.0	1.83 ± 0.07	0.37 ± 0.04	0.9900
3	PEC	TiO_2	PFOA	5	76.4	1.83 ± 0.04	0.38 ± 0.02	0.9875
4	EC	$GOTiO_2$	PFOA	5	97.5	0.86 ± 0.09	0.80 ± 0.05	0.9446
5	EC	TiO_2	PFOA	5	95.1	1.06 ± 0.11	0.65 ± 0.05	0.9363
6	PEC	$GOTiO_2$	PFOS	0.5	100	0.42 ± 0.00	1.65 ± 0.25	0.9725
7	PEC	$GOTiO_2$	PFOS	5	100	0.71 ± 0.01	0.97 ± 0.09	0.9429

doi:10.6342/NTU202201196

The electrode potential affects the PFOA degradation efficiency in a PEC system by manipulating the electron transfer capability and •OH production(Lin et al., 2012; Ma et al., 2015; Zhuo et al., 2011). Four different electrode potentials from 3 to 6 V were applied in the PEC system. The photochemical experiment represents 0 V. **Figure 4-11** shows the rate constant for PFOA degradation at each electrode potential (the corresponding current density is also provided). PFOA did not obviously degrade at a potential of 0 V. Even at a potential of 3 V, the degradation of PFOA was negligible, with a pseudo-first-order rate constant of 0.01 $hour^{-1}$. Above 3 V (J = 2 mA cm^{-2}), an increase in voltage resulted in an increase in the degradation efficiency of PFOA. When the voltage increased from 4 to 6 V (J = 4–16.7 mA cm^{-2}), and the degradation rate constant increased from 0.04 to 0.37 $hour^{-1}$. Peng et al. (2017) noted that an increase in the electrode potential leads to a decrease in the electron-hole recombination rate, which facilitates the generation of reactive species and accordingly enhances the electrochemical performance.

doi:10.6342/NTU202201196

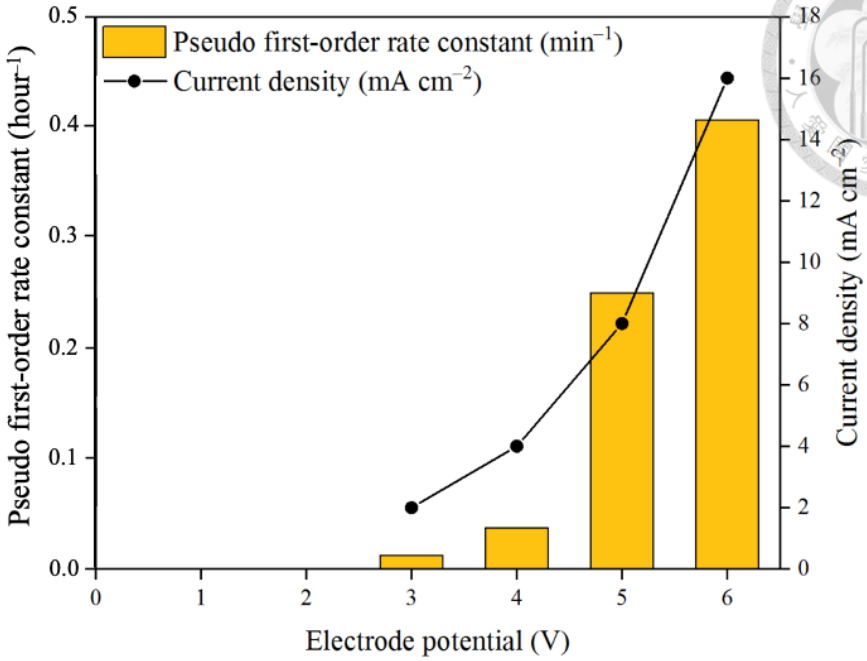

Figure 4-11. The rate constants of PFOA and current densities in the PEC system at different electrode potentials on PFOA degradation in the PEC and EC systems ([NaCl] = 50 mM, initial solution pH = 5.3).

doi:10.6342/NTU202201196

The solution pH also influences the degradation efficiency of PFOA. Three different initial pH values (2, 5.3, and 10) were studied in the PEC system (**Figure 4-12**). The rate constant (0.44 $hour^{-1}$) at pH 2 was the highest, and that at pH 5.3 (0.37 $hour^{-1}$) was slightly lower; however, the rate constant at pH 10 (0.20 $hour^{-1}$) was much lower than that at pH 2. This trend is consistent with previous literature that stated that an acidic pH favors PFOA oxidative degradation (Ma et al., 2015). At low pH, the H^+ concentration is high, hindering the production of •OH; thus, the achievement of a high PFOA decomposition efficiency in the PEC system depends on the direct electrochemical oxidation process.

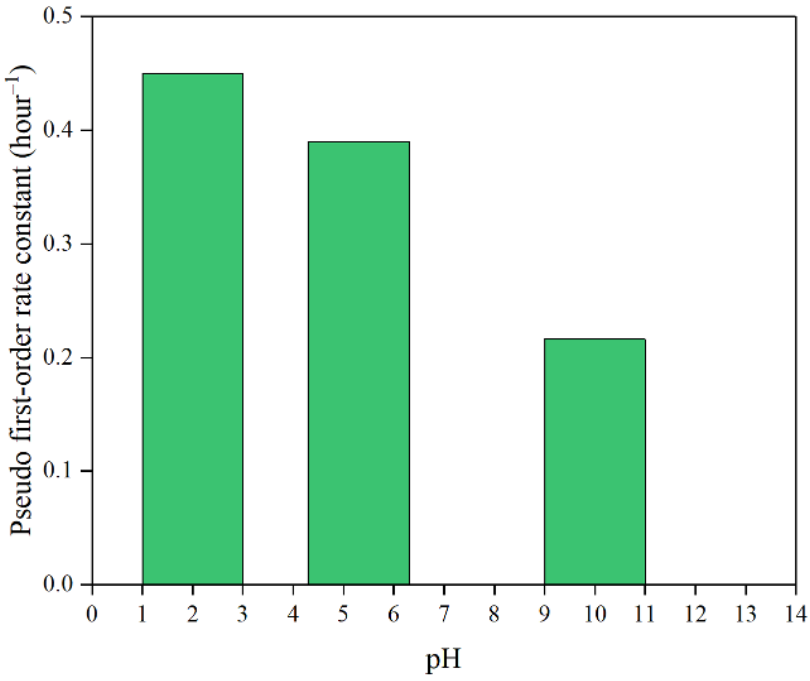

Figure 4-12. The rate constants of PFOA in the PEC system at different pH values on PFOA degradation in the PEC and EC systems ([NaCl] = 50 mM, initial solution pH = 5.3).

doi:10.6342/NTU202201196

Comparative experiments were conducted to investigate the PFOA degradation efficiency (**Figure 4-13**) with $GOTiO_2$ and TiO_2 as the anodic materials under PEC and EC conditions. The degradation of PFOA followed pseudo-first-order kinetics in the PEC and EC processes. In the PEC experiments, the degradation rate constants of the two anodes were nearly the same (0.37 ± 0.04 $hour^{-1}$ for $GOTiO_2$ and 0.38 ± 0.02 $hour^{-1}$ for TiO_2). However, in the EC systems, the $GOTiO_2$ electrode showed higher PFOA degradation rate constants than did the TiO_2 electrode; the rate constants were 0.80 ± 0.05 and 0.65 ± 0.05 $hour^{-1}$, respectively.

In **Figure 4-13**, we can observe that the degradation efficiency in the EC system was higher than that in the PEC system (97.5 and 76 % removal in 4 h in the EC and PEC systems, respectively). The limited effect of UV irradiation on the electrochemical process is likely due to the competition between multiple reactive species. Further explanation will be given in **Section 4.2.2**. Two other studies indicated a similar phenomenon. Cotillas et al. (2016) and Rubí-Juárez et al. (2016) investigated sulfamethoxazole and glyphosate degradation, respectively, and both found that the degradation efficiency in the PEC system was lower than that in the EC system.

doi:10.6342/NTU202201196

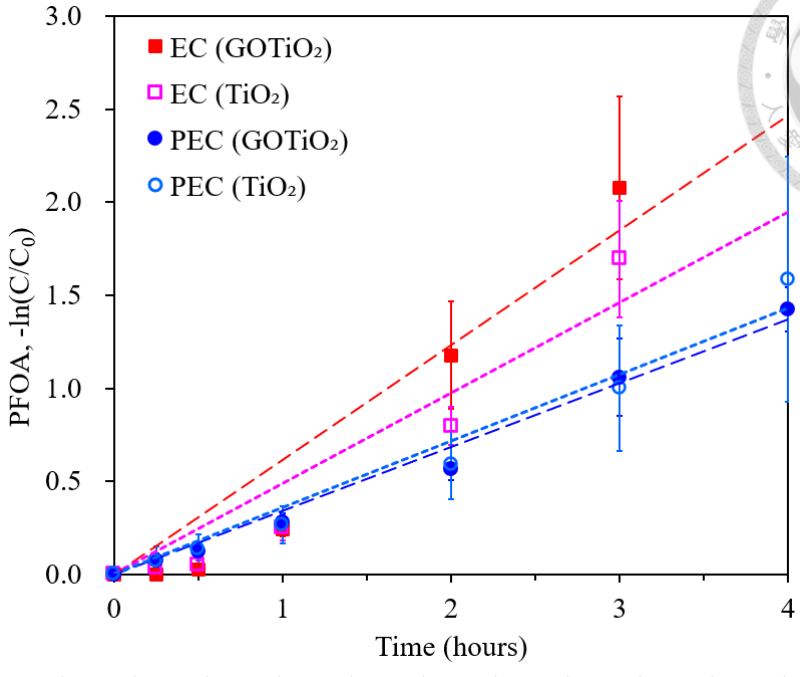

Figure 4-13. The effect of the $GOTiO_2$ and TiO_2 electrodes on PFOA degradation in the PEC and EC systems ([NaCl] = 50 mM, initial solution pH = 5.3).

doi:10.6342/NTU202201196

4.2.2. Degradation mechanism in the PEC process

PFOS degradation mechanism in the PEC process

In the PEC system with sodium perchlorate as the electrolyte, multiple radical chain reactions occurred, and several ROSs were generated as follows (Liu et al., 2019; Muruganandham and Swaminathan, 2004):

$$OH^- \rightarrow \bullet OH + e^- \quad (4\text{-}1)$$

$$H_2O \rightarrow \bullet OH + H^+ + e^- \quad (4\text{-}2)$$

$$2\bullet OH \rightarrow H_2O_2 \quad (4\text{-}3)$$

$$H_2O_2 + h\nu \rightarrow 2\bullet OH \quad (4\text{-}4)$$

$$H_2O_2 \rightarrow O_2 + 2H^+ + 2e^- \quad (4\text{-}5)$$

$$O_2 + e^- \rightarrow \bullet O_2^- \quad (4\text{-}6)$$

Equations (4-1) and **(4-2)** show the hydroxyl radical (•OH) generated on the surface of the $GOTiO_2$ photoelectrode through an electron transfer reaction. **Equation (4-3)** shows the production of hydrogen peroxide (H_2O_2) from the •OH self-recombination reaction; simultaneously, H_2O_2 will also absorb UV light and transform into •OH (**Equation (4-5)**). In addition, H_2O_2 will be oxidized into O_2, which further reacts with electrons to generate superoxide radicals ($\bullet O_2^-$) (**Equations (4-5)** and **(4-6)**).

doi:10.6342/NTU202201196

To elucidate the participation of reactive species in PFOS degradation in the PEC system, scavenger experiments and probe tests were performed. Scavengers including benzoic acid, p-benzoquinone and potassium iodide (each of 30 mM) were utilized and individually spiked into the solutions. Benzoic acid and *p*-benzoquinone can scavenge •OH and $•O_2^-$, with reaction rate constants of 5.9×10^9 M^{-1} s^{-1} (Chen et al., 2003; Zrinyi and Pham, 2017) and 9×10^9 $M^{-}1$ s^{-1} (Greenstock and Miller, 1975; Palominos et al., 2009), respectively. The results in **Figure 4-14** show that the presence of benzoic acid and *p*-benzoquinone led to the inhibition of PFOS degradation; among the two scavengers, *p*-benzoquinone suppressed PFOS degradation to a larger extent (the degradation rate decreased from 94.83 to 79.99 % and 56.23 % by the addition of benzoic acid and p-benzoquinone, respectively). This implied the involvement of •OH and $•O_2^-$ in the degradation of PFOS, in which $•O_2^-$ played a relatively important role. The abundances of •OH and $•O_2^-$ were further measured using the probe reagents nitrobenzene and hydroquinone (each at 5 μM), respectively(Fang et al., 2014; Guo et al., 2017). To investigate [•OH]ss and [$•O_2^-$]ss in the PEC and EC processes, nitrobenzene was used as the probe reagent of •OH. The reaction rate constant between nitrobenzene and •OH ($k_{•OH/nitrobenzene}$) was 3.9×10^9 M^{-1} s^{-1} (Fang et al., 2014; Guo et al., 2017). Hydroquinone was used as the probe reagent for •OH and $•O_2^-$, and the reaction rate constants $k_{•OH/hydroquinone}$ and $k_{•O2^-/hydroquinone}$ were 5.2×10^9 and 1.7×10^7 M^{-1} s^{-1} (Buxton et al.,

doi:10.6342/NTU202201196

1988), respectively. (Experimental conditions: $[NB]_0 = [HQ]_0 = 5$ μM, reaction time = 15 min, and J = 20 mA cm^{-2} with a 16 W UVC lamp (for the PEC process)). The pseudo-first-order reaction of NB and HQ is shown by the following equation:

$$R_{NB} = -d[NB]/dt = k_{obs}[NB] = k_{\bullet OH/NB}\,[\bullet OH]_{ss}\,[NB]$$

$$\rightarrow k_{obs} = k_{\bullet OH/NB}\,[\bullet OH]_{ss} \quad (4\text{-}7)$$

$$R_{HQ} = -d[HQ]/dt = k_{obs}[HQ] = k_{\bullet OH/HQ}\,[\bullet OH]_{ss}\,[HQ] + k_{\bullet O_2^-/HQ}\,[\bullet O_2^-]_{ss}\,[HQ]$$

$$\rightarrow k_{obs} = k_{\bullet OH/HQ}\,[\bullet OH]_{ss} + k_{\bullet O_2/HQ}[\bullet O_2^-]_{ss} \quad (4\text{-}8)$$

In our experiment, the k_{obs} values for NB and HQ were 0.1285 and 0.3048 min^{-1} in the PEC process, respectively. Accordingly, [•OH]ss and $[\bullet O_2^-]$ss were determined to be 5.49×10^{-7} μM and 1.31×10^{-4} μM in the PEC process, respectively. The steady-state concentration of $\bullet O_2^-$ in the PEC system was significantly higher (~240 times) than that of [•OH]. This result corresponded with the observation from the scavenger experiments, which noted the predominant role of $\bullet O_2^-$ in PFOS degradation compared with that of •OH. On the other hand, we observed that iodide anion (I^-) spiking resulted in significant inhibition of PFOS degradation (the $\boldsymbol{\eta}$ values decreased from 94.83 to 46.56 %) (**Figure 4-14**). The I^- present can compete with existing anions in the solution (e.g., PFOS anion and OH^-) for sorption onto the $GOTiO_2$ photoelectrode surface and further inhibit the electron transfer reaction contributed by the PFOS anion and OH^- (Fang et al., 2013; Wang and Zhang, 2011); thus, inhibition by I^- addition suggested that the electron

doi:10.6342/NTU202201196

transfer pathway also participated in PFOS degradation. Overall, the above results demonstrated that •OH, $•O_2^-$ and electron transfer reactions were all responsible for PFOS degradation during the PEC process.

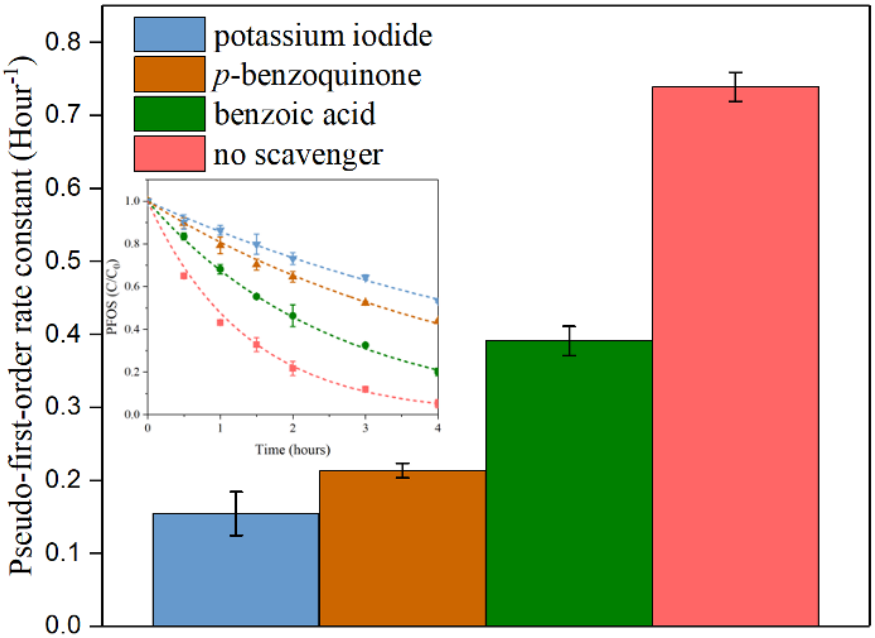

Figure 4-14. Effects of benzoic acid, p-benzoquinone and potassium iodide on PFOS degradation in the PEC system.

doi:10.6342/NTU202201196

PFOA degradation mechanism in the PEC process using chloride anion electrolyte

On the other hand, the influences of Cl^- in PEC process were examined. The predominant reactions in the EC system (**Equations (4-9)**−**(4-13)**) and PEC system (**Equations (4-9)**−**(4-15)**) using Cl^- as an electrolyte are as follows (Cho and Hoffmann, 2014; Cho et al., 2014; Cotillas et al., 2016; Liu et al., 2019).

$$H_2O \rightarrow \bullet OH + H^+ + e^- \quad (4\text{-}9)$$

$$\bullet OH + Cl^- \rightarrow OH^- + \bullet Cl \quad (4\text{-}10)$$

$$\bullet Cl + Cl^- \rightarrow \bullet Cl_2^- \quad (4\text{-}11)$$

$$\bullet OH + Cl^- \rightarrow HOCl + e^- \quad (4\text{-}12)$$

$$HOCl \rightarrow OCl^- + H^+ \; pKa = 7.5 \quad (4\text{-}13)$$

$$HOCl + h\nu \rightarrow \bullet OH + \bullet Cl \quad (4\text{-}14)$$

$$OCl^- + h\nu \rightarrow \bullet O^- + \bullet Cl \quad (4\text{-}15)$$

Equation (4-9) shows the generation of •OH by electron transfer on the surface of the TiO_2 anode. **Equations (4-10)**−**(4-13)** show the production of •Cl and $HOCl/OCl^-$ through the reaction between •OH and Cl^-; •Cl will also react with Cl^- to generate $\bullet Cl_2^-$. In the PEC system, in the presence of UV irradiation, $HOCl/OCl^-$ will be transformed into $\bullet OH/\bullet O^-$ and •Cl, as shown in **Equations (4-14)**−**(4-15)**. These reactions imply that the mechanism of PFOA decomposition in the PEC and EC processes varies. To investigate •OH, nitrobenzene (10 μM) was used as the probe compound

doi:10.6342/NTU202201196

($k_{•OH/nitrobenzene} = 3.9 \times 10^9\ M^{-1}\ s^{-1}$) (Fang et al., 2014; Guo et al., 2017). The [•OH]ss values were calculated to be 1.42×10^{-7} and 1.66×10^{-7} μM in the PEC system and EC system, respectively; on the other hand, [HOCl] was measured at 56 mg L^{-1} in the PEC system and 82 mg L^{-1} in the EC system (**Table 4-3**). The pseudo-first-order reaction of NB is shown by **Equation (4-7)**. These results showed that both concentrations of the reactive species •OH and HOCl were lower in the PEC system than in the EC system, which suggests competition among multiple species in the PEC system, thereby leading to a decrease in the reactive species in the system and consequently decreasing the degradation rate. Although there might be other species (e.g., other RCS) coexisting in the systems, the results of the •OH and HOCl measurement implied that the different amounts of reactive species possibly lead to different byproduct formation trends in the PEC and the EC systems; further investigation on the reactive species contribution will be discussed in the following paragraphs.

Table 4-3. $[•OH]_{ss}$ and [HOCl] measurements in the PEC and EC systems.

	PEC system	**EC system**
$[•OH]_{ss}$	1.42×10^{-7} μM	1.66×10^{-7} μM
[HOCl]	56 mg L^{-1}	82 mg L^{-1}

doi:10.6342/NTU202201196

To further explore the contribution of reactive species involved in PFOA degradation in the PEC and EC systems, the radical scavenger experiments (by the addition of excess amounts of nitrobenzene and *t*-BuOH; 36 mM) were conducted. Nitrobenzene was used as the •OH scavenger; it possesses a high reactivity with •OH ($k_{•OH/nitrobenzene} = 3.9 \times 10^9\ M^{-1}s^{-1}$), but its reactivity with free chlorine ($HOCl/OCl^-$) and other RCS (e.g., •Cl) is negligible (Fang et al., 2014; Guo et al., 2017). *tert*-Butyl alcohol (*t*-BuOH) can quench both •OH and •Cl; the rate constants for the reaction of *t*-BuOH with •OH and •Cl are $k_{•OH/t\text{-}BuOH} = 6.0 \times 10^8\ M^{-1}s^{-1}$ and $k_{•Cl/t\text{-}BuOH} = 3.0 \times 10^8\ M^{-1}s^{-1}$, respectively (Lai et al., 2017; Ma et al., 2018; Watts and Linden, 2007). **Figure 4-15** shows the PFOA degradation with and without the presence of scavengers. Without scavengers in the PEC and EC systems, the PFOA degradation rate constants were 0.37 $\pm$ 0.04 in the PEC system and 0.80 ± 0.05 $hour^{-1}$ in the EC system. The addition of nitrobenzene led to the decrease in the PFOA degradation rate constants from 0.37 ± 0.04 to 0.032 ± 0.01 $hour^{-1}$ in the PEC system and from 0.80 ± 0.05 to 0.038 ± 0.02 $hour^{-1}$ in the EC system. This result suggested that the contributions of •OH were 15.1 and 53 % in the PEC and EC systems, respectively. Additionally, in the presence of *t*-BuOH, due to both •OH and RCS generated in the systems being scavenged, the PFOA degradation rate constants decreased to 0.020 ± 0.03 and 0.24 ± 0.01 $hour^{-1}$ in the PEC and EC systems, respectively. Thus, RCS contributed 29.5 and 17.1 % for PFOA degradation in

doi:10.6342/NTU202201196

the PEC and EC systems, respectively. On the other hand, we observed that PFOA degradation could not be completely scavenged by the addition of the *t*-BuOH scavenger; this observation was possibly because of the participation of the electron transfer pathway for PFOA degradation in the two systems. Overall, based on the results in **Figure 4-15**, the contributions of electron transfer pathway, •OH and RCS for PFOA degradation were 55.4, 15.1 and 29.5 % in the PEC system and 29.9, 53 and 17.1 % in the EC system. These values corresponded with the discussion in previous paragraph. The different reactive species that dominate in the PEC and EC systems result in the variation in the degradation pathways of PFOA. However, further in-depth investigation is still required to explore the relationship between the reactive species participation and the degradation byproducts generation.

doi:10.6342/NTU202201196

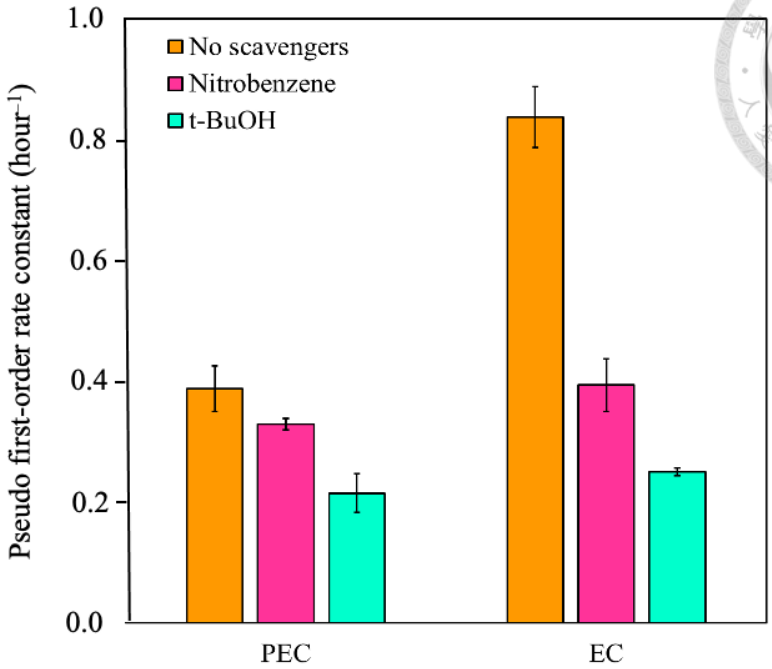

Figure 4-15. Effects of nitrobenzene and *t*-BuOH on PFOA degradation in the PEC and EC systems. ($[PFOA]_0 = 12$ μM, [NaCl] = 50 mM, nitrobenzene (or *t*-BuOH) =36 mM, initial solution pH = 5.3).

doi:10.6342/NTU202201196

4.2.3. Transformation byproducts and pathways of the PEC process

PFOS transformation byproducts and pathways of the PEC process

During the PEC reaction, PFOS undergoes various degradation pathways and is further transformed into various byproducts. To fully explore the overall transformation pathway and elucidate the detailed reaction mechanism, this study not only used PFOS but also separately utilized eight main byproducts, PFOA, PFHpA, PFHxA, PFPeA, PFBA, PFPrA, PFHxS and PFBS, which were detected during PFOS degradation as the target pollutants to conduct the PEC reaction. The results in **Figure 4-16 (a)** and **(b)–(i)** represent PFOS and its 8 main byproducts of degradation/transformation via the PEC reaction, respectively (the dotted lines represent the degradation of target pollutants, formation of F^- and SO_4^{2-}, which correspond to the left y-axis, and the solid lines with solid symbols and the open symbols represent the byproduct evolution, corresponding to the byproducts (nM and peak area/10^4) on the right y-axis, respectively). In this work, a total of 25 PFOS transformation byproducts were observed. Detailed QTOFMS spectrometry parameter information on the 25 detected byproducts is presented in **Table 4-4**, and the mass spectra and structures of the product ions scanned are shown in **Figure 4-17**. These byproducts can be categorized into five groups, including 5 PFSAs, 6 PFCAs, 5 PFALs, 4 HFCs and 5 others. Notably, the byproduct PFSAs (P9 and P15), PFALs and

doi:10.6342/NTU202201196

HFCs were identified for the first time. On the other hand, the results in most of the figures in **Figure 4-16** revealed that the transformation byproducts with different carbon chain lengths possess distinct degradation efficiencies; the concentration of the long-chain byproducts first increases and then decreases, while the concentration of shorter-chain byproducts continuously increases with time. Furthermore, among the degradation of all studied PFAA target compounds (the dotted line in **Figure 4-16**), it was observed that PFAAs with longer chain lengths have a higher degradation rate than PFAAs with shorter chain lengths; the relationship between carbon chain length and PFAA reactivity is discussed further in **Section 4.2.5**.

doi:10.6342/NTU202201196

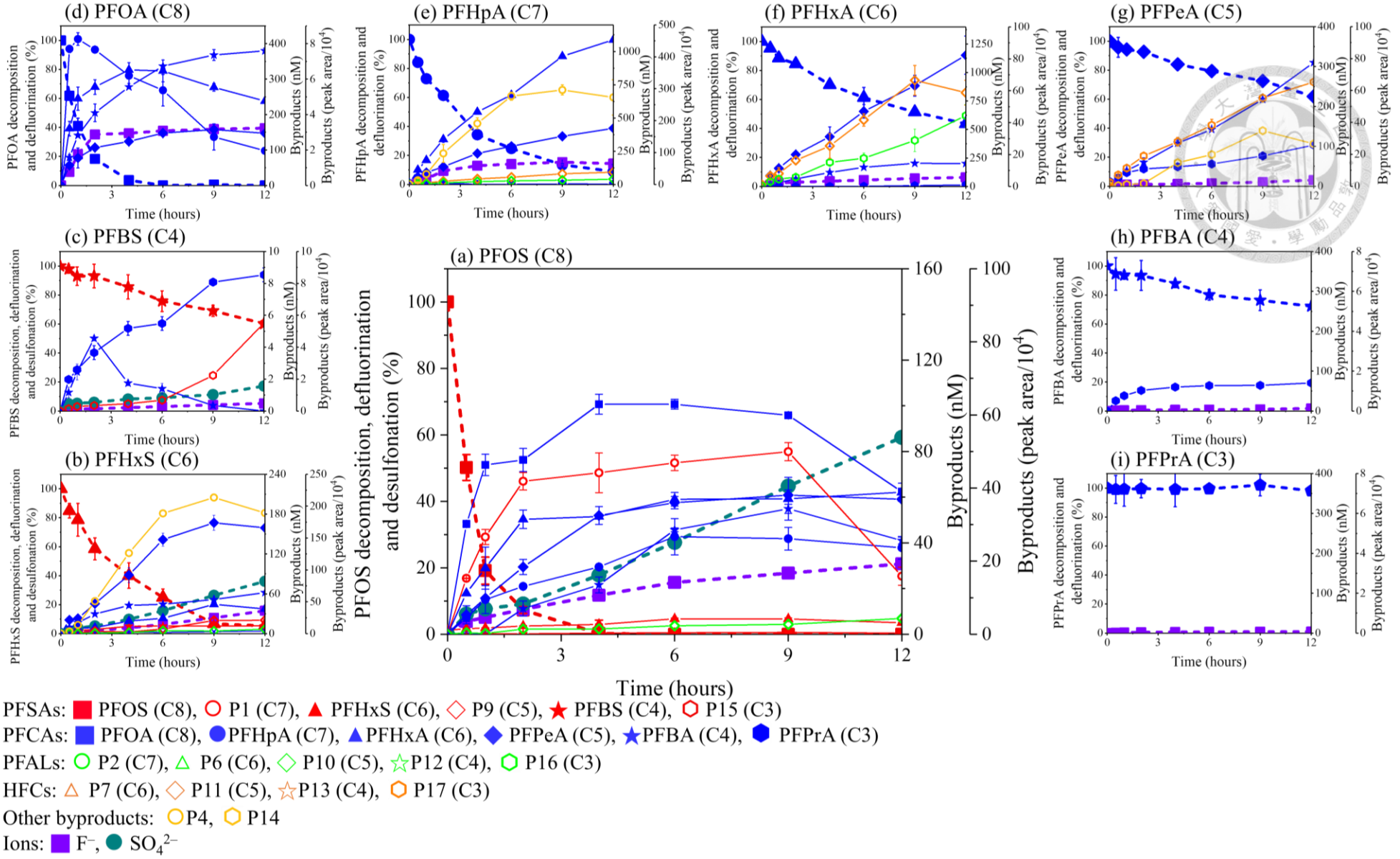

Figure 4-16. Formation of the transformation byproducts, F^- and SO_4^{2-} from (a) PFOS, (b) PFHxS, (c) PFBS, (d) PFOA, (e) PFHpA, (f) PFHxA, (g) PFPeA, (h) PFBA, and (i) PFPrA degradation in PEC systems. ($[PFAAs]_0$ = 40 μM, $[NaClO_4]$ = 50 mM, initial solution pH = 5.64, current density = 30 mA cm^{-2})

doi:10.6342/NTU202201196

(a)

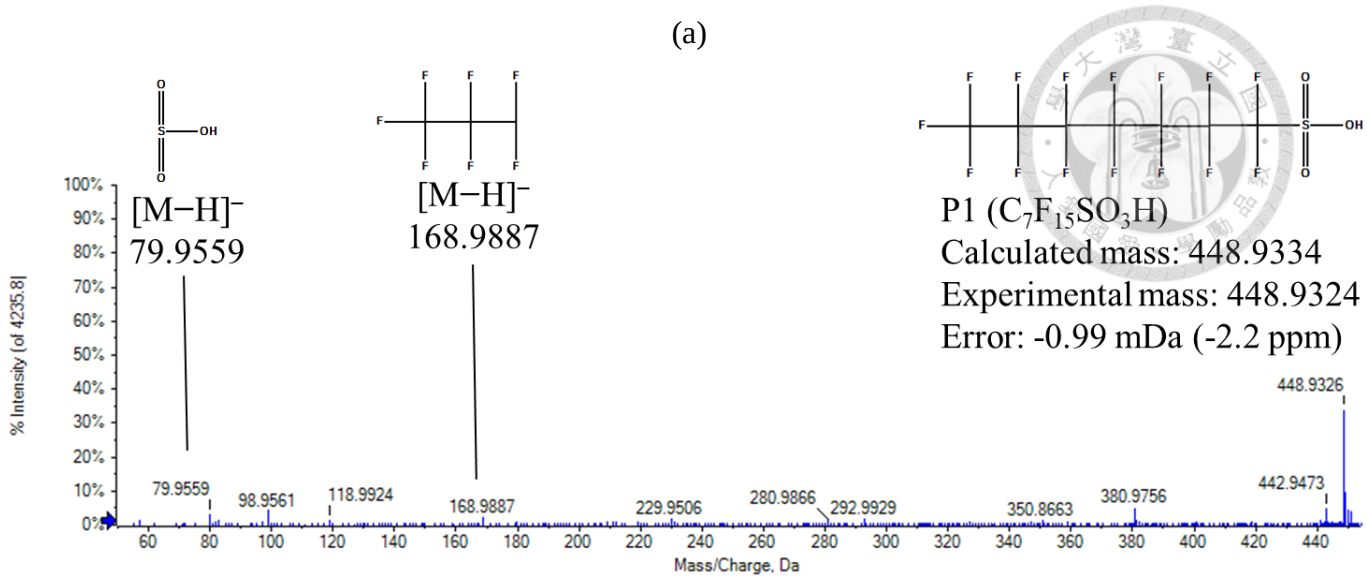

(b)

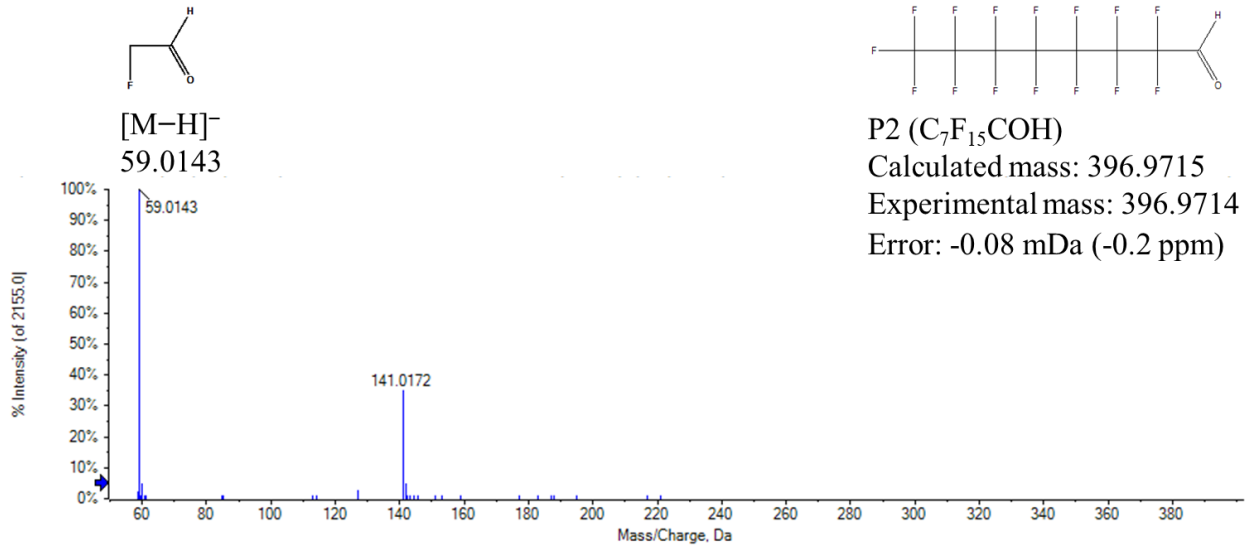

(c)

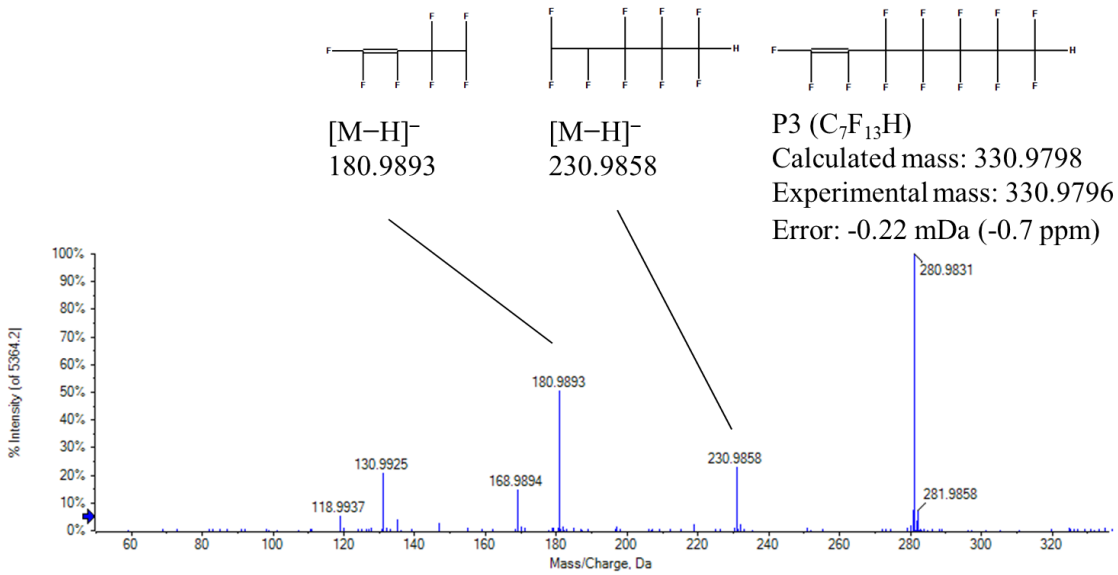

doi:10.6342/NTU202201196

(d)

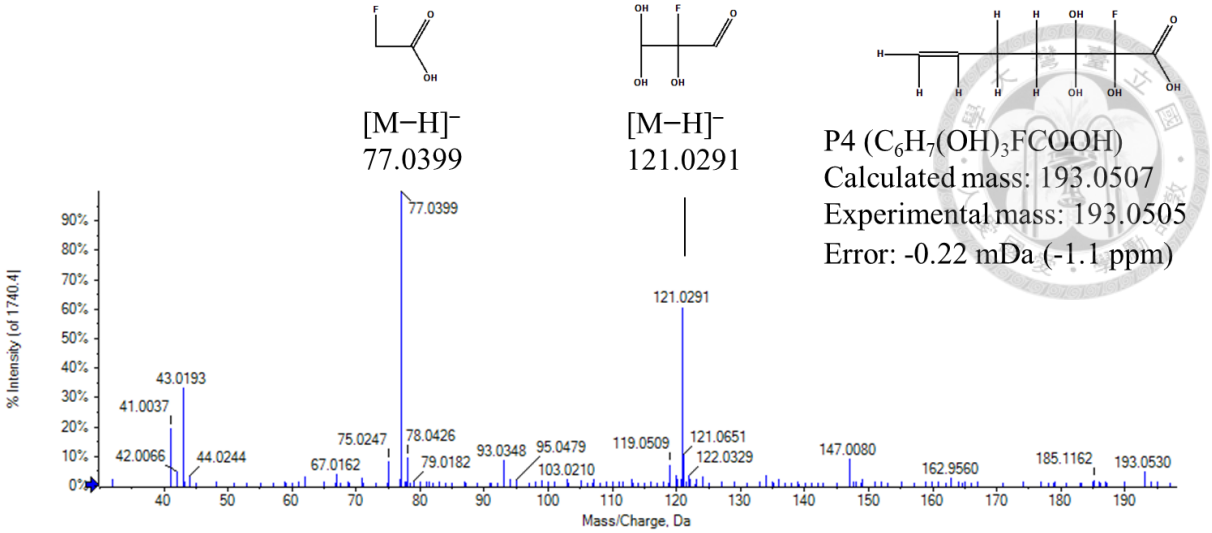

(e)

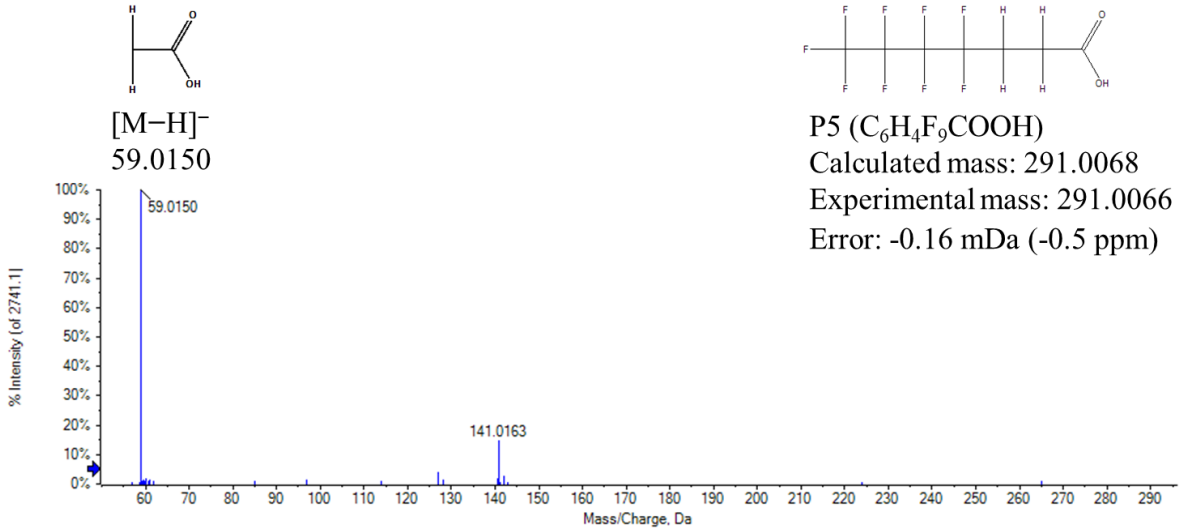

(f)

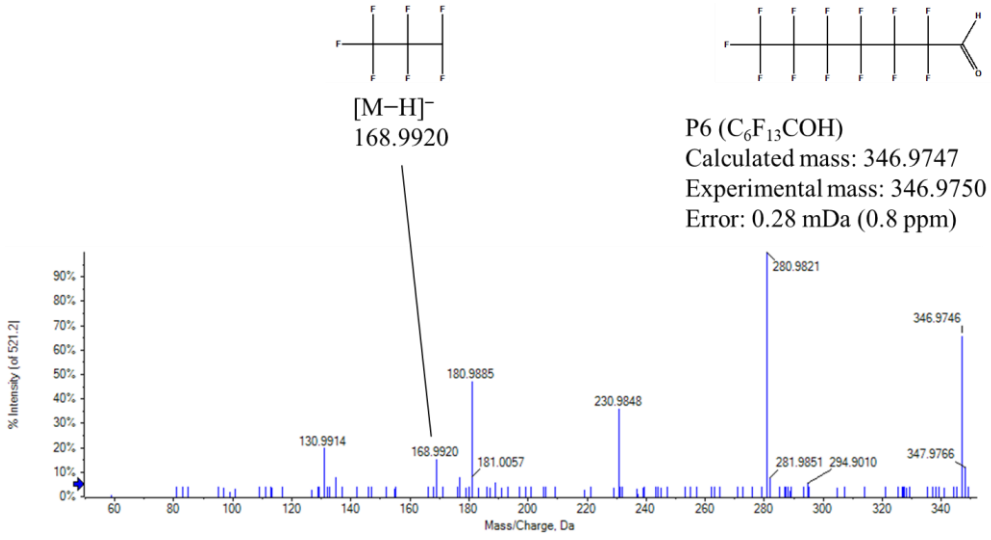

doi:10.6342/NTU202201196

(j)

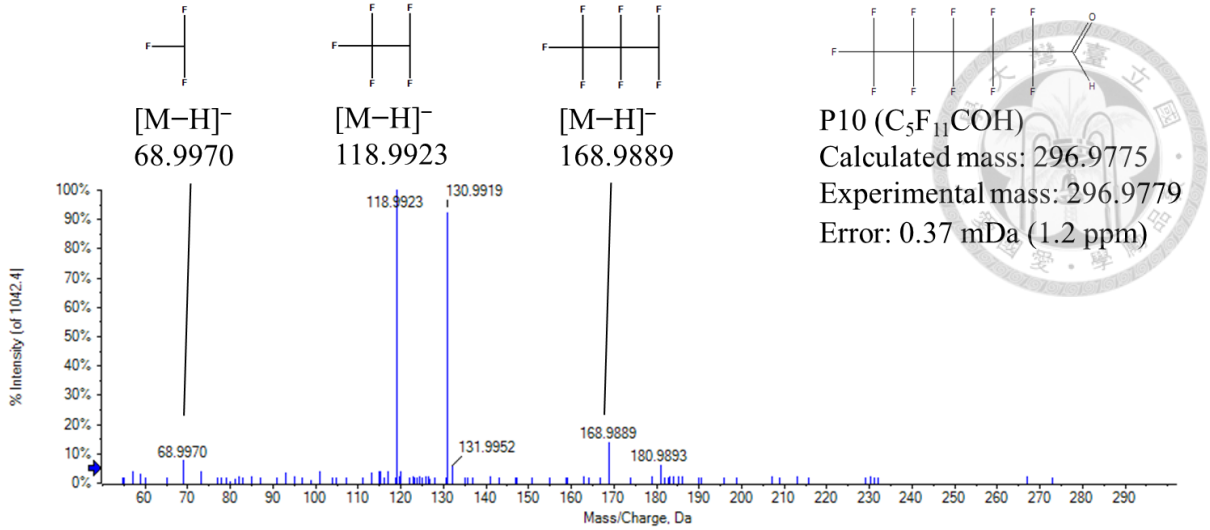

(k)

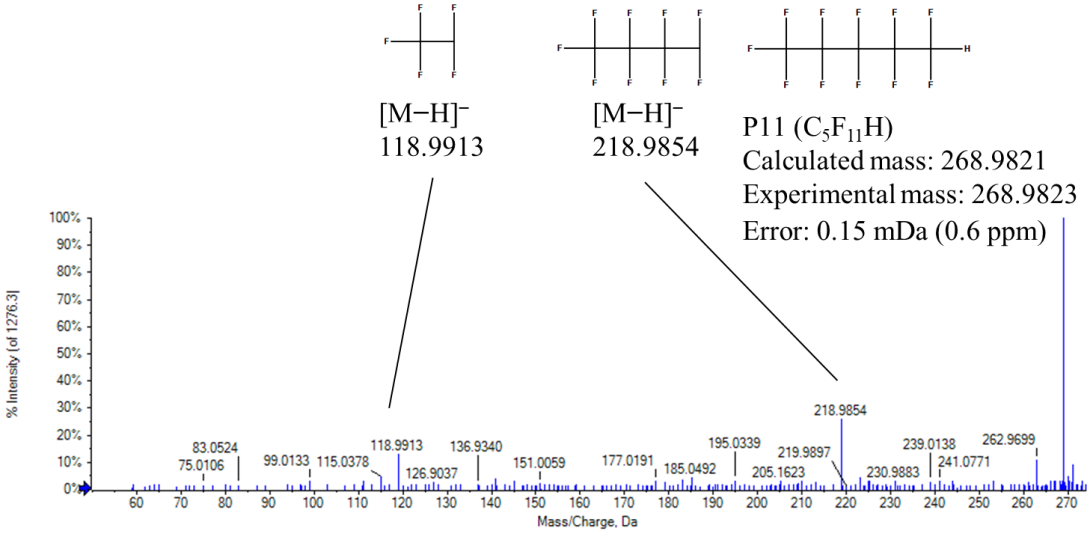

(l)

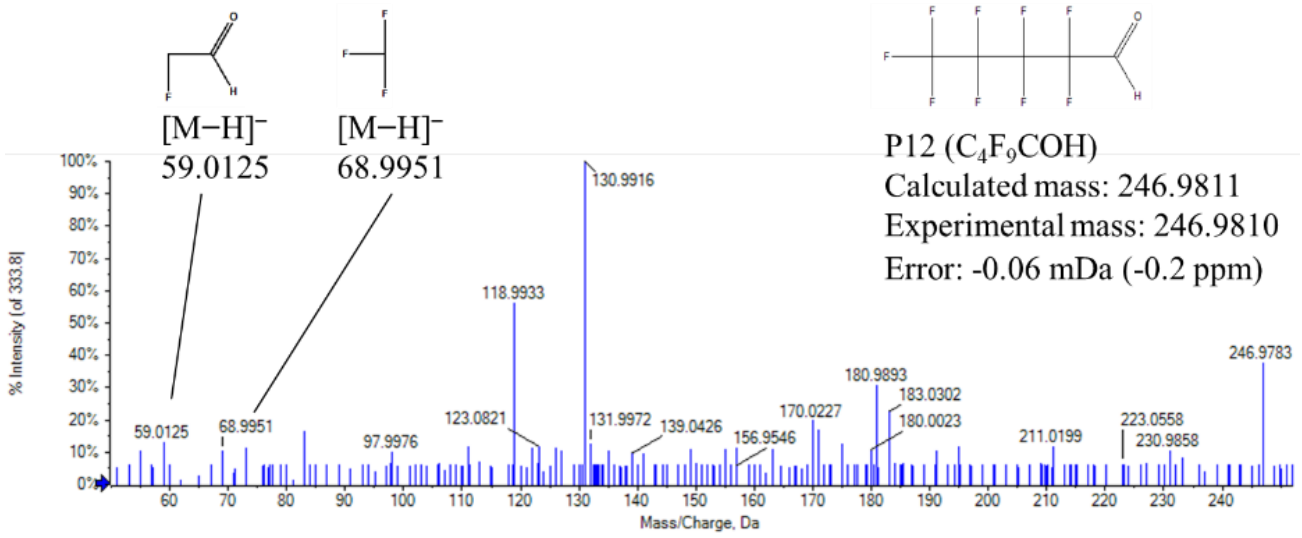

doi:10.6342/NTU202201196

(m)

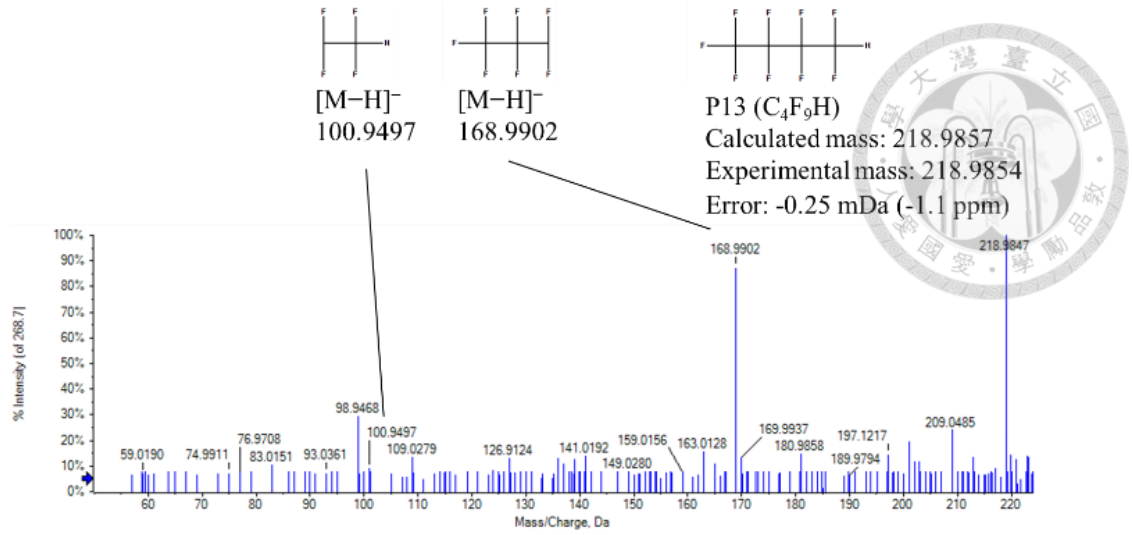

(n)

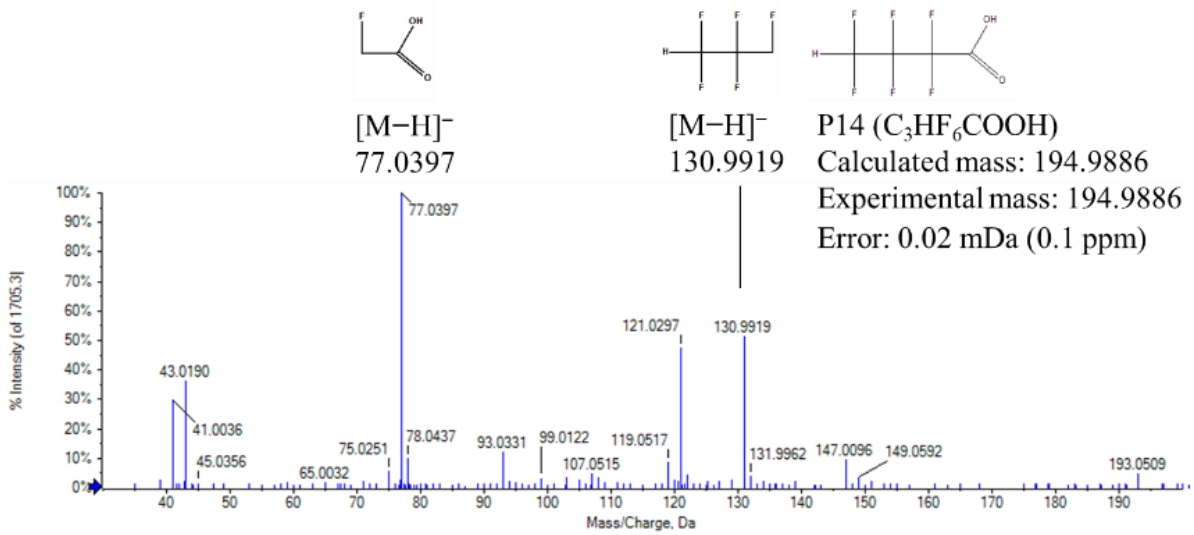

(o)

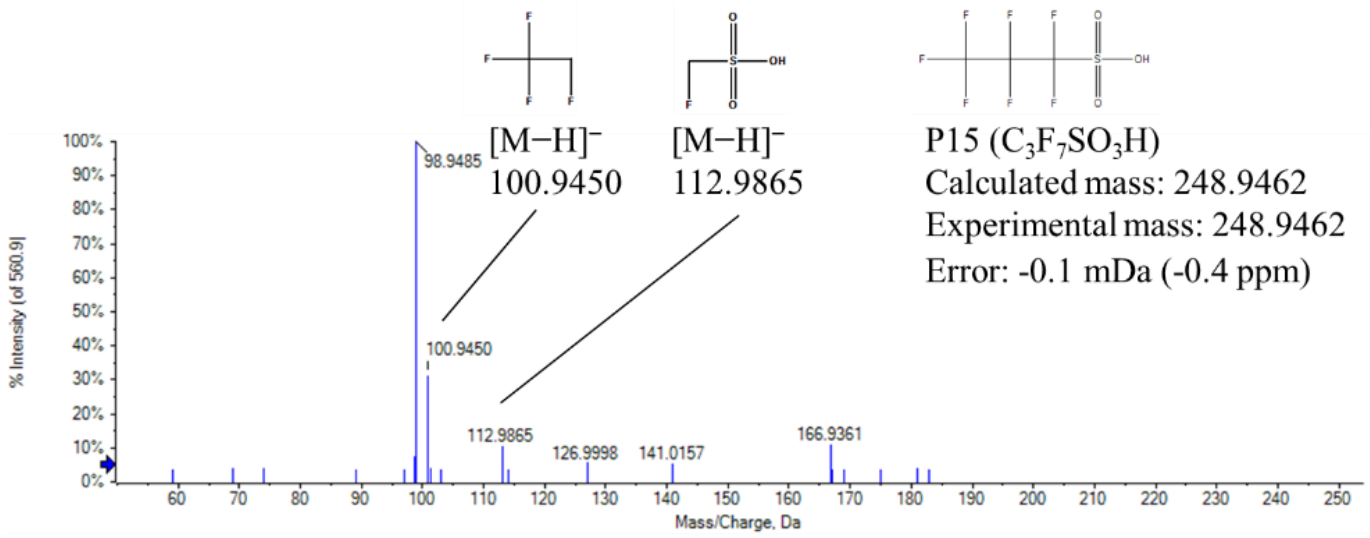

doi:10.6342/NTU202201196

(p)

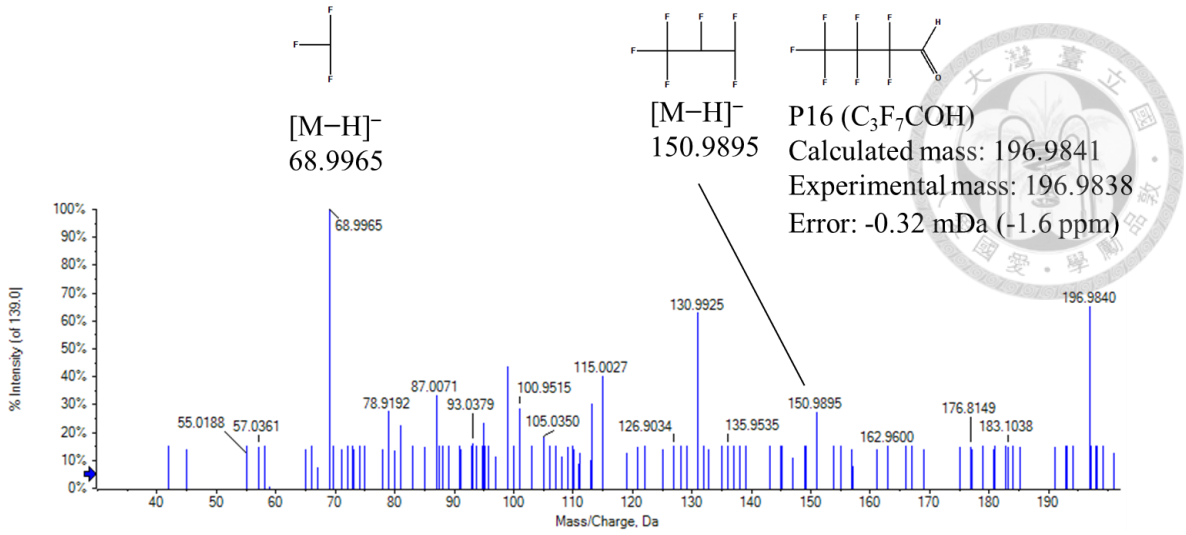

(q)

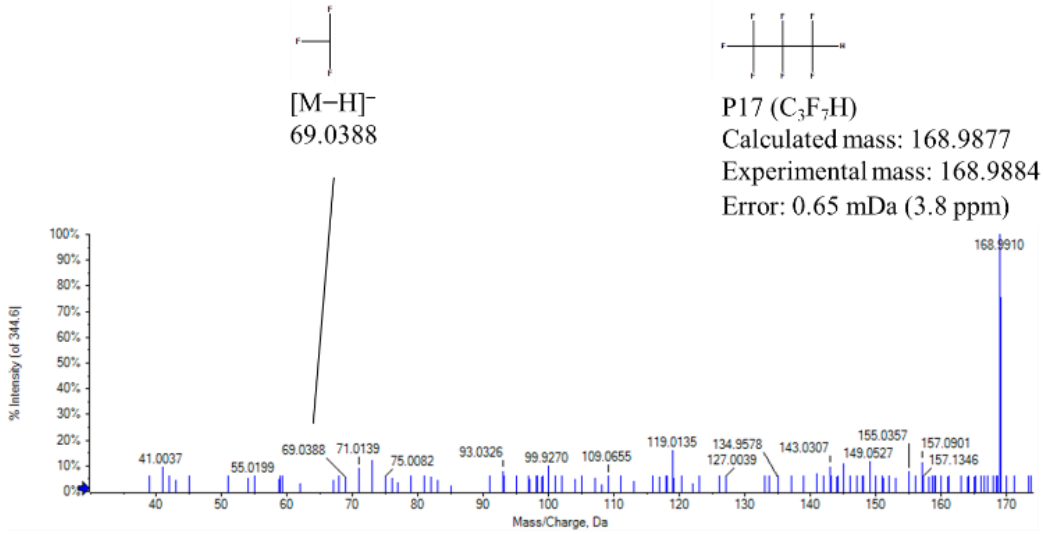

Figure 4-17. Mass spectra and structures of the product ions (a) P1, (b) P2, (c) P3, (d) P4, (e) P5, (f) P6, (g) P7, (h) P8, (i) P9, (j) P10, (k) P11, (l) P12, (m) P13, (n) P14, (o) P15, (p) P16 and (q) P17.

doi:10.6342/NTU202201196

Table 4-4. Accurate mass measurements obtained by UHPLC–QTOFMS for PFOS and the identified byproducts.

Compound	Formula	Mass [M-H]$^-$ (m/z)		Retention time	Mass error	
		Calculated	Experimental	(min)	(ppm)	mDa
Target compounds						
PFOS	$C_8F_{17}SO_3H$	498.9302	498.931	2.99	1.6	0.8
PFAAs byproducts (8 compounds)						
PFHxS	$C_6F_{13}SO_3H$	398.9366	398.9370	2.62	0.9	0.4
PFBS	$C_4F_9SO_3H$	298.9430	298.9430	2.44	0	0
PFOA	$C_7F_{15}COOH$	412.9664	412.9668	2.78	1	0.4
PFHpA	$C_6F_{13}COOH$	362.9696	362.9693	2.66	-0.8	-0.3
PFHxA	$C_5F_{11}COOH$	312.9728	312.9727	2.55	-0.4	-0.1
PFPeA	C_4F_9COOH	262.9760	262.9760	2.43	0.1	0
PFBA	C_3F_7COOH	212.9792	212.9790	2.35	-1.2	-0.2
PFPrA	C_2F_5COOH	162.9824	162.9823	2.07	-0.5	-0.1
PFOS byproducts (19 compounds)						
P1	$C_7F_{15}SO_3H$	448.9334	448.9324	1.37	-2.2	-0.99
P2	$C_7F_{15}COH$	396.9715	396.9714	1.57	-0.2	-0.08
P3	$C_7F_{13}H$	330.9798	330.9796	2.75	-0.7	-0.22
P4	$C_6H_7(OH)_3FCOOH$	193.0507	193.0505	2.21	-1.1	-0.22
P5	$C_6H_4F_9COOH$	291.0068	291.0066	1.61	-0.5	-0.16
P6	$C_6F_{13}COH$	346.9747	346.9750	2.75	0.8	0.28
P7	$C_6F_{13}H$	318.9796	318.9795	2.63	-0.2	-0.07
P8	$C_6F_{11}H$	280.9823	280.9827	2.52	1.5	0.42
P9	$C_5F_{11}SO_3H$	348.9398	348.9400	2.18	0.6	0.22
P10	$C_5F_{11}COH$	296.9775	296.9779	2.60	1.2	0.37
P11	$C_5F_{11}H$	268.9821	268.9823	2.51	0.6	0.15
P12	C_4F_9COH	246.9811	246.9810	2.51	-0.2	-0.06
P13	C_4F_9H	218.9857	218.9854	2.45	-1.1	-0.25
P14	C_3HF_6COOH	194.9886	194.9886	2.08	0.1	0.02
P15	$C_3F_7SO_3H$	248.9462	248.9461	1.85	-0.4	-0.1
P16	C_3F_7COH	196.9841	196.9838	2.41	-1.6	-0.32
P17	C_3F_7H	168.9877	168.9884	2.28	3.8	0.65

doi:10.6342/NTU202201196

Based on the identified byproduct information in this work and other relevant studies on PFOS degradation (Duan et al., 2020; Shi et al., 2019), the mechanism and pathways of PFOS transformation in the PEC system were proposed, as shown in **Figure 4- 18.** Initially, PFOS is transformed to PFOS radicals through direct electron transfer on the surface of the GOTiO_2 photoelectrode (**Equation (4-16)**). Then, this radical is desulfonated to form •C_8F_{17} and sulfur trioxide (SO_3) (**Equation (4-17)**). After desulfonation, •C_8F_{17} reacts with •OH to generate the unstable alcohol $C_8F_{17}OH$ (**Equation (4-18)**); $C_8F_{17}OH$ rapidly decomposed into $C_7F_{15}COF$ with F^- release (**Equations (4-18)** and **(4-19)**). Subsequently, $C_7F_{15}COF$ underwent a hydrolysis reaction and generated $C_7F_{15}COO^-$ (PFOA, C8) and $C_7F_{15}C(O)^-$ with the release of another F^- (**Equation (4-20)**). Through electron transfer and subsequent decarboxylation or decarbonylation, PFOA and $C_7F_{15}C(O)^-$ were further converted to •C_7F_{15} (**Equations (4-21)** and **(4-22)**). •C_7F_{15} and other shorter-chain-length •C_nF2_{n+1} (n= 3–6) underwent further reactions and transformed into $C_7F_{13}H$ and other HFCs (**Equation (4-23)**). On the other hand, •C_7F_{15} also reacted with •SO_3^- (generated from the electron transfer reaction of SO_3) and formed $C_7F_{15}SO_3^-$ (PFSAs, C7) (**Equations (4-24)** and **(4-25)**). Stepwise, PFOS was gradually decomposed into short-chain PFAAs and finally mineralized into CO_2, SO_4^{2-} and F^-. On the other hand, PFOS also underwent defluorination and hydroxylation pathways, of which P5 and P14 were the defluorinated byproducts, while

doi:10.6342/NTU202201196

P4 was the hydroxylated byproduct. Additionally, regarding the transformation trend of the hydroxylated byproduct (P4), we observed that most of its concentrations continuously increased or reached a plateau (**Figure 4-16**), implying that it was recalcitrant and generated at the later stage of PFOS transformation. In summary, the complete PFOS degradation pathways include (a) desulfonation, (b) oxidation followed by defluorination, (c) decarboxylation, (d) decarbonylation, (e) sulfonation, (f) defluorination and (g) hydroxylation. The transformation byproducts include PFCAs ($C_nF_{2n+1}C(O)OH$, n= 2−7), PFSAs ($C_mF_{2m+1}SO_3H$, m= 3−7), PFALs ($C_pF_{2p+1}C(O)H$, p= 3−6), HFCs ($C_qF_{2q+1}H$, q= 3−7) and others (P3−5, P8 and P14). However, given that the authentic standards of some of the byproducts (e.g., PFALs and HFCs) were not acquired in this work, the production yields among all types of byproducts as well as the contribution of each transformation pathway could not be comprehensively elucidated/compared; further investigation is required.

$$C_8F_{17}SO_3^- \rightarrow \bullet C_8F_{17}SO_3 + e^- \quad (4\text{-}16)$$

$$\bullet C_8F_{17}SO_3 \rightarrow \bullet C_8F_{17} + SO_3 \quad (4\text{-}17)$$

$$\bullet C_8F_{17} + \bullet OH \rightarrow C_8F_{17}OH \quad (4\text{-}18)$$

$$C_8F_{17}OH \rightarrow C_7F_{15}COF + H^+ + F^- \quad (4\text{-}19)$$

$$C_7F_{15}COF + H_2O \rightarrow C7F_{15}COO^-/\ C_7F_{15}C(O)^- + 2H^+ + F^- \quad (4\text{-}20)$$

$$C_7F_{15}COO^- / C_7F_{15}C(O)^- \rightarrow \bullet C_7F_{15}COO / \bullet C_7F_{15}C(O) + e^- \quad (4\text{-}21)$$

doi:10.6342/NTU202201196

$$\bullet C_7F_{15}COO / \bullet C_7F_{15}C(O) \rightarrow \bullet C_7F_{15} + CO_2 / CO \quad (4\text{-}22)$$

$$\bullet C_7F_{15} + 3e^- \rightarrow C_7F_{13}^- + 2F^- \quad (4\text{-}23)$$

$$SO_3 + e^- \rightarrow \bullet SO_3^- \quad (4\text{-}24)$$

$$\bullet C_7F_{15} + \bullet SO_3^- \rightarrow C_7F_{15}SO_3^- \quad (4\text{-}25)$$

doi:10.6342/NTU202201196

Comparison of the PFOS degradation mechanisms between EC and PEC processes

The transformation byproduct generation in the EC system was also elucidated (as shown in **Figure 4-19**) to facilitate better understanding the photo-electro synergistic mechanism. Comparing the results in **Figure 4-16 (a)** and **Figure 4-19**, despite the similarity of the types of transformation byproducts observed between the EC and PEC systems, their transformation trends were distinctly different. During the PEC process, the byproducts were continuously generated and further degraded over time, while most of the byproducts in the EC system were slowly and continuously formed. The detected trends of the parent compound PFOS as well as the associated byproducts in the two systems revealed that not only a faster PFOS degradation rate but also a rapid byproduct evolution profile occurred in the PEC process. This suggested that the applied UV radiation can synergistically benefit the associated PEC reactions, likely decreasing electron-hole recombination and subsequently promoting the electron transfer reaction and reactive species production (Peng et al., 2017; Zhao and Zhu, 2006), thus leading to faster PFOS decomposition and byproduct evolution/degradation. However, further elucidation of the detailed synergistic mechanism is still needed.

doi:10.6342/NTU202201196

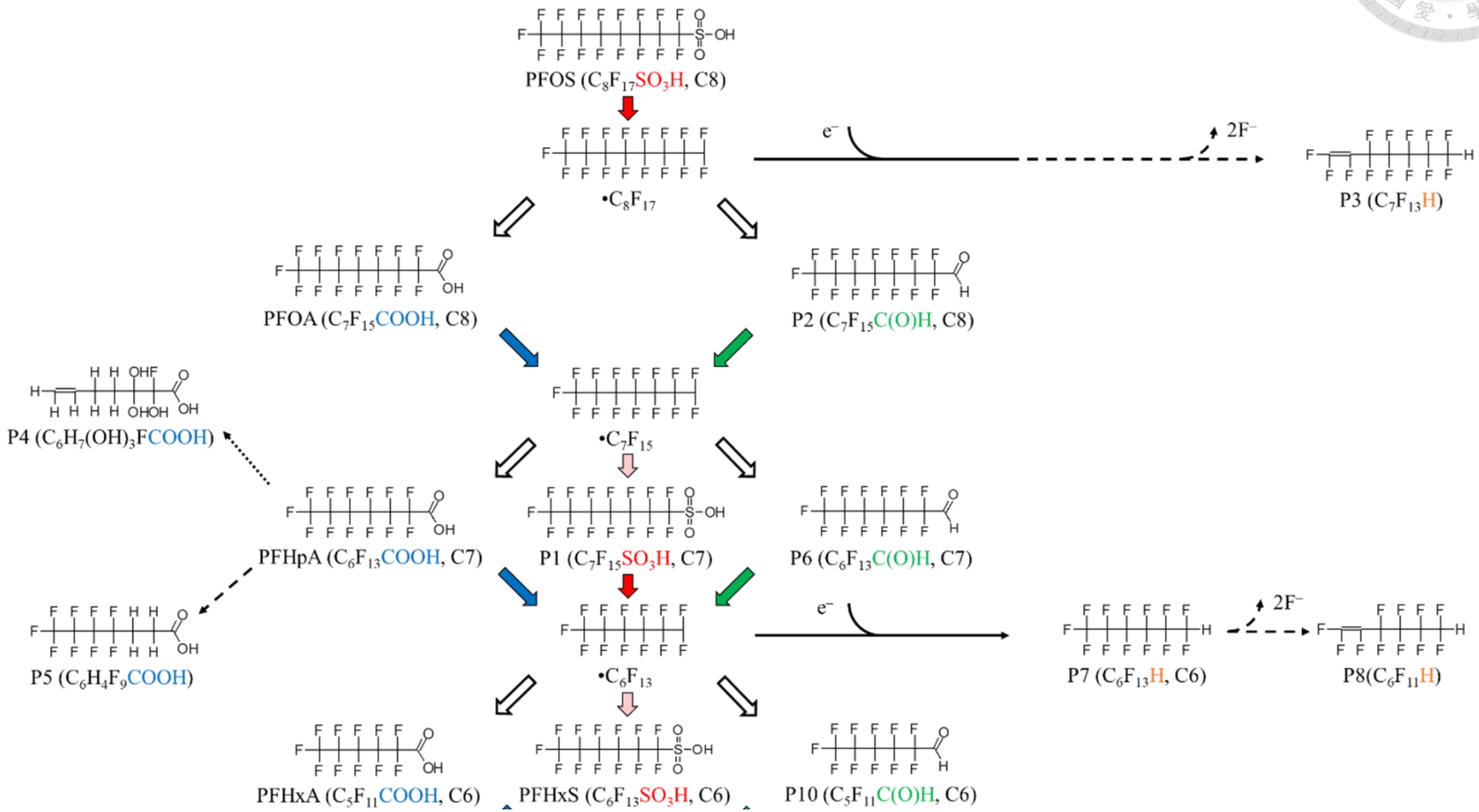

doi:10.6342/NTU202201196

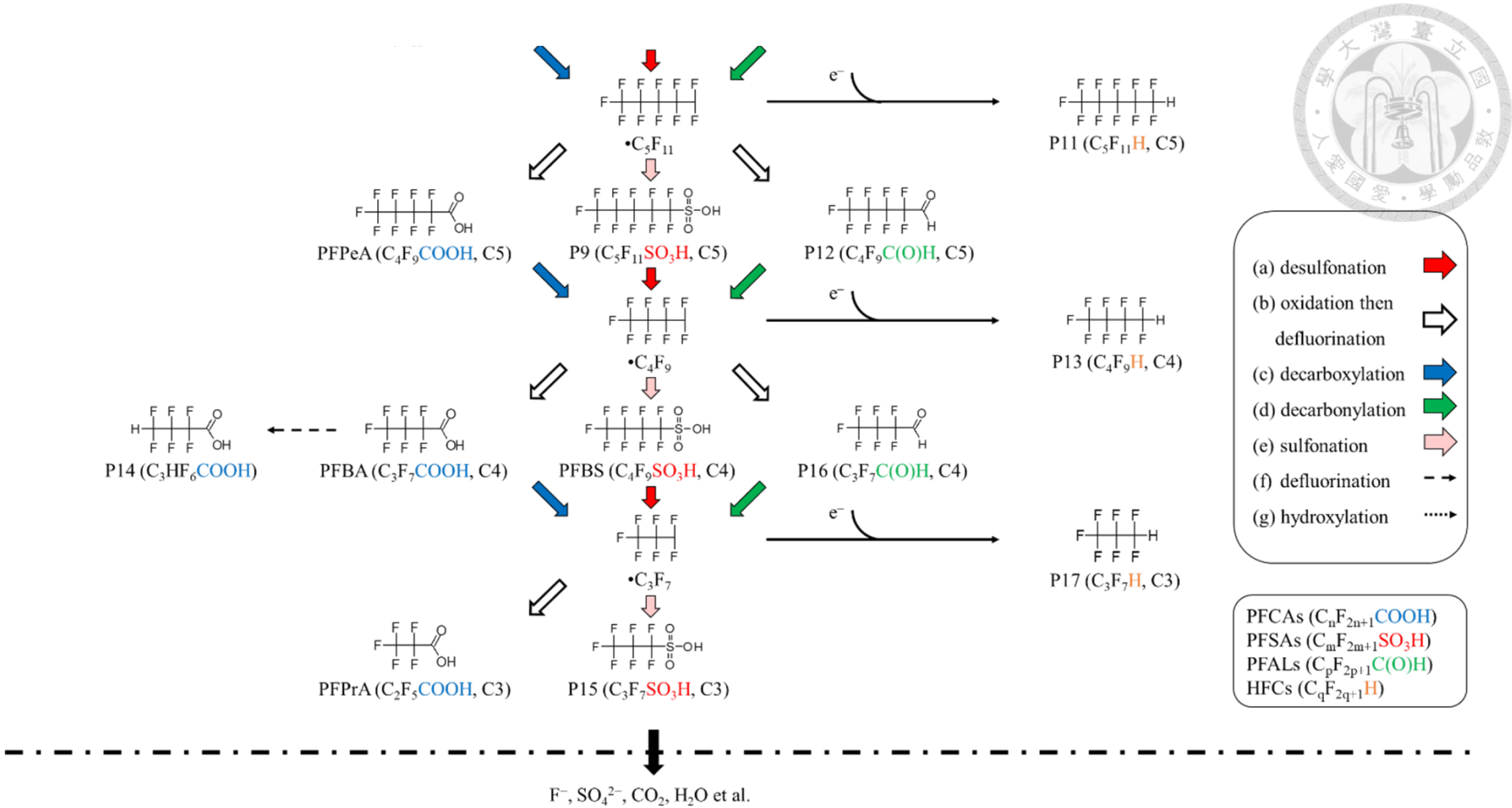

Figure 4- 18. Proposed degradation pathway of PFOS in the PEC system.

doi:10.6342/NTU202201196

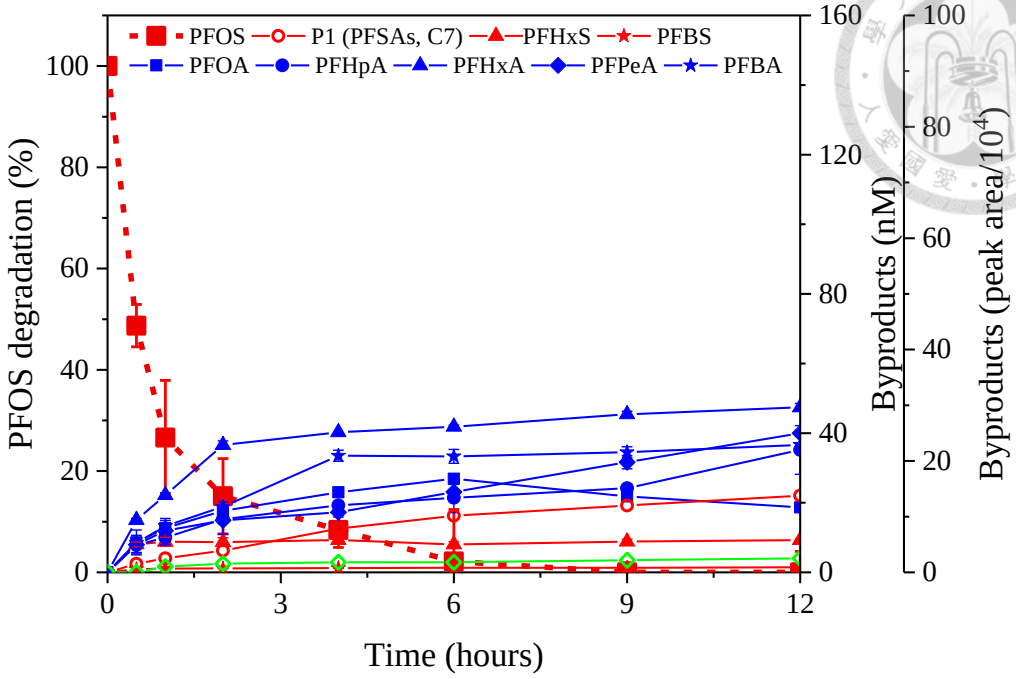

Figure 4-19. Formation of the transformation byproducts of PFOS degradation in the EC system. The dotted lines represent the degradation of target pollutants and correspond to the left y-axis, and the solid lines with solid symbols and the open symbols represent the byproduct evolution, corresponding to the byproducts (nM and peak area/10^4) on the right y-axis, respectively ($[PFOS]_0$ = 40 μM, $[NaClO_4]$ = 50 mM, initial solution pH = 5.64, current density = 30 mA cm^{-2}).

doi:10.6342/NTU202201196

PFOA transformation byproducts and pathways of the PEC process using chloride anion electrolyte

Equations (4-9)−(4-15) imply that the mechanism of PFOA decomposition in the PEC and EC processes varies. Based on the observed byproducts (discussed in the following paragraphs), the degradation pathways are proposed for PFOA. In the present study, the transformation byproducts and pathways of the PEC process using Cl^- as an electrolyte was also provided (using PFOA as the model compound). A total of 18 byproducts were observed during PFOA degradation; five of the byproducts (short-chain C7−C3 PFAAs) were confirmed by standard authentication, and the other 13 byproducts (P6, P10, P16 and P18−P27) were identified by UHPLC–QTOFMS and semiquantified with the calibration curves of the target compounds PFOA. Byproduct information is provided in **Table 4-5**, and their mass spectra are shown in **Figure 4-21**. **Figure 4-20** shows the major byproducts generated during PFOA degradation in the PEC and EC systems with the $GOTiO_2$ electrode. Based on these byproducts, four PFOA degradation pathways are proposed in **Figure 4-22**: (a) decarboxylation followed by oxidation, (b) defluorination, (c) hydroxylation and (d) Cl atom substitution.

doi:10.6342/NTU202201196

(a)

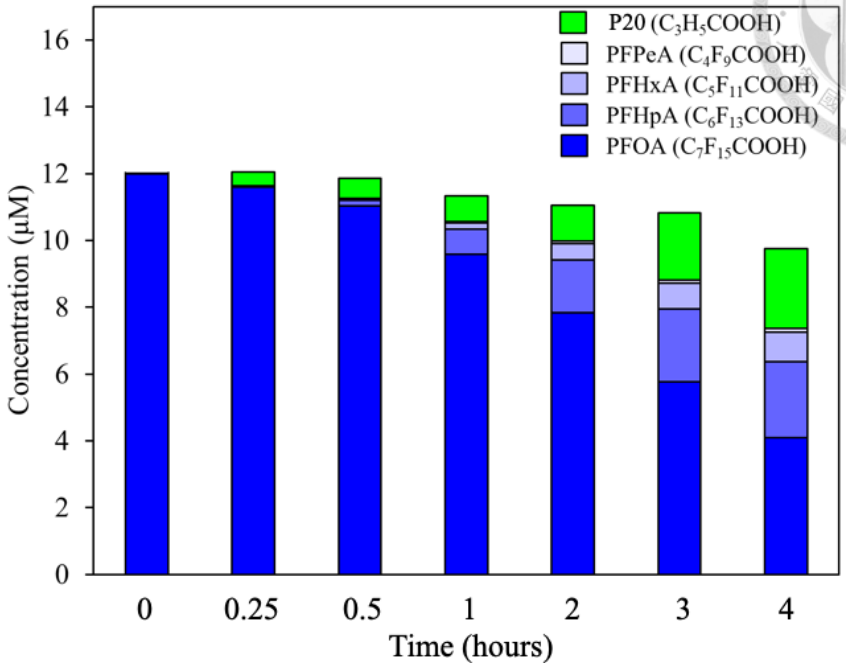

(b)

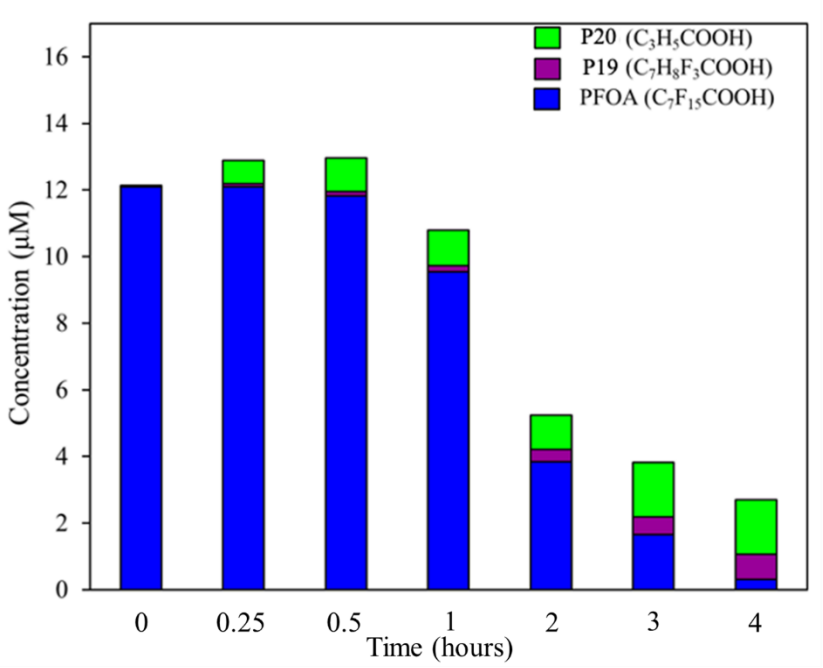

Figure 4-20. Major byproducts generated during PFOA degradation in (a) the PEC system and (b) the EC system with the GOTiO_2 electrode ($[PFOA]_0$ = 12 μM, [NaCl] = 50 mM, initial solution pH = 5.3).

doi:10.6342/NTU202201196

(a)

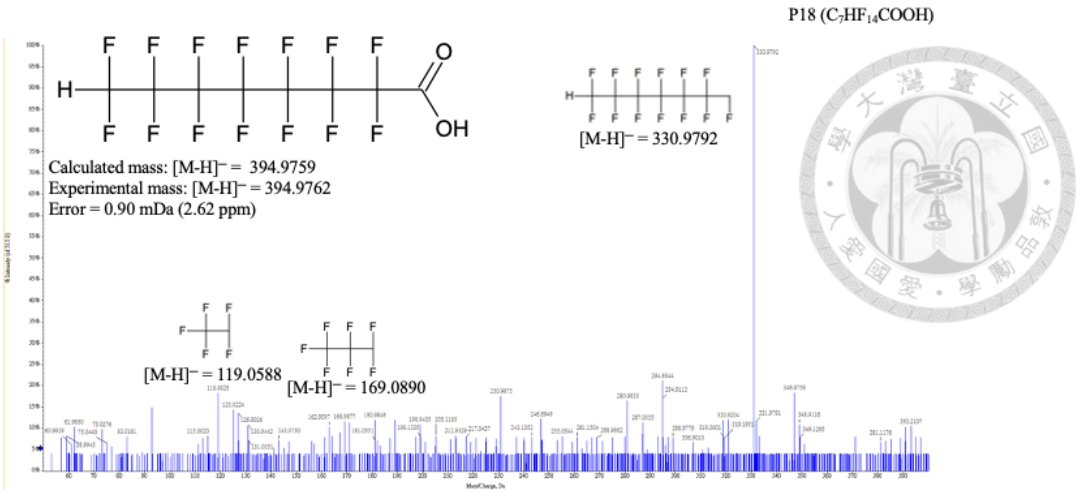

(b)

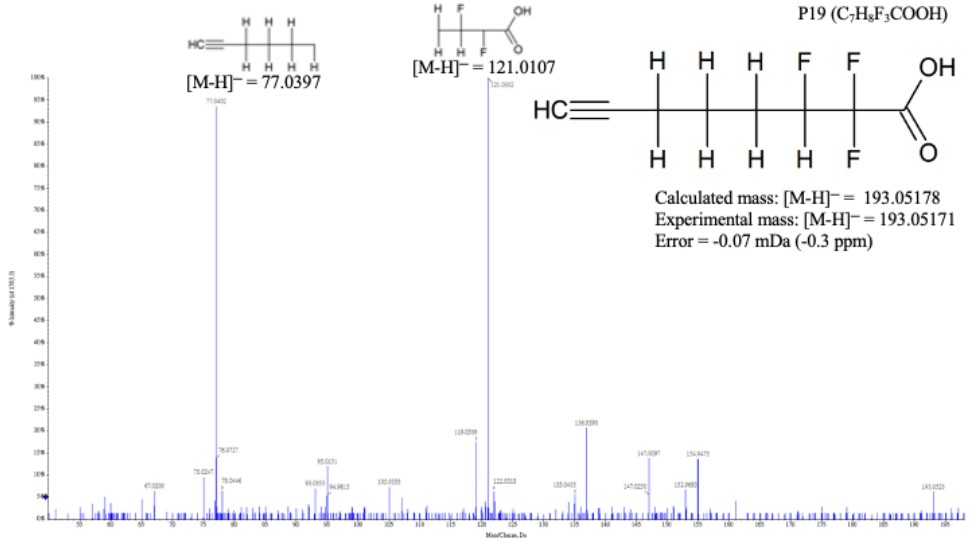

(c)

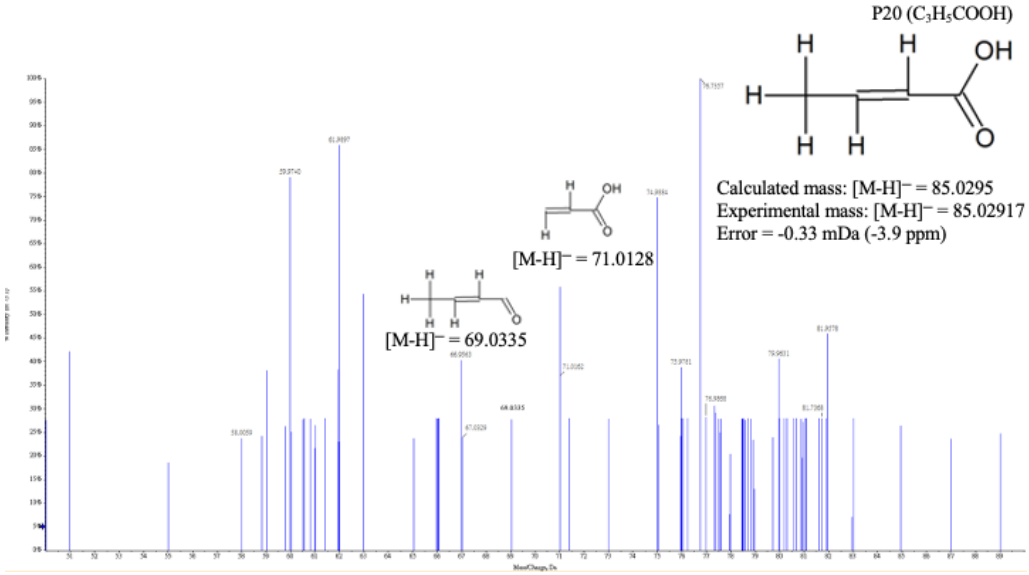

doi:10.6342/NTU202201196

(d)

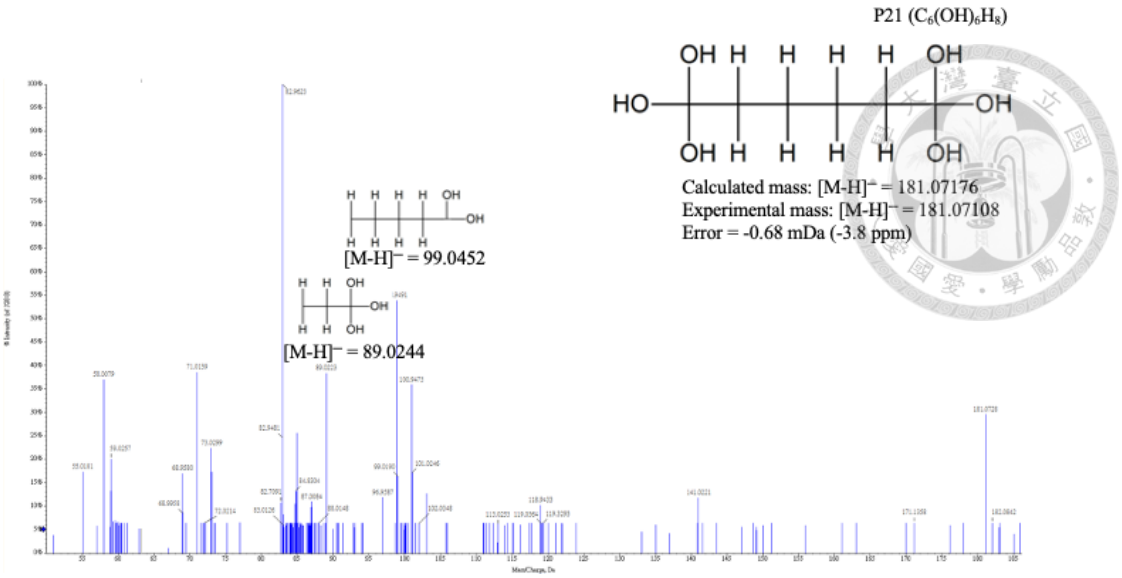

(e)

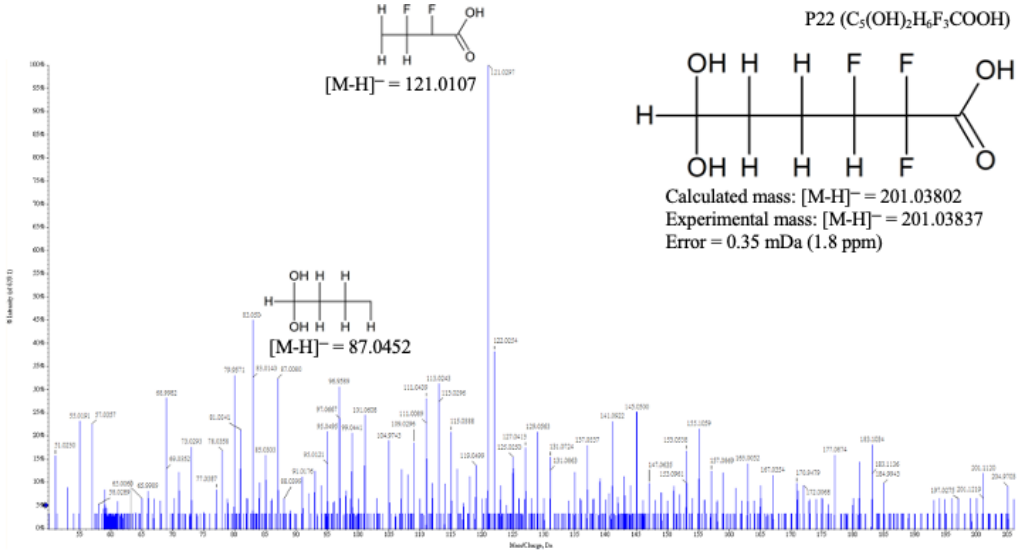

(f)

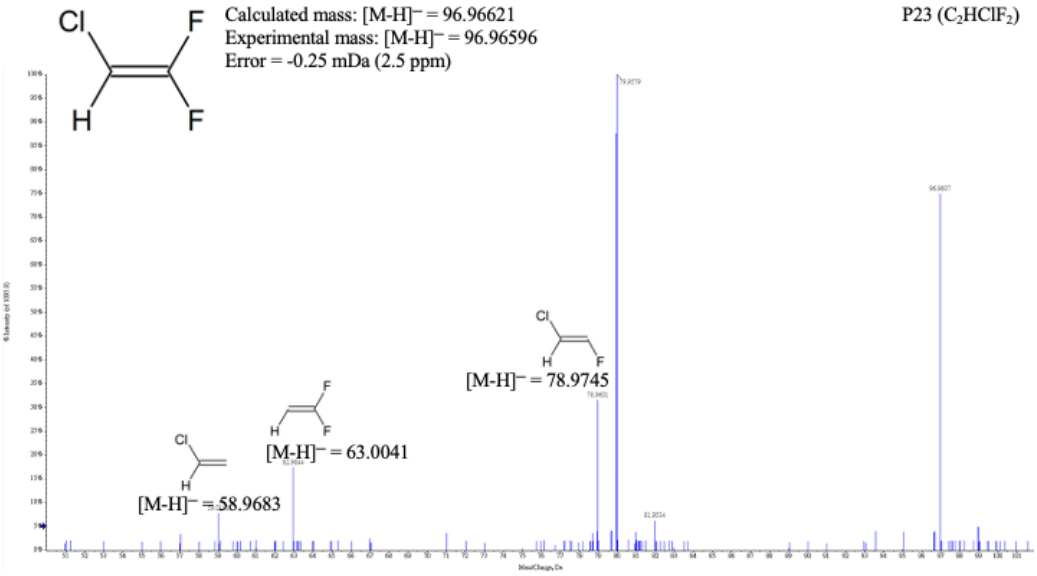

doi:10.6342/NTU202201196

(g)

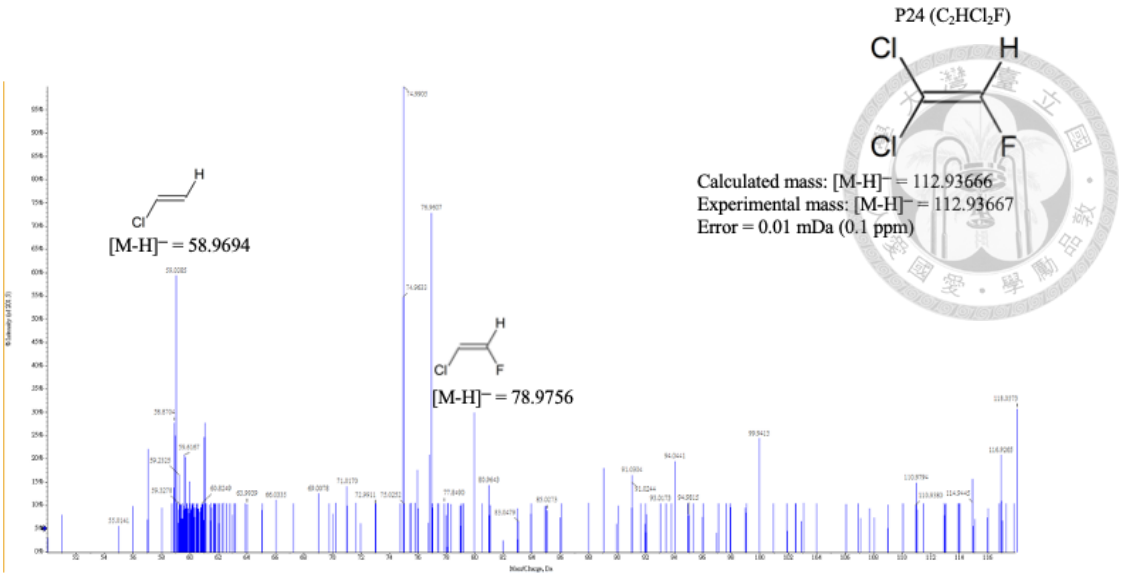

(h)

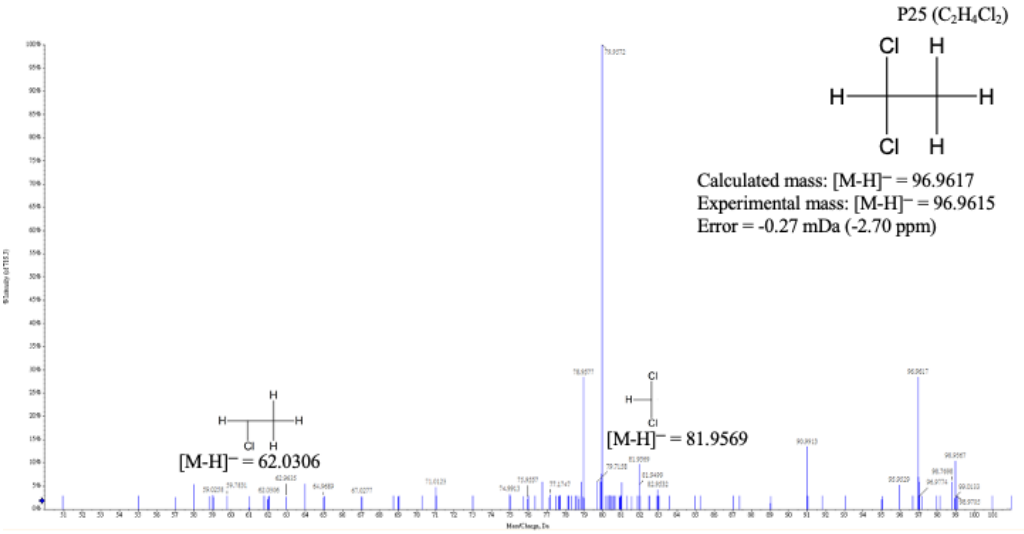

(i)

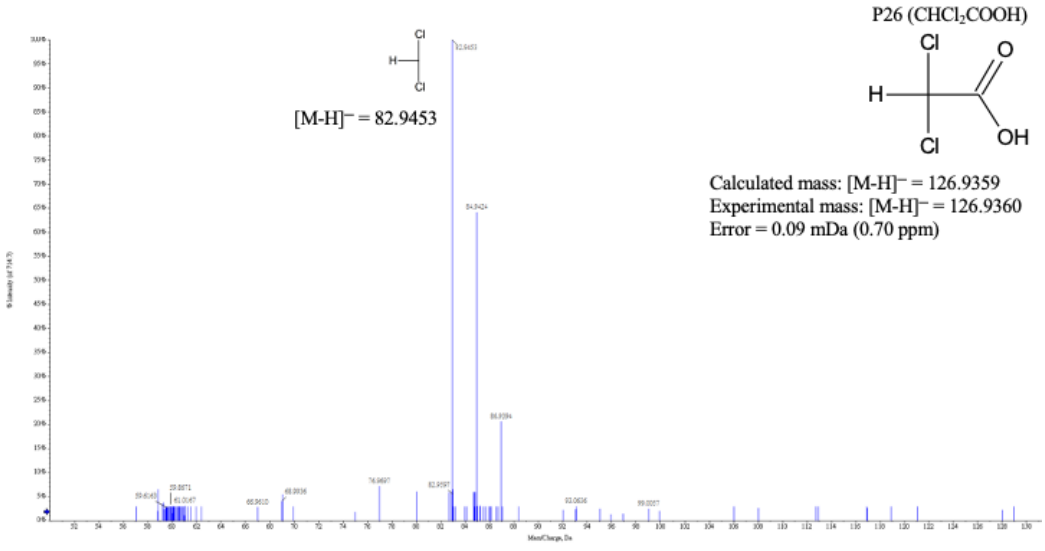

doi:10.6342/NTU202201196

(j)

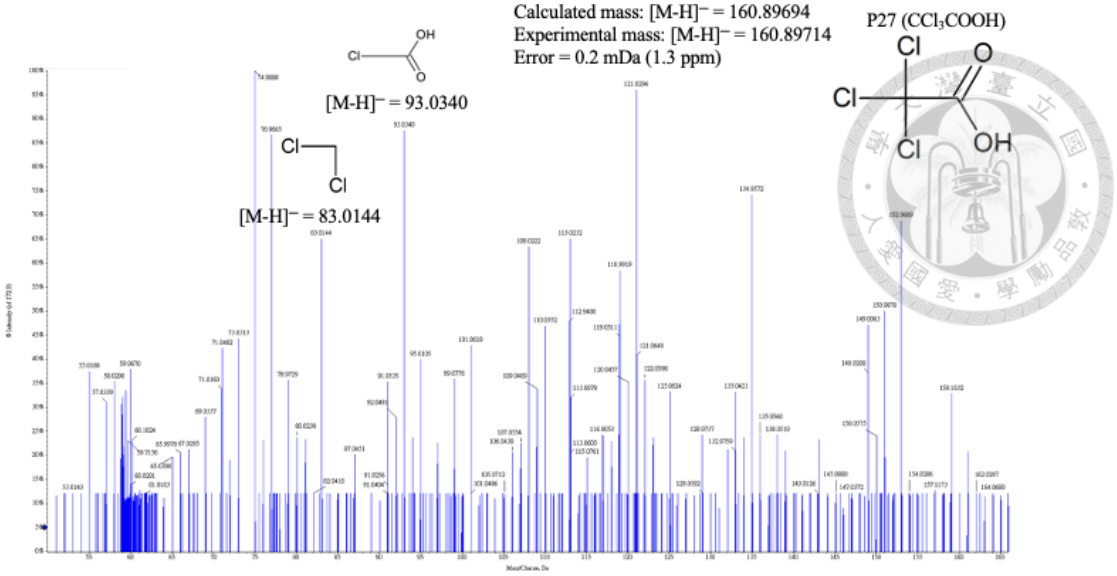

(k)

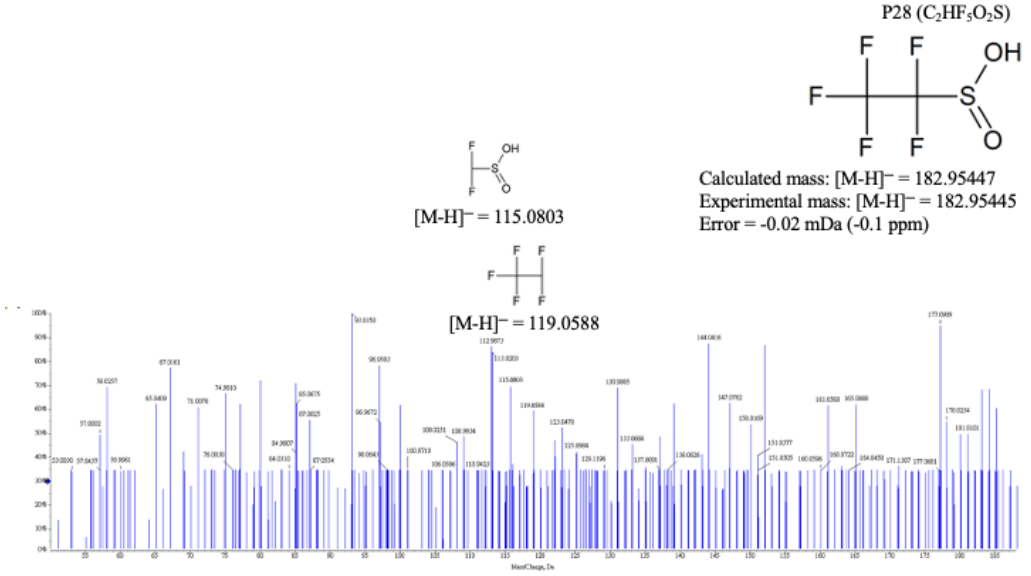

(l)

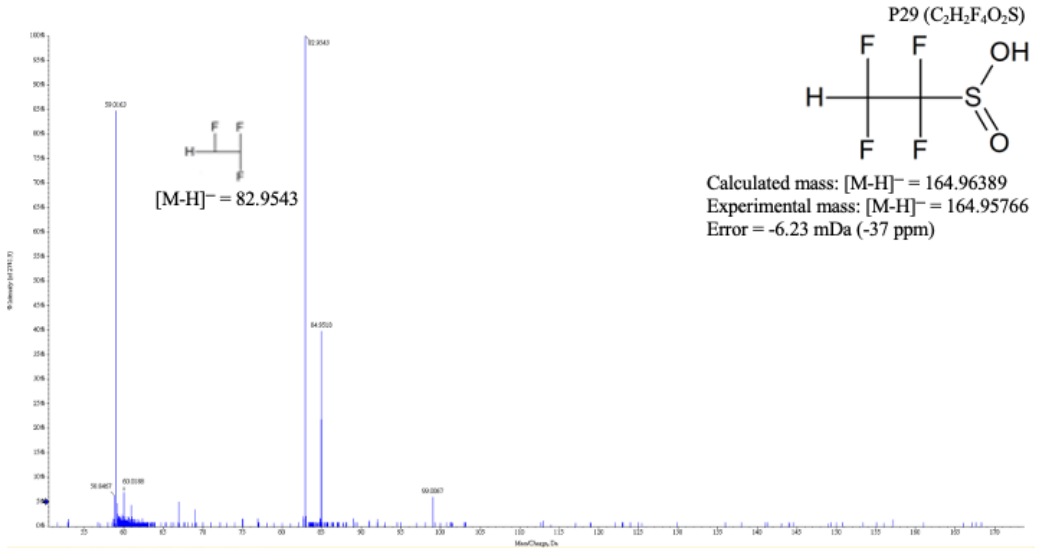

doi:10.6342/NTU202201196

(m)

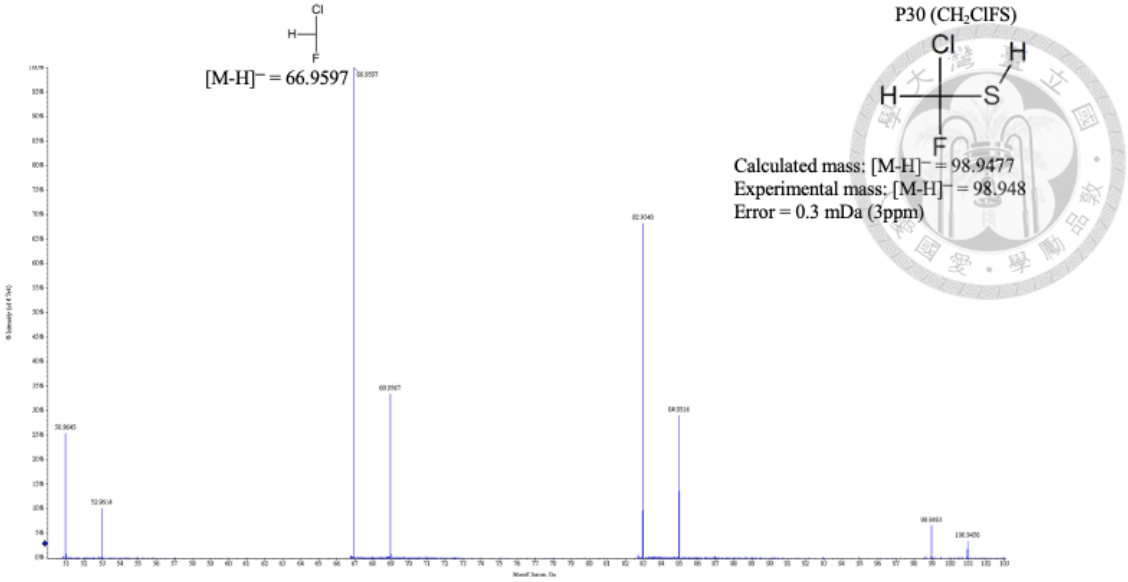

Figure 4-21. Mass spectra and structures of the product ions (a) P18, (b) P19, (c) P20, (d) P21, (e) P22, (f) P23, (g) P24, (h) P25, (i) P26, (j) P27, (k) P28, (l) P29 and (m) P30 in the PEC and EC systems using chloride anion as electrolyte.

doi:10.6342/NTU202201196

Table 4-5. Accurate mass measurements obtained by UHPLC–QTOFMS for PFOA, PFOS and the identified byproducts.

Compound	Formula	Mass [M-H]$^-$ (m/z)		Retention time (min)	Mass error		DBE
		Calculated	Experimental		(ppm)	mDa	
Target compounds							
PFOA	$C_7F_{15}COOH$	412.9664	412.9648	3.01	-3.90	-1.60	1
PFOS	$C_8F_{17}SO_3H$	498.9302	498.9310	2.99	1.60	0.78	0
PFOA byproducts (18 compounds)							
PFHpA	$C_6F_{13}COOH$	362.9696	362.9691	2.78	-1.30	-0.48	1
PFHxA	$C_5F_{11}COOH$	312.9728	312.9717	2.67	-3.50	-1.11	1
PFPeA	C_4F_9COOH	262.9760	262.9757	2.58	-1.20	-0.32	1
PFBA	C_3F_7COOH	212.9792	212.9792	2.50	-0.10	-0.03	1
PFPrA	C_2F_5COOH	162.9824	162.9824	2.38	0.10	0.03	1
P6	$C_6F_{13}COH$	346.9747	346.9739	3.07	-2.40	-0.85	1
P10	$C_5F_{11}COH$	296.9779	296.9777	2.81	-0.50	-0.16	1
P16	C_3F_7COH	196.9843	196.9845	2.62	0.90	0.18	1
P18	$C_7HF_{14}COOH$	394.9759	394.9762	3.02	0.90	0.34	1
P19	$C_7H_8F_3COOH$	193.0518	193.0517	2.40	-0.30	-0.07	3
P20	C_3H_5COOH	85.0295	85.0292	6.58	-3.90	-0.33	2
P21	$C_6(OH)_6H_8$	181.0718	181.0711	1.67	-3.80	-0.68	0
P22	$C_5(OH)_2H_6F_3COOH$	201.0380	201.0384	2.36	1.80	0.35	1
P23	C_2HClF_2	96.9662	96.9660	7.45	-2.50	-0.25	1
P24	C_2HCl_2F	112.9367	112.9367	2.55	0.10	0.01	1
P25	$C_2H_4Cl_2$	96.9617	96.9615	7.45	-2.70	-0.27	0
P26	$CHCl_2COOH$	126.9359	126.9360	1.76	0.70	0.09	1
P27	CCl_3COOH	160.8969	160.8971	2.40	1.30	0.20	1
PFOS byproducts (including the following 4 byproducts, PFOA and 18 PFOA byproducts)							
P1	$C_7F_{15}SO_3H$	448.9334	448.9333	2.74	-0.20	-0.08	0
P28	$C_2HF_5O_2S$	182.9545	182.9545	2.73	-0.10	-0.02	0
P29	$C_2H_2F_4O_2S$	164.9639	164.9577	1.46	-37.70	-6.23	0
P30	CH_2ClFS	98.9477	98.9480	1.43	3.00	0.30	0

doi:10.6342/NTU202201196

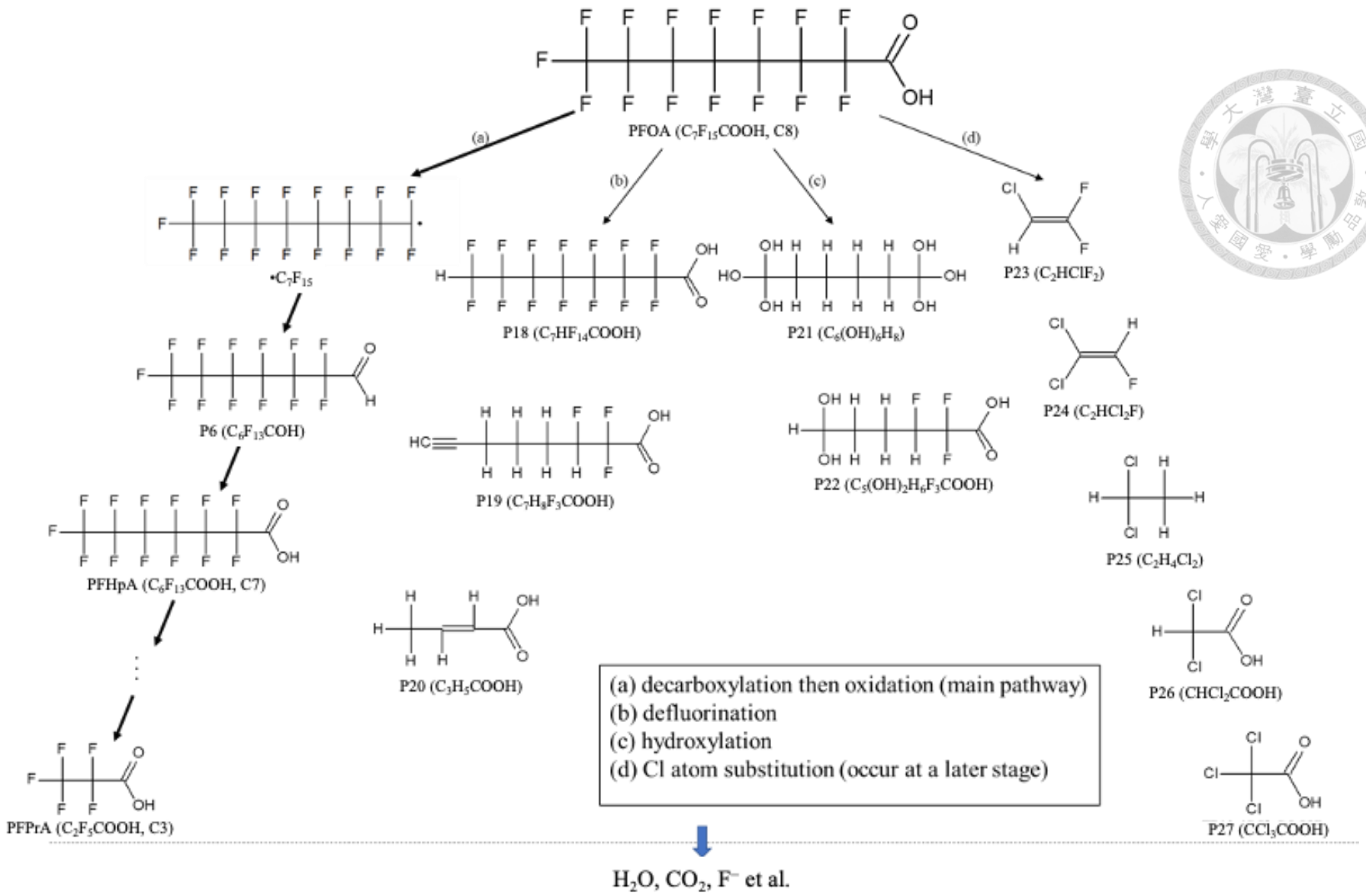

Figure 4-22. Proposed degradation pathways of PFOA in the PEC and EC systems.

doi:10.6342/NTU202201196

Pathway (a) (**Figure 4-22**), decarboxylation followed by oxidation, seems to be the main degradation pathway of PFOA in the PEC system. The production yield of the corresponding byproducts (PFHpA, PFHxA, PFPeA) was 45.7 % with a 4-hour reaction time (**Figure 4-20 (a)**). **Figure 4-23** shows that PFOA exhibited stepwise decomposition via release of $-CF_2$ groups and transformation into short-chain PFAAs (Li et al., 2017; Peng et al., 2017); the concentrations of the PFAA byproducts increased with increasing reaction time in the PEC system, and the order of their concentrations was PFHpA (C7) >PFHxA (C6) >PFPeA (C5) > PFBA (C4) > PFPrA (C3). Based on the above PFAA byproduct composition and other studies investigating PFOA decomposition (Lin et al., 2012; Ma et al., 2015; Niu et al., 2012; Peng et al., 2017; Zhuo et al., 2011), the degradation mechanism of PFOA is proposed: PFOA is converted to PFOA radical through a direct electron transfer from the carboxyl group to the TiO_2 anode (**Equation (4-26)**). Then, this radical is decarboxylated to form $\bullet C_7F_{15}$; this bond cleavage reaction is followed Kolbe decarboxylation (**Equation (4-27)**). After decarboxylation, $\bullet C_7F_{15}$ could react with •OH to generate $C_7F_{15}OH$ (**Equation (4-28)**), which is a thermally unstable alcohol that can rapidly decompose into $C_6F_{13}COF$ while releasing F^- (**Equation (4-29)**). Next, $C_6F_{13}OF$ undergoes hydrolysis and subsequently generates $C_6F_{13}COOH$ (i.e., PFHpA) with another F^- release (**Equation (4-30)**).

doi:10.6342/NTU202201196

$$C_7F_{15}COO^- \rightarrow \bullet C_7F_{15}COO + e^- \quad (4\text{-}26)$$

$$\bullet C_7F_{15}COO \rightarrow \bullet C_7F_{15} + CO_2 \quad (4\text{-}27)$$

$$\bullet C_7F_{15} + \bullet OH \rightarrow C_7F_{15}OH \quad (4\text{-}28)$$

$$C_7F_{15}OH \rightarrow C_6F_{13}COF + H^+ + F^- \quad (4\text{-}29)$$

$$C_6F_{13}COF + H_2O \rightarrow C_6F_{13}COO^- + 2H^+ + F^- \quad (4\text{-}30)$$

Compared with the PEC system, no short-chain PFAA (C7−C3) byproducts were observed in the EC system (**Figure 4-20 (b)**). The significant difference in the main byproducts generated in the PEC and EC systems is possibly due to the different reactive species dominating the reaction; this also leads to different degradation rates of PFOA in the two systems. In the PEC system, the existing HOCl in the solution would be activated by irradiation, generating •OH and •Cl in the PEC system (**Equations (4-14)**−**(4-15)**); however, these different species could react with/scavenge each other. Based on **Equations (4-9)**−**(4-15)**, in the PEC and EC systems, •OH is possibly one of the dominant species; HOCl may also be an important species among all the reactive chlorine species. Thus, •OH and HOCl were detected in these two systems accordingly.

Other PFOA degradation pathways are as follows. PFOA underwent defluorination to generate P18−20, of which P20 had a high production yield (12.2 % after 4 hours of reaction) (**Figure 4-20**). Hydroxylation of PFOA resulted in the generation of P21 and

doi:10.6342/NTU202201196

P22, as shown in **Figure 4-22**. Furthermore, PFOA underwent Cl atom substitution and generated several chlorinated byproducts (P23−27); this result confirmed that RCS were also involved in PFOA degradation. We also observed that all the detected chlorinated byproducts (P23−27) had smaller molecular structures (containing only two carbons) than the other byproducts, implying that P23−27 were generated in the later steps of PFOA degradation and transformation. In summary, it is possible that PFOA mainly undergoes direct electron transfer initially, followed by reactions that generate shorter-chain products, and is further attacked by RCS in the later stage of degradation; however, further studies are needed for elucidation.

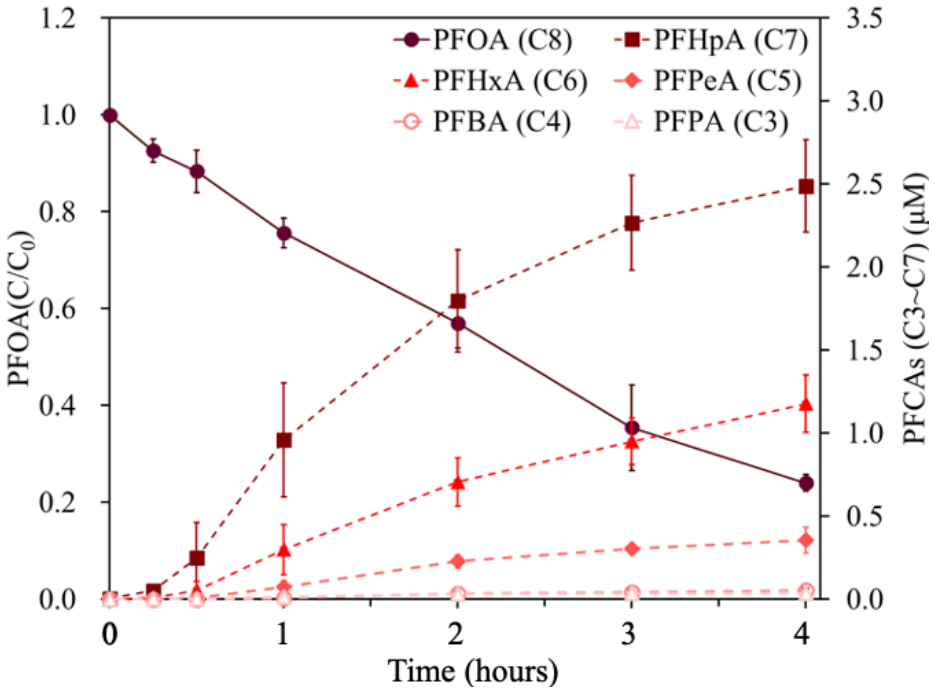

Figure 4-23. Byproducts generated during the PEC degradation of PFOA with the GOTiO$_2$ electrode ([PFOA]$_0$ = 12 μM, [NaCl] = 50 mM, initial solution pH = 5.3).

doi:10.6342/NTU202201196

A comparison of the PFOA degradation pathway in the PEC and EC systems with the $GOTiO_2$ and TiO_2 electrodes is illustrated in **Figure 4-20** and **Figure 4-24**. The principal byproducts were PFHpA, PFHxA, and PFPeA. P20 was detected with only the $GOTiO_2$ electrode, while P19, P23 and P27 were detected with only the TiO_2 electrode. These results indicated that the Cl atom substitution pathway was slightly more favorable with the TiO_2 electrode, while defluorination was more favorable with the $GOTiO_2$ electrode. Moreover, **Figure 4-20 (b)** and **Figure 4-24 (b)** show the PFOA degradation byproducts formed in the EC system with the $GOTiO_2$ and TiO_2 electrodes, respectively. The corresponding byproducts were nearly the same, except P20 was formed with the $GOTiO_2$ electrode. These results showed that the PFOA degradation pathway was not greatly affected by the anodic material.

doi:10.6342/NTU202201196

(a)

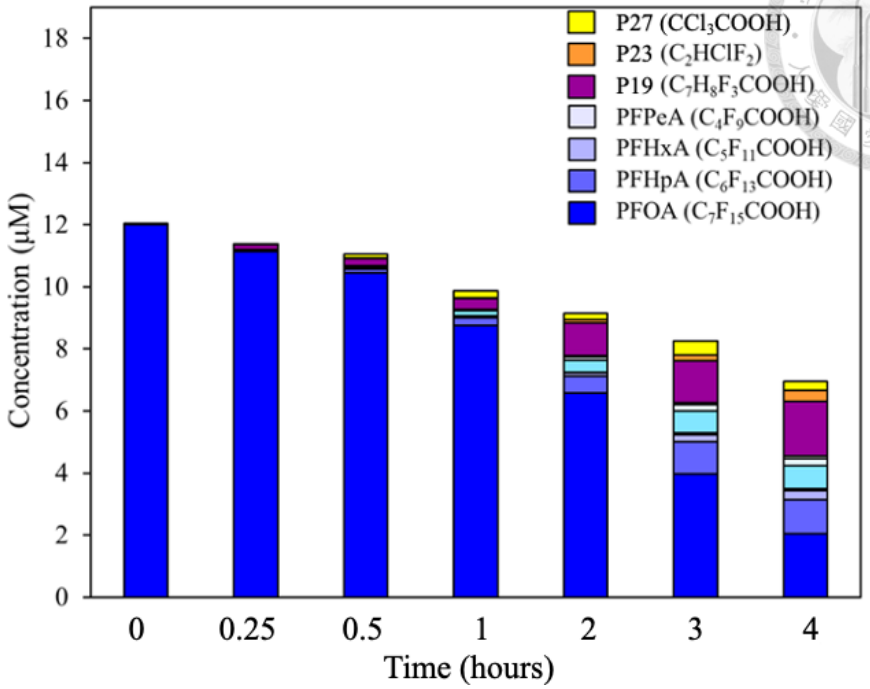

(b)

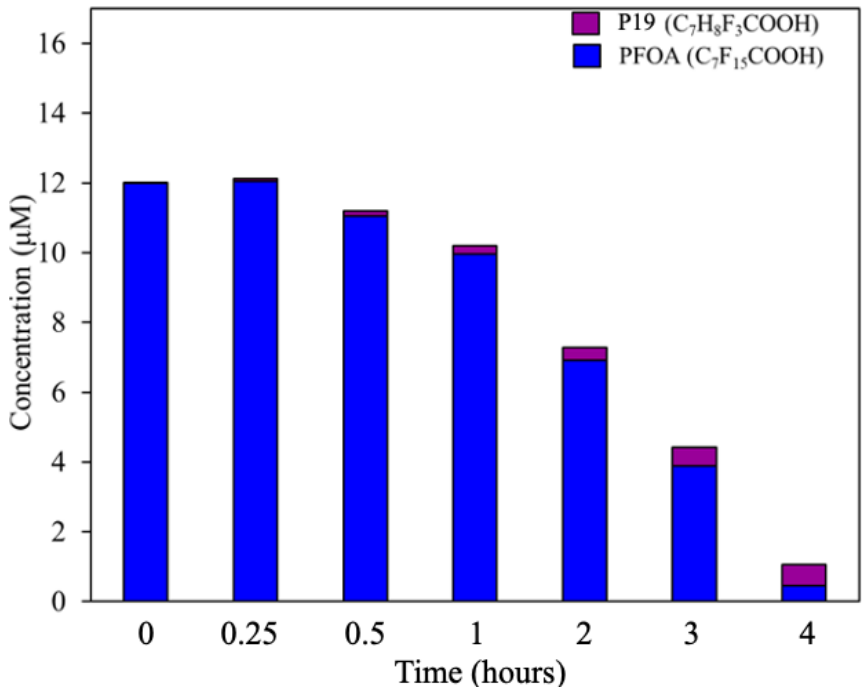

Figure 4-24. Byproducts generated during PFOA degradation in the (a) PEC system and (b) EC system with the TiO_2 electrode ($[PFOA]_0$ = 12 μM, [NaCl] = 50 mM, initial solution pH = 5.3).

doi:10.6342/NTU202201196

PFOS degradation in the PEC system using chloride anion as an electrolyte

In addition to PFOA, another perfluorinated chemical, PFOS, was also studied in the PEC system employing $GOTiO_2$ as the electrode. Similar to PFOA, a low concentration of PFOS resulted in a high degradation efficiency under PEC conditions (**Figure 4-25**). Additionally, under similar PEC conditions, a higher degradation efficiency for PFOS than PFOA was obtained; the degradation rate constants were 0.97 ± 0.09 and $0.37 \pm 0.04\ hour^{-1}$, respectively. Schaefer et al. (2015) also observed a higher PFOS degradation efficiency relative to that of PFOA during EC treatment of groundwater influenced by aqueous film-forming foams (AFFFs). **Figure 4-26** shows PFOS degradation and the main byproducts (with the highest signal intensity) generated in the PEC system. In the case of PFOS, four byproducts (P1 and P28−30) along with PFOA and their 18 byproducts were identified (**Table 4-5**). The proposed pathways are shown in **Figure 4-27**. Four degradation pathways were observed including (a) oxidation then decarboxylation, (b) defluorination, (c) hydroxylation and (d) Cl atom substitution. According to **Figure 4-26**, PFOS was completely removed after 4 h of treatment, and the byproduct yield in this study was 20 %, indicating the generation of other CF_2-containing unidentified byproducts. Short-chain PFAAs were detected during PFOS degradation, and their concentrations increased with the reaction time (**Figure 4-28**). Notably, the highest concentration of PFOA generated was approximately 10 nM, which is 3 orders of

doi:10.6342/NTU202201196

magnitude lower than the initial concentration of PFOS (10 μM). PFOA probably forms via the release of a sulfonate group ($-SO_3H$) from PFOS through electron transfer and further oxidation. The short-chain PFAAs are generated through stepwise defluorination, as evidenced by the presence of short-chain PFAAs (**Figure 4-28**). Due to the low yield of these short-chain compounds, this pathway might not be a main pathway of PFOS decomposition. The production yield of the other byproducts (P19, P20, P21, P23, P25, P27, P28 and P30) was 20 % for a 4-hour reaction time. The highest production yield among the byproducts of PFOS was for P20, i.e., 13 % with a 4-hour reaction time. The formation of P20 likely occurs through the defluorination pathway. Overall, in this work, the results regarding PFOS degradation byproducts and mechanisms are still limited; further studies are required for investigation.

doi:10.6342/NTU202201196

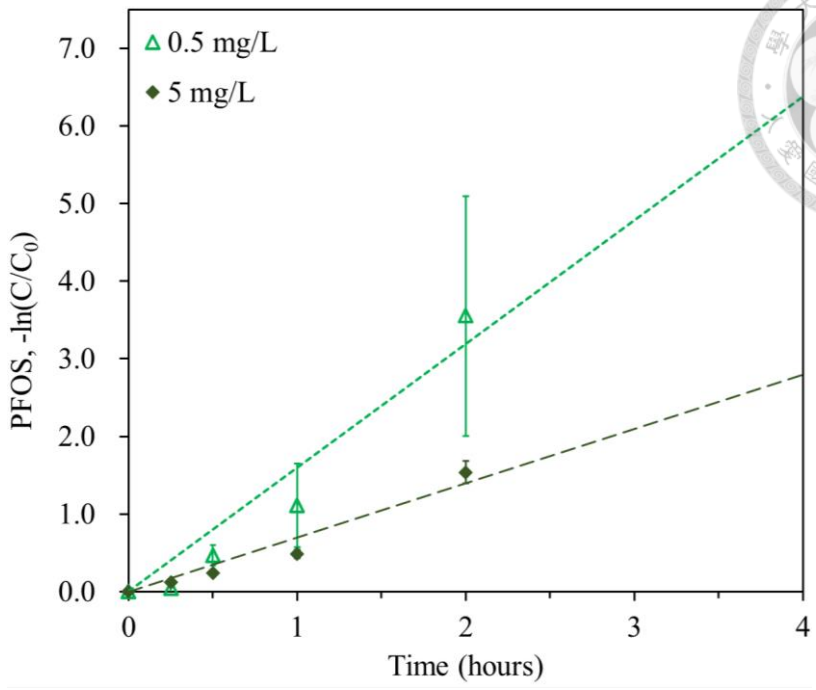

Figure 4-25. Effect of the PFOS concentration on PEC degradation using chloride anion as electrolyte with the GOTiO$_2$ electrode ([NaCl] = 50 mM).

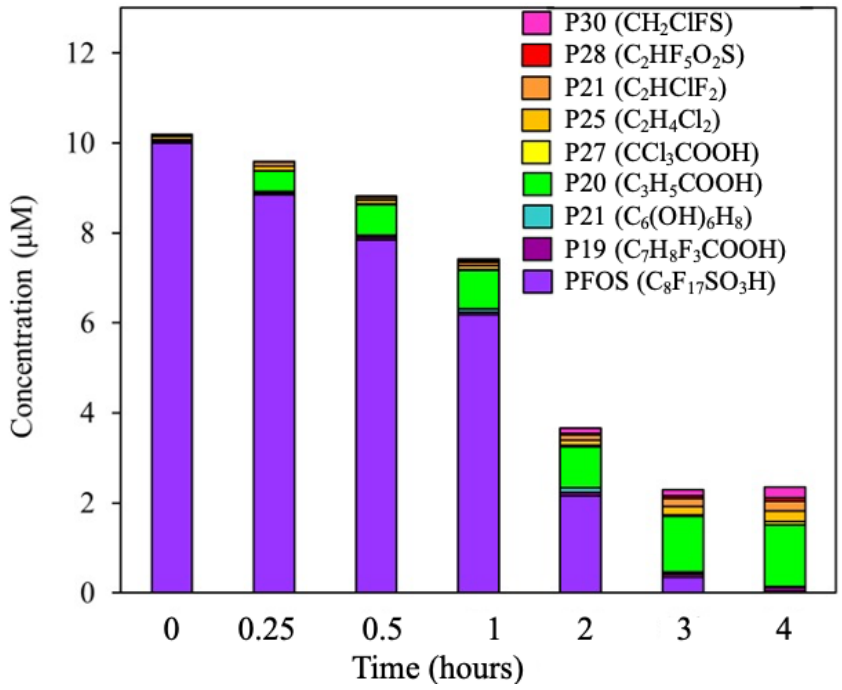

Figure 4-26. Major byproducts generated during PFOS degradation in the PEC system with the GOTiO$_2$ electrode ([PFOS]$_0$ = 10 μM, [NaCl] = 50 mM, initial solution pH = 5.3).

doi:10.6342/NTU202201196

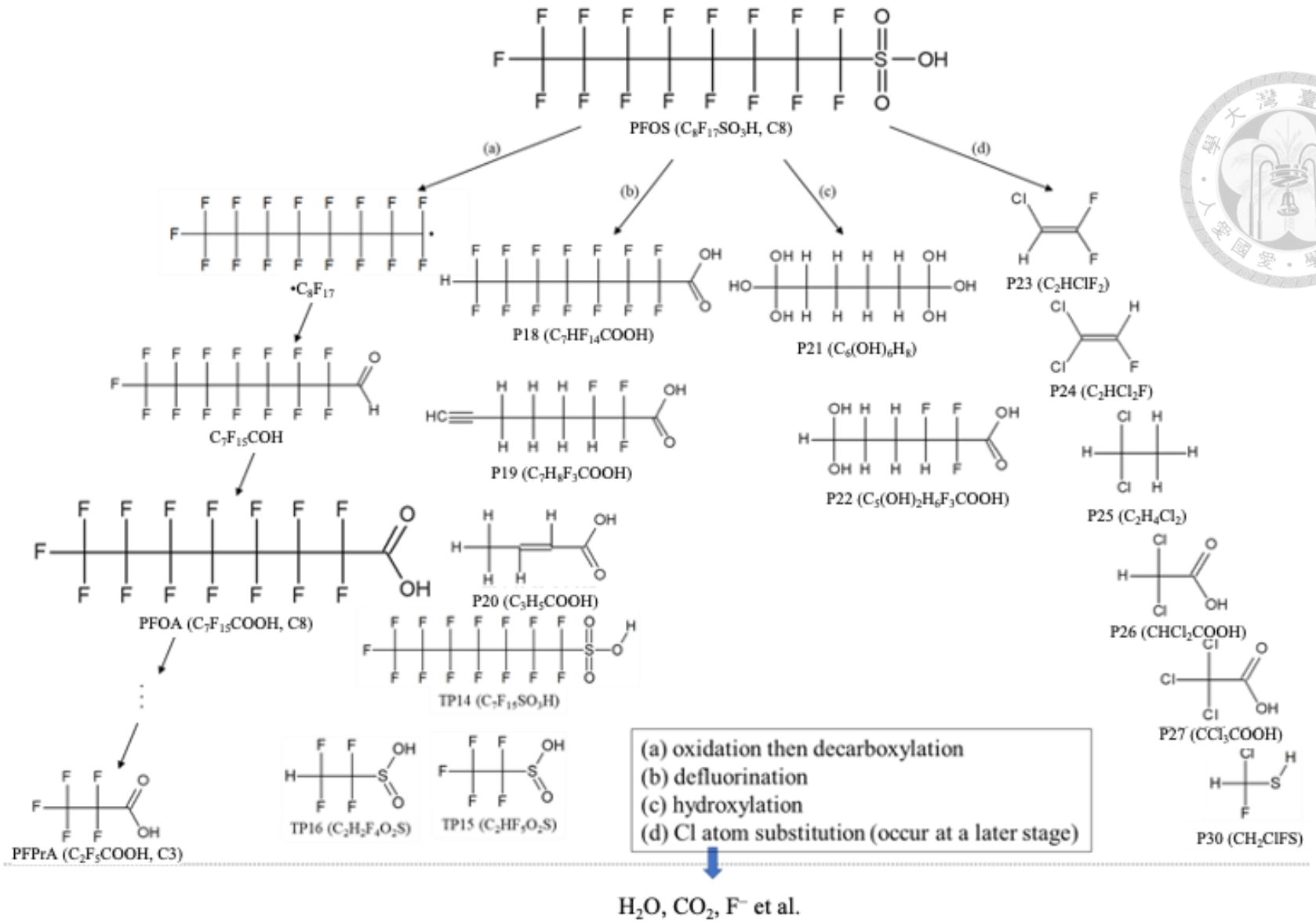

Figure 4-27. Proposed degradation pathways of PFOS in the PEC and EC systems.

doi:10.6342/NTU202201196

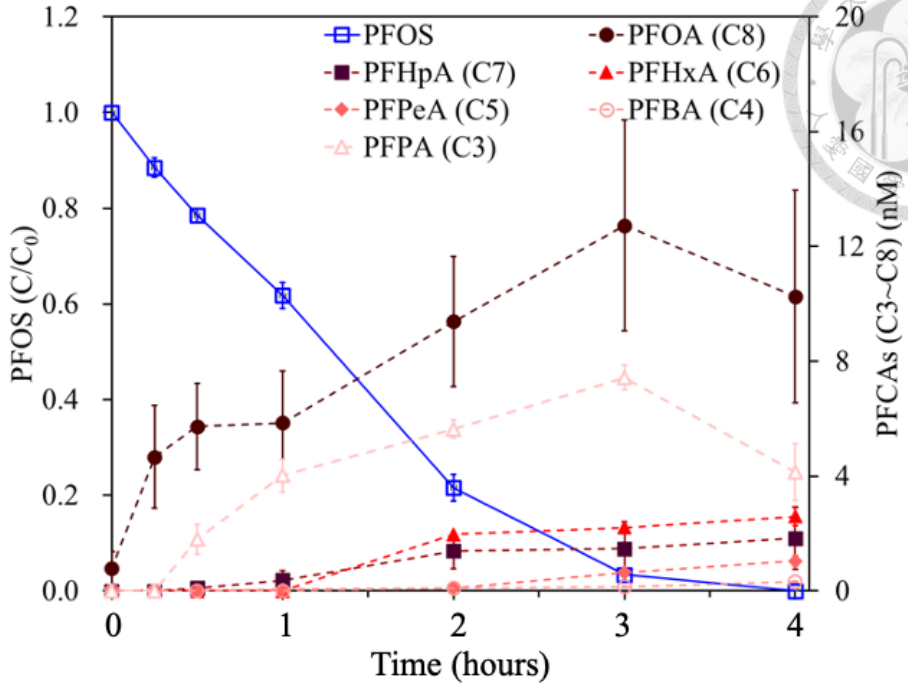

Figure 4-28. Byproducts generated during the PEC degradation of PFOS with the $GOTiO_2$ electrode ($[PFOS]_0$ = 10 μM, [NaCl] = 50 mM, initial solution pH = 5.3).

doi:10.6342/NTU202201196

4.2.4. Detoxification of PFOS during the PEC process

The generation of byproducts via target compound decomposition leads to a change in toxicity during the treatment process (Lai et al., 2017; Yin et al., 2018). However, to date, very few studies have examined the toxicity of PFOS byproducts following the application of PEC treatment. The toxicity behavior during PFOS degradation via the PEC process is shown in **Figure 4-29**. The results show that the toxicity gradually increased from 0.13 to 11.89 within the first 6 h during PFOS degradation; conversely, the toxicity decreased from 11.89 to 2.57 after 6 h of reaction. On the other hand, regarding the results of the ion formation trend during PFOS degradation in the PEC system (**Figure 4-16 (a)**), the concentrations of fluoride and sulfate ions constantly increased over 12 h, with significant production yields of 21.2 and 59.2 %, respectively, which suggested the possible decomposition of PFOS during the PEC process. Overall, according to the comparison of the byproduct transformation and ion formation (**Figure 4-16 (a)**) with the toxicity trends, PFOS was continuously decomposed into small-fragment byproducts, which possess low toxicity. This demonstrated that the PEC system developed in this work is a promising treatment process for PFOS removal.

doi:10.6342/NTU202201196

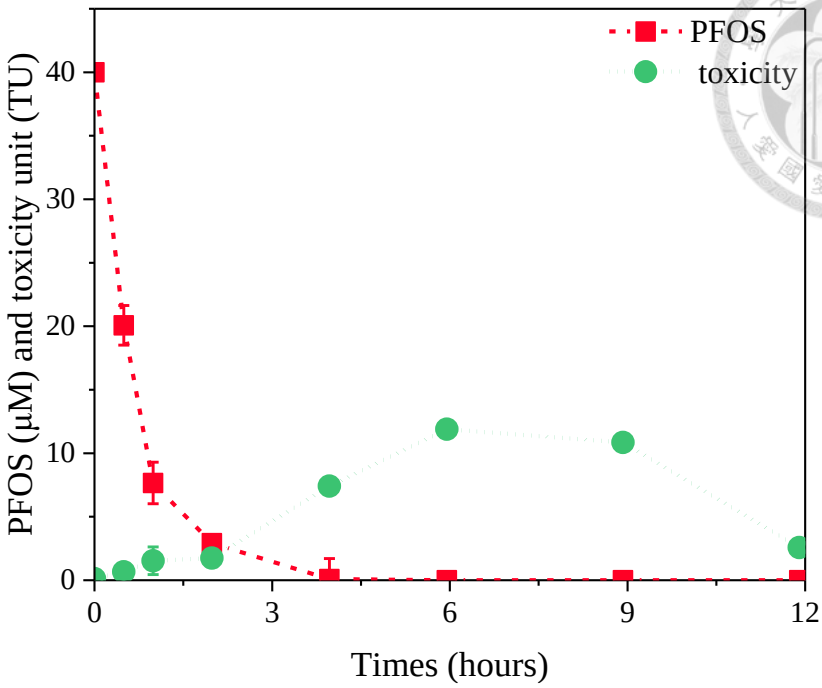

Figure 4-29. Toxicity of PFOS degradation in the PEC system ($[PFOS]_0$ = 40 μM, $[NaClO_4]$ = 50 mM, initial solution pH = 5.64, current density = 30 mA cm^{-2}).

doi:10.6342/NTU202201196

4.2.5. The reactivity and competitive inhibition behavior of PFAAs

In **Section 4.2.3**, we observed that PFOS is transformed into variable-chain-length PFSA and PFCA byproducts, which contain sulfonate groups (−SO_3H) and carboxylic groups (−COOH), respectively. To further explore their reactivity and competitive inhibition behavior, the degradation of PFSAs and PFCAs with different carbon chain lengths in the PEC system was examined individually and in a mixture system. The detailed observed degradation efficiencies (***η***) and rate constants (***k***) are provided in **Table 4-6**. In the individual solution (solution containing a single compound), the results show that PFSAs and PFCAs with shorter carbon chains exhibited lower degradation rates; the ***η*** value decreased in the following order: PFOS > PFHxS > PFBS (for PFSAs); PFOA > PFHpA > PFHxA > PFPeA > PFBA > PFPrA (for PFCAs), as shown in **Figure 4-30 (a)** and **(b)**. This phenomenon was also observed in other studies, which indicated that PFAAs with shorter carbon chain lengths were more persistent in EC systems (Niu et al., 2012; Wang et al., 2020).

doi:10.6342/NTU202201196

Table 4-6. Summary of the molecular volumes and degradation of PFAAs in the PEC system in the individual and mixed solutions ($[PFAAs]_0$ = 0.5 μM, $[NaClO_4]$ = 50 mM, initial solution pH = 5.64, current density = 30 mA cm^{-2}).

No.	Target compound	Molecular volume (cm^3 mol^{-1})[a]	Individual		Mixture	
			Degradation efficiency (η, %)	Pseudo-first-order rate constant (k, $hour^{-1}$)	Degradation efficiency (η, %)	Pseudo-first-order rate constant (k,$hour^{-1}$)
PFSAs						
1	PFOS	272.1	99.67 %	4.10 ± 0.37	99.16 %	3.74 ± 0.13
2	PFHxS	217.2	77.75 %	0.75 ± 0.08	35.73 %	0.23 ± 0.01
3	PFBS	162.3	9.27 %	0.04 ± 0.01	5.87 %	0.01 ± 0.00
PFCAs						
4	PFOA	237.3	98.09 %	1.92 ± 0.11	65.45 %	0.53 ± 0.05
5	PFHpA	209.8	47.56 %	0.32 ± 0.04	0.74 %	0.01 ± 0.00
6	PFHxA	182.0	30.05 %	0.16 ± 0.03	5.36 %	0.02 ± 0.00
7	PFHeA	154.9	25.29 %	0.14 ± 0.01	0.81 %	0.01 ± 0.00
8	PFBA	127.5	19.95 %	0.11 ± 0.01	3.53 %	0.02 ± 0.00
9	PFPrA	100.0	5.80 %	0.04 ± 0.01	2.78 %	0.02 ± 0.00

a. The molecular volumes of PFAAs were estimated using ACDLabs Chemsketh software.

doi:10.6342/NTU202201196

(a)

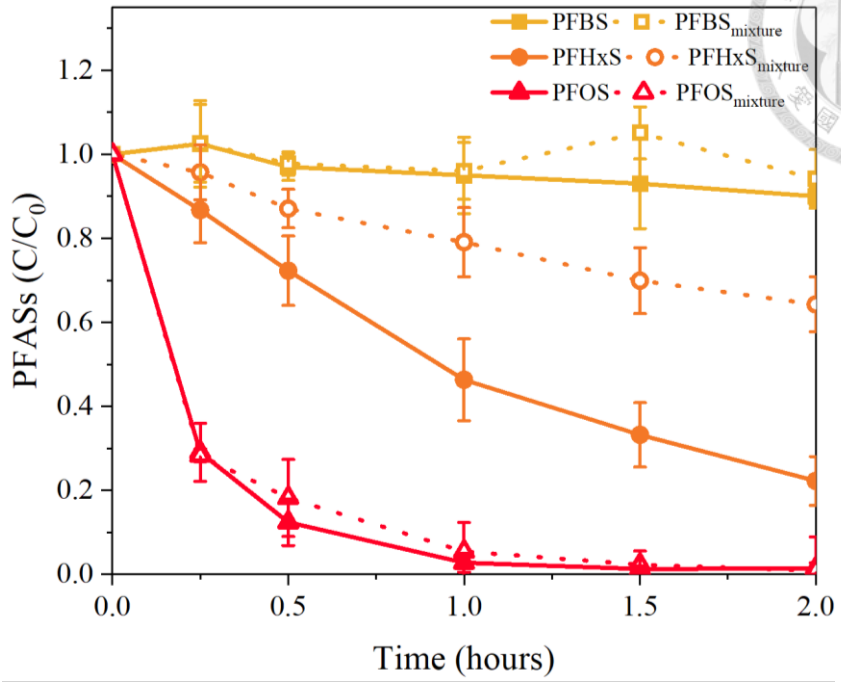

(b)

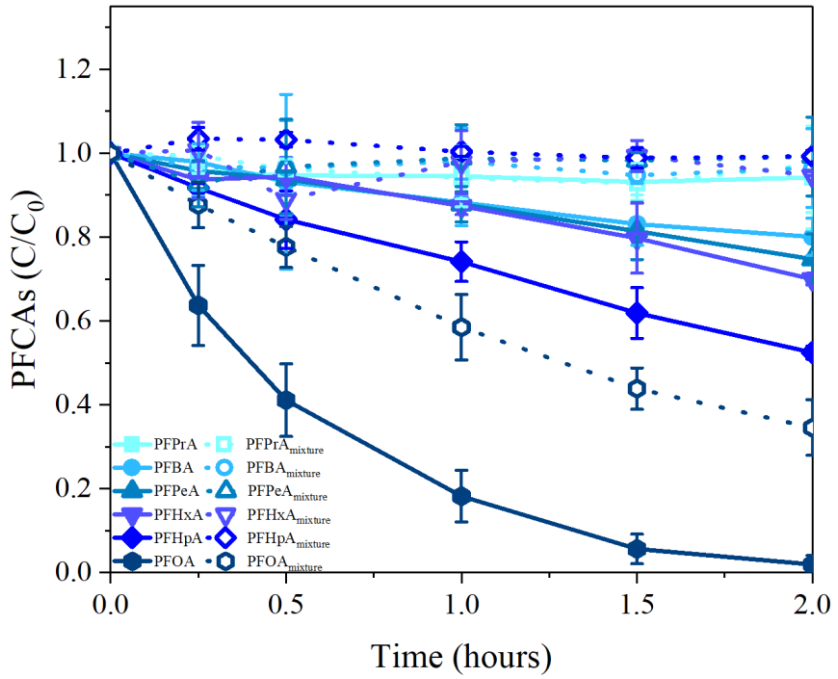

doi:10.6342/NTU202201196

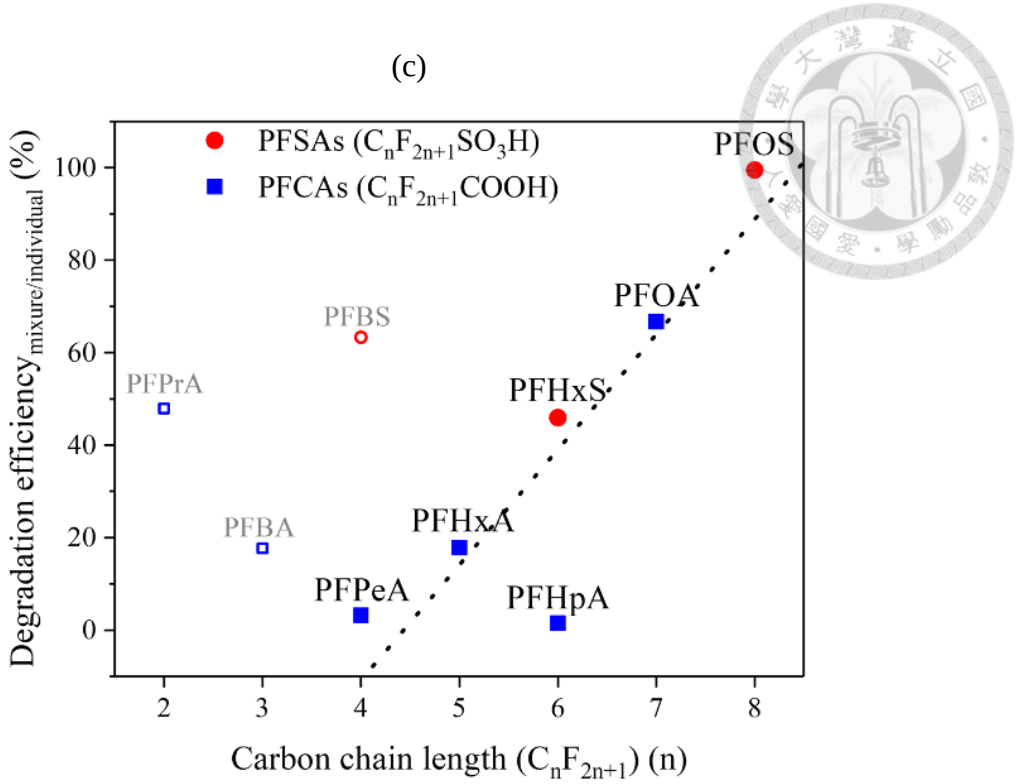

Figure 4-30. The degradation of (a) PFSAs and (b) PFCAs in the PEC system (solid line: in the individual solutions; dotted line: in the mixed solution) and (c) the relationship between the carbon chain length and degradation efficiency ratio ($\eta_{mixture}/\eta_{individual}$) of PFAAs ($[PFAAs]_0$ = 1 μM, $[NaClO_4]$ = 50 mM, initial solution pH = 5.64, current density = 30 mA cm^{-2}).

doi:10.6342/NTU202201196

Furthermore, we compared the relationship between the carbon chain length and degradation efficiency ratio ($\eta_{mixture}/\eta_{individual}$) for different PFAAs, as shown in **Figure 4-30 (c)**. $\eta_{mixture}/\eta_{individual}$ represents the degree of competitive inhibition that occurred for each PFAA in the mixture system compared with that in the individual system. Based on the results, we observed that PFAAs with longer carbon chain lengths exhibited weaker competitive inhibition behavior. For instance, PFOS is the longest carbon chain PFAA studied in this work; its degradation rates in the individual solution and in the mixture solution were very similar (the $\eta_{mixture}/\eta_{individual}$ value is 99.5 % (nearly 100 %)), suggesting minimal competitive inhibition occurred (**Figure 4-30 (a)** and **(c)**). However, for most of the other studied PFAAs (except for PFBS, PFBA and PFPrA), their degradation rates in the mixture solution were obviously slower than those in the individual solutions (**Figure 4-30 (a)** and **(b)**), with the $\eta_{mixture}/\eta_{individual}$ value decreasing greatly with decreasing chain length (**Figure 4-30 (c)**). The difference in the competitive inhibition behavior for each PFAA is explained as follows. PFAAs with longer chain lengths possess greater molecular volumes; hence, they might have more opportunities to contact the photoanode and undergo further degradation. According to **Table 4-6**, PFOS (showing the highest $\eta_{mixture}/\eta_{individual}$ value) bears the largest molecular volume (272.1 cm^3 mol^{-1}) among the observed PFAAs, hence resulting in its weakest competitive inhibition behavior. It should be noted that the three shorter-chain compounds, PFBS,

doi:10.6342/NTU202201196

PFBA and PFPrA, exhibited minimal degradation in the individual solutions (their $\eta_{individual}$ values were all < 20 %); thus, the calculated $\eta_{mixture}/\eta_{individual}$ values are relatively high, which does not accurately reflect the actual competitive inhibition behavior; hence, they are excluded from discussion.

doi:10.6342/NTU202201196

5. Conclusions, environmental implication and suggestions

5.1. Conclusions

1. The decomposition of PFOS and PFOA in a PEC system was successfully achieved in this work by utilizing a fabricated $GOTiO_2$ photoelectrode; new insights into the PFOS degradation mechanism have also been comprehensively elucidated for the first time.
2. The presence of GO decreased the optical band gap and increased the surface area of the $GOTiO_2$ photoelectrode, contributing to its higher capacitance and hence leading to better PEC performance in PFOS and PFOA degradation.
3. With a current density of 20 mA cm^{-2}, electrode distance of 5 mm, initial pH of 5.64, $[PFOS]_0$ of 0.5 μM, and $[NaClO_4]$ of 50 mM, PFOS was completely decomposed in 4 hours, the rate constants was 0.80 $hour^{-1}$.
4. With a current density of 16.7 mA cm^{-2}, initial pH of 5.3, $[PFOA]_0$ of 0.5 mg L^{-1}, and [NaCl] of 50 mM, PFOA was completely decomposed in 4 h via PEC process using NaCl as an electrolyte, the rate constants was 0.74 $hour^{-1}$.
5. The scavenger/probe experiments showed that PFOS degradation was attributed to the electron transfer reaction and •OH and $•O_2^-$ attack, further leading to its decomposition; in the PEC system using Cl^- as electrolyte, PFOA degradation was

doi:10.6342/NTU202201196

attributed to the electron transfer reaction and •OH and RCSs attack, further leading to its decomposition.

6. During the pathways of desulfonation, oxidation then defluorination, decarboxylation, decarbonylation, sulfonation, defluorination and hydroxylation, PFOS was transformed into various byproducts, including PFSAs, PFCAs, PFALs, HFCs and others; further decomposition of PFOS led to its mineralization with the formation of fluoride ions and sulfate ions.
7. Four different possible reaction pathways for PFOA degradation in the PEC and EC systems using Cl^- as an electrolyte, namely, decarboxylation followed by oxidation, defluorination, hydroxylation and Cl atom substitution, were proposed in this study along with the widely reported Kolbe reactions, and decarboxylation followed by oxidation was the primary degradation pathway, PFOA degradation products, including short-chain-length PFAAs and other byproducts. The Cl-containing short-chain byproducts observed in the PEC and EC systems during the decomposition of PFOA indicated that RCS were involved in the reactions.
8. Regarding the reactivity of PFOS, PFOA and other PFAAs, the results from this work demonstrated that the degradation rates of PFAAs depend on their carbon chain length.

doi:10.6342/NTU202201196

9. PFAAs with shorter chain lengths possess lower degradation rates. In addition, when PFAAs coexist, greater competitive inhibition behavior was observed for the shorter-chain-length PFAA.

doi:10.6342/NTU202201196

5.2. Environmental implications

This study observes that PFOS and PFOA were completely decomposed via PEC process. The PEC process will likely be applied to WWTPs wastewater effluents and designed the flow-through PEC process to increase the PFOS and PFOA decomposition efficiency. The electrode have incorporated boron-doped diamond (BDD) anodes and nickel alloy stainless steel cathodes, which are chemically inert and have, high electrochemical, chemical stability and corrosion. The wastewater effluents contain high salt which could enhance the application of PEC processes.

In addition, due to the PFOS and PFOA are being regulated by many countries and have been discontinued by many manufacturers, the manufacture and use of shorter chain lengths PFAAs has increased for the replacement. Nevertheless, this study observes that the shorter chain lengths PFAAs possess lower degradation rates and greater competitive inhibition behavior in mixture. This information could be helpful for lawmakers that the shorter chain lengths PFAAs should also be regulated or limited to minimize the environmental impact. In conclusion, the implications from this study accentuates the need for more attention of the reactivity and competitive inhibition behavior among PFAAs in the aquatic environment.

doi:10.6342/NTU202201196

5.3. Suggestions

1. New degradation pathways were identified; a total of 30 PFOS byproducts are reported in this work. However, given that the authentic standards of some of the byproducts (e.g., PFALs and HFCs) were not acquired in this work, the production yields among all types of byproducts as well as the contribution of each transformation pathway could not be comprehensively elucidated/compared; further investigation is required.

   Approach:

   To purchase the authentic standards of byproducts to quantitative and qualitative the PFOS byproduct in this study. On the other hand, LC–MSMS and QTOFMS were not the best analytical instruments to identify the byproducts, gas chromatography–mass spectrometry (GC–MS) can be used to identify the byproducts (e.g., PFALs and HFCs), and acquire more complete information on the production yields among all types of byproducts as well as the contribution of each transformation pathway.

doi:10.6342/NTU202201196

2. Through the scavenger experiments, this study elucidated the participation of reactive species such as •OH, $•O_2^-$ and electron transfer in the PEC system. However, the scavenger experiments and probe tests are two of the more indirect methods for verification. Further in-depth investigation is required to examine the presence of specific radical species.

Approach:

To determine the reactive species by electron paramagnetic resonance (EPR) spectroscopy. EPR spectroscopy can be used to clarify the generation of reactive species in-situ, such as •OH and $•O_2^-$.

3. This study indicated that the excellent decomposition efficiency achieved by the PEC system; however, the defluorination efficiency was less than 21.2 %. Therefore, modification and improvement of electrodes are needed to achieve higher defluorination.

Approach:

To improve the defluorination efficiency in the PEC system, the different electrodes materials and the compositions of electrodes need further investigations. Anodes such as metal-organic framework (MOF) anode, highly boron-doped diamond (BDD) anode, electrospun nanoparticles on carbon nano fibers anode.

doi:10.6342/NTU202201196

4. It is possible that PFOA mainly undergoes direct electron transfer initially, followed by reactions that generate shorter-chain products, and is further attacked by RCSs in the later stage of degradation; however, further studies are needed for elucidation.

Approach:

The stable electrolyte (e.g., $NaClO_4$) can be used to confirm the non-Cl-containing byproducts (P6, P10, P16 and P18-P22) in this study; the Cl-containing short-chain byproducts (P23-P30) should not be observed in the PEC system using $NaClO_4$ as an electrolyte.

5. In the experiments studying the pH effect, this study elucidated that the concentration of OH^- increased with increasing pH, which led to competition between the PFOS anion and OH^- for the sorption sites on the anode, thereby leading to the lowest PFOS removal at pH 11, however, in heterogeneous degradation, the charge associated with the surface functionality of material is an important characteristic.

Approach:

To determine the point of zero charge (PZC) of $GOTiO_2$ photoelectrode, and examine the relationship between the PZC of $GOTiO_2$ photoelectrode, pK_a of PFOS and PFOA and the degradation rate constants of different pH values.

doi:10.6342/NTU202201196

6. References

Ahrens, L. 2011. Polyfluoroalkyl compounds in the aquatic environment: a review of their occurrence and fate. Journal of environmental monitoring : JEM 13 1, 20-31.

Akter, J., Lee, J.-y., Ha, H.-J., Yi, I.G., Hong, D.-H., Park, C.-M., Lee, M.-Y. and Kim, I. 2022. Degradation of Organics and Change Concentration in Per-Fluorinated Compounds (PFCs) during Ozonation and UV/H_2O_2 Advanced Treatment of Tertiary-Treated Sewage. Sustainability 14(9), 5597.

Aleboyeh, A., Moussa, Y. and Aleboyeh, H. 2005. The effect of operational parameters on UV/H_2O_2 decolourisation of Acid Blue 74. Dyes and Pigments 66(2), 129-134.

Aquino, J.M., Rocha-Filho, R.C., Ruotolo, L.A.M., Bocchi, N. and Biaggio, S.R. 2014. Electrochemical degradation of a real textile wastewater using β-PbO_2 and DSA® anodes. Chemical Engineering Journal 251, 138-145.

Becker, A.M., Gerstmann, S. and Frank, H. 2008. Perfluorooctane surfactants in waste waters, the major source of river pollution. Chemosphere 72(1), 115-121.

Bräunig, J., Baduel, C., Heffernan, A., Rotander, A., Donaldson, E. and Mueller, J.F. 2017. Fate and redistribution of perfluoroalkyl acids through AFFF-impacted groundwater. Science of The Total Environment 596-597, 360-368.

Brillas, E. and Martínez-Huitle, C.A. 2015. Decontamination of wastewaters containing synthetic organic dyes by electrochemical methods. An updated review. Applied Catalysis B: Environmental 166-167, 603-643.

Brooke, D., Footitt, A. and Nwaogu, T. 2004. Environmental risk evaluation report: Perfluorooctanesulphonate (PFOS). Environmental Agency 1.

Brown, G.M. and Gu, B. (2006) Perchlorate: Environmental Occurrence, Interactions and Treatment. Gu, B. and Coates, J.D. (eds), pp. 17-47, Springer US, Boston, MA.

Buxton, G.V., Greenstock, C.L., Helman, W.P. and Ross, A.B. 1988. Critical Review of rate constants for reactions of hydrated electrons, hydrogen atoms and hydroxyl radicals (·OH/·O^- in Aqueous Solution. Journal of Physical and Chemical Reference Data 17(2), 513-886.

Carter, K.E. and Farrell, J. 2008. Oxidative Destruction of Perfluorooctane Sulfonate Using Boron-Doped Diamond Film Electrodes. Environmental Science & Technology 42(16), 6111-6115.

Chen, J., Pehkonen, S.O. and Lin, C.-J. 2003. Degradation of monomethylmercury chloride by hydroxyl radicals in simulated natural waters. Water Research 37(10), 2496-2504.

doi:10.6342/NTU202201196

Cheng, J.-h., Liang, X.-y., Yang, S.-w. and Hu, Y.-y. 2014. Photochemical defluorination of aqueous perfluorooctanoic acid (PFOA) by VUV/Fe^{3+} system. Chemical Engineering Journal 239, 242-249.

Cho, K. and Hoffmann, M.R. 2014. Urea Degradation by Electrochemically Generated Reactive Chlorine Species: Products and Reaction Pathways. Environmental Science & Technology 48(19), 11504-11511.

Cho, K. and Hoffmann, M.R. 2015. $Bi_xTi_{1-x}O_z$ Functionalized Heterojunction Anode with an Enhanced Reactive Chlorine Generation Efficiency in Dilute Aqueous Solutions. Chemistry of Materials 27(6), 2224-2233.

Cho, K., Kwon, D. and Hoffmann, M.R. 2014. Electrochemical treatment of human waste coupled with molecular hydrogen production. Rsc Advances 4(9), 4596-4608.

Compton, O.C., Cranford, S.W., Putz, K.W., An, Z., Brinson, L.C., Buehler, M.J. and Nguyen, S.T. 2012. Tuning the Mechanical Properties of Graphene Oxide Paper and Its Associated Polymer Nanocomposites by Controlling Cooperative Intersheet Hydrogen Bonding. ACS Nano 6(3), 2008-2019.

Conder, J.M., Hoke, R.A., Wolf, W.d., Russell, M.H. and Buck, R.C. 2008. Are PFCAs Bioaccumulative? A Critical Review and Comparison with Regulatory Criteria and Persistent Lipophilic Compounds. Environmental Science & Technology 42(4), 995-1003.

Cotillas, S., de Vidales, M.J.M., Llanos, J., Saez, C., Canizares, P. and Rodrigo, M.A. 2016. Electrolytic and electro-irradiated processes with diamond anodes for the oxidation of persistent pollutants and disinfection of urban treated wastewater. Journal of Hazardous Materials 319, 93-101.

de S. Furtado, R.X., Sabatini, C.A., Zaiat, M. and Azevedo, E.B. 2021. Perfluorooctane sulfonic acid (PFOS) degradation by optimized heterogeneous photocatalysis (TiO_2/UV) using the response surface methodology (RSM). Journal of Water Process Engineering 41, 101986.

Devi, L.G. and Kavitha, R. 2013. A review on non metal ion doped titania for the photocatalytic degradation of organic pollutants under UV/solar light: Role of photogenerated charge carrier dynamics in enhancing the activity. Applied Catalysis B: Environmental 140-141, 559-587.

Dhangar, K. and Kumar, M. (2021) Contaminants in Drinking and Wastewater Sources: Challenges and Reigning Technologies. Kumar, M., Snow, D.D., Honda, R. and Mukherjee, S. (eds), pp. 405-436, Springer Singapore, Singapore.

Duan, P., Hu, X., Ji, Z., Yang, X. and Sun, Z. 2018. Enhanced oxidation potential of Ti/SnO_2-Cu electrode for electrochemical degradation of low-concentration ceftazidime in aqueous solution: Performance and degradation pathway. Chemosphere 212, 594-603.

doi:10.6342/NTU202201196

Duan, X., Wang, W., Wang, Q., Sui, X., Li, N. and Chang, L. 2020. Electrocatalytic degradation of perfluoroocatane sulfonate (PFOS) on a 3D graphene-lead dioxide (3DG-PbO_2) composite anode: Electrode characterization, degradation mechanism and toxicity. Chemosphere 260, 127587.

Duong, H.T., Kadokami, K., Shirasaka, H., Hidaka, R., Chau, H.T.C., Kong, L., Nguyen, T.Q. and Nguyen, T.T. 2015. Occurrence of perfluoroalkyl acids in environmental waters in Vietnam. Chemosphere 122, 115-124.

EC. 2006 Directive 2006/122/EC of the European Parliament and of the council of 12 December 2006, amending for the 30th time Council Directive 76/769/EEC on the approximation of the laws, regulations and administrative provisions of the Member States relating to restrictions on the marketing and use of certain dangerous substances and preparations. (perfluorooctane sulfonates).
https://eur-lex.europa.eu/LexUriServ/LexUriServ.do?uri=OJ:L:2006:372:0032:0034:EN:PDF.

EC. 2017 Commission Regulation (EU) 2017/1000 of 13 June 2017 amending Annex XVII to Regulation (EC) No 1907/2006 of the European Parliament and of the Council concerning the Registration, Evaluation, Authorisation and Restriction of Chemicals (REACH) as regards perfluorooctanoic acid (PFOA), its salts and PFOA-related substances.
https://eur-lex.europa.eu/legal-content/EN/TXT/PDF/?uri=CELEX:32017R1000&from=EN.

Fang, H., Gao, Y., Li, G., An, J., Wong, P.-K., Fu, H., Yao, S., Nie, X. and An, T. 2013. Advanced Oxidation Kinetics and Mechanism of Preservative Propylparaben Degradation in Aqueous Suspension of TiO_2 and Risk Assessment of Its Degradation Products. Environmental Science & Technology 47(6), 2704-2712.

Fang, J., Fu, Y. and Shang, C. 2014. The Roles of Reactive Species in Micropollutant Degradation in the UV/Free Chlorine System. Environmental Science & Technology 48(3), 1859-1868.

Fujishima, A. and Honda, K. 1972. Electrochemical Photolysis of Water at a Semiconductor Electrode. Nature 238(5358), 37-38.

Fujishima, A., Zhang, X. and Tryk, D.A. 2008. TiO_2 photocatalysis and related surface phenomena. Surface Science Reports 63(12), 515-582.

Garcia-Segura, S. and Brillas, E. 2017. Applied photoelectrocatalysis on the degradation of organic pollutants in wastewaters. Journal of Photochemistry and Photobiology C: Photochemistry Reviews 31, 1-35.

Garcia-Segura, S., Dosta, S., Guilemany, J.M. and Brillas, E. 2013. Solar photoelectrocatalytic degradation of Acid Orange 7 azo dye using a highly stable

doi:10.6342/NTU202201196

TiO_2 photoanode synthesized by atmospheric plasma spray. Applied Catalysis B-Environmental 132, 142-150.

Georgieva, J., Valova, E., Armyanov, S., Philippidis, N., Poulios, I. and Sotiropoulos, S. 2012. Bi-component semiconductor oxide photoanodes for the photoelectrocatalytic oxidation of organic solutes and vapours: A short review with emphasis to TiO_2–WO_3 photoanodes. Journal of Hazardous Materials 211-212, 30-46.

Greenstock, C.L. and Miller, R.W. 1975. The oxidation of tiron by superoxide anion. Kinetics of the reaction in aqueous solution and in chloroplasts. Biochimica et Biophysica Acta (BBA) - Bioenergetics 396(1), 11-16.

Guo, K., Wu, Z., Shang, C., Yao, B., Hou, S., Yang, X., Song, W. and Fang, J. 2017. Radical Chemistry and Structural Relationships of PPCP Degradation by UV/Chlorine Treatment in Simulated Drinking Water. Environmental Science & Technology 51(18), 10431-10439.

Hagfeldt, A., Boschloo, G., Sun, L., Kloo, L. and Pettersson, H. 2010. Dye-Sensitized Solar Cells. Chemical Reviews 110(11), 6595-6663.

Hansen, K.J., Johnson, H.O., Eldridge, J.S., Butenhoff, J.L. and Dick, L.A. 2002. Quantitative Characterization of Trace Levels of PFOS and PFOA in the Tennessee River. Environmental Science & Technology 36(8), 1681-1685.

Harada, K., Saito, N., Sasaki, K., Inoue, K. and Koizumi, A. 2003. Perfluorooctane sulfonate contamination of drinking water in the Tama River, Japan: estimated effects on resident serum levels. Bulletin of environmental contamination and toxicology 71(1), 0031-0036.

Hassan, M., Zhao, Y. and Xie, B. 2016. Employing TiO_2 photocatalysis to deal with landfill leachate: Current status and development. Chemical Engineering Journal 285, 264-275.

Hoffmann, M.R., Martin, S.T., Choi, W. and Bahnemann, D.W. 1995. Environmental Applications of Semiconductor Photocatalysis. Chemical Reviews 95(1), 69-96.

Hori, H., Hayakawa, E., Einaga, H., Kutsuna, S., Koike, K., Ibusuki, T., Kiatagawa, H. and Arakawa, R. 2004. Decomposition of Environmentally Persistent Perfluorooctanoic Acid in Water by Photochemical Approaches. Environmental Science & Technology 38(22), 6118-6124.

Hu, X., Yu, Y. and Sun, Z. 2016a. Preparation and characterization of cerium-doped multiwalled carbon nanotubes electrode for the electrochemical degradation of low-concentration ceftazidime in aqueous solutions. Electrochimica Acta 199, 80-91.

Hu, X.C., Andrews, D.Q., Lindstrom, A.B., Bruton, T.A., Schaider, L.A., Grandjean, P., Lohmann, R., Carignan, C.C., Blum, A., Balan, S.A., Higgins, C.P. and Sunderland, E.M. 2016b. Detection of Poly- and Perfluoroalkyl Substances (PFASs) in U.S.

doi:10.6342/NTU202201196

Drinking Water Linked to Industrial Sites, Military Fire Training Areas, and Wastewater Treatment Plants. Environmental Science & Technology Letters 3(10), 344-350.

Hunge, Y.M., Yadav, A.A., Dhodamani, A.G., Suzuki, N., Terashima, C., Fujishima, A. and Mathe, V.L. 2020. Enhanced photocatalytic performance of ultrasound treated GO/TiO_2 composite for photocatalytic degradation of salicylic acid under sunlight illumination. Ultrasonics Sonochemistry 61, 104849.

Hurley, S., Houtz, E., Goldberg, D., Wang, M., Park, J.-S., Nelson, D.O., Reynolds, P., Bernstein, L., Anton-Culver, H., Horn-Ross, P. and Petreas, M. 2016. Preliminary Associations between the Detection of Perfluoroalkyl Acids (PFAAs) in Drinking Water and Serum Concentrations in a Sample of California Women. Environmental Science & Technology Letters 3(7), 264-269.

Jin, L., Zhang, P., Shao, T. and Zhao, S. 2014. Ferric ion mediated photodecomposition of aqueous perfluorooctane sulfonate (PFOS) under UV irradiation and its mechanism. Journal of Hazardous Materials 271, 9-15.

Key, B.D., Howell, R.D. and Criddle, C.S. 1997. Fluorinated Organics in the Biosphere. Environmental Science & Technology 31(9), 2445-2454.

Khannam, M., Sharma, S., Dolui, S. and Dolui, S.K. 2016. A graphene oxide incorporated TiO_2 photoanode for high efficiency quasi solid state dye sensitized solar cells based on a poly-vinyl alcohol gel electrolyte. RSC Advances 6(60), 55406-55414.

Kim, T.-H., Lee, S.-H., Kim, H.Y., Doudrick, K., Yu, S. and Kim, S.D. 2019. Decomposition of perfluorooctane sulfonate (PFOS) using a hybrid process with electron beam and chemical oxidants. Chemical Engineering Journal 361, 1363-1370.

Koo, M.S., Cho, K., Yoon, J. and Choi, W. 2017. Photoelectrochemical Degradation of Organic Compounds Coupled with Molecular Hydrogen Generation Using Electrochromic TiO_2 Nanotube Arrays. Environmental Science & Technology 51(11), 6590-6598.

Lai, W.W.-P., Hsu, M.-H. and Lin, A.Y.-C. 2017. The role of bicarbonate anions in methotrexate degradation via UV/TiO_2: Mechanisms, reactivity and increased toxicity. Water Research 112, 157-166.

Lai, W.W.-P., Lin, Y.-C., Tung, H.-H., Lo, S.-L. and Lin, A.Y.-C. 2016. Occurrence of pharmaceuticals and perfluorinated compounds and evaluation of the availability of reclaimed water in Kinmen. Emerging Contaminants 2(3), 135-144.

Láng, G.G., Sas, N.S., Ujvári, M. and Horányi, G. 2008. The kinetics of the electrochemical reduction of perchlorate ions on rhodium. Electrochimica Acta 53(25), 7436-7444.

doi:10.6342/NTU202201196

Lehmler, H.-J. 2005. Synthesis of environmentally relevant fluorinated surfactants—a review. Chemosphere 58(11), 1471-1496.

Leung, S.C.E., Shukla, P., Chen, D., Eftekhari, E., An, H., Zare, F., Ghasemi, N., Zhang, D., Nguyen, N.-T. and Li, Q. 2022. Emerging technologies for PFOS/PFOA degradation and removal: A review. Science of The Total Environment 827, 153669.

Li, M., Feng, C., Hu, W., Zhang, Z. and Sugiura, N. 2009. Electrochemical degradation of phenol using electrodes of Ti/RuO_2–Pt and Ti/IrO_2–Pt. Journal of Hazardous Materials 162(1), 455-462.

Li, M.J., Yu, Z.B., Liu, Q., Sun, L. and Huang, W.Y. 2016. Photocatalytic decomposition of perfluorooctanoic acid by noble metallic nanoparticles modified TiO_2. Chemical Engineering Journal 286, 232-238.

Li, S., Zhang, G.S., Zhang, W., Zheng, H.S., Zhu, W.Y., Sun, N., Zheng, Y.J. and Wang, P. 2017. Microwave enhanced Fenton-like process for degradation of perfluorooctanoic acid (PFOA) using Pb-$BiFeO_3$/rGO as heterogeneous catalyst. Chemical Engineering Journal 326, 756-764.

Li, X., Chen, S., Quan, X. and Zhang, Y. 2011. Enhanced Adsorption of PFOA and PFOS on Multiwalled Carbon Nanotubes under Electrochemical Assistance. Environmental Science & Technology 45(19), 8498-8505.

Lin, A.Y.-C., Panchangam, S.C., Chang, C.-Y., Hong, P.K.A. and Hsueh, H.-F. 2012. Removal of perfluorooctanoic acid and perfluorooctane sulfonate via ozonation under alkaline condition. Journal of Hazardous Materials 243, 272-277.

Lin, A.Y.-C., Panchangam, S.C. and Ciou, P.-S. 2010. High levels of perfluorochemicals in Taiwan's wastewater treatment plants and downstream rivers pose great risk to local aquatic ecosystems. Chemosphere 80(10), 1167-1174.

Lin, A.Y.-C., Panchangam, S.C. and Lo, C.-C. 2009. The impact of semiconductor, electronics and optoelectronic industries on downstream perfluorinated chemical contamination in Taiwanese rivers. Environmental Pollution 157(4), 1365-1372.

Lin, Y.-C., Lai, W.W.-P., Tung, H.-h. and Lin, A.Y.-C. 2015. Occurrence of pharmaceuticals, hormones, and perfluorinated compounds in groundwater in Taiwan. Environmental Monitoring and Assessment 187(5), 256.

Liu, X., Chen, C., Chen, X.a., Qian, G., Wang, J., Wang, C., Cao, Z. and Liu, Q. 2018. WO_3 QDs enhanced photocatalytic and electrochemical perfomance of GO/TiO_2 composite. Catalysis Today 315, 155-161.

Liu, X.J., Pan, L.K., Zhao, Q.F., Lv, T., Zhu, G., Chen, T.Q., Lu, T., Sun, Z. and Sun, C.Q. 2012. UV-assisted photocatalytic synthesis of ZnO-reduced graphene oxide composites with enhanced photocatalytic activity in reduction of Cr(VI). Chemical Engineering Journal 183, 238-243.

doi:10.6342/NTU202201196

Liu, Y., Chen, S., Quan, X., Yu, H., Zhao, H. and Zhang, Y. 2015. Efficient Mineralization of Perfluorooctanoate by Electro-Fenton with H_2O_2 Electro-generated on Hierarchically Porous Carbon. Environmental Science & Technology 49(22), 13528-13533.

Liu, Y.-J., Hu, C.-Y. and Lo, S.-L. 2019. Direct and indirect electrochemical oxidation of amine-containing pharmaceuticals using graphite electrodes. Journal of Hazardous Materials 366, 592-605.

Llorca, M., Farré, M., Picó, Y., Müller, J., Knepper, T.P. and Barceló, D. 2012. Analysis of perfluoroalkyl substances in waters from Germany and Spain. Science of The Total Environment 431, 139-150.

Loos, R., Locoro, G., Comero, S., Contini, S., Schwesig, D., Werres, F., Balsaa, P., Gans, O., Weiss, S., Blaha, L., Bolchi, M. and Gawlik, B.M. 2010. Pan-European survey on the occurrence of selected polar organic persistent pollutants in ground water. Water Research 44(14), 4115-4126.

Lu, D., Sha, S., Luo, J., Huang, Z. and Zhang Jackie, X. 2020. Treatment train approaches for the remediation of per- and polyfluoroalkyl substances (PFAS): A critical review. Journal of Hazardous Materials 386, 121963.

Lv, N., Li, Y., Huang, Z., Li, T., Ye, S., Dionysiou, D.D. and Song, X. 2019. Synthesis of GO/TiO_2/Bi_2WO_6 nanocomposites with enhanced visible light photocatalytic degradation of ethylene. Applied Catalysis B: Environmental 246, 303-311.

Ma, L., Wang, C., Li, H., Peng, F. and Yang, Z. 2018. Degradation of geosmin and 2-methylisoborneol in water with UV/chlorine: Influencing factors, reactive species, and possible pathways. Chemosphere 211, 1166-1175.

Ma, Q., Liu, L., Cui, W., Li, R., Song, T. and Cui, Z. 2015. Electrochemical degradation of perfluorooctanoic acid (PFOA) by Yb-doped Ti/SnO_2–Sb/PbO_2 anodes and determination of the optimal conditions. RSC Advances 5(103), 84856-84864.

Mak, Y.L., Taniyasu, S., Yeung, L.W.Y., Lu, G., Jin, L., Yang, Y., Lam, P.K.S., Kannan, K. and Yamashita, N. 2009. Perfluorinated Compounds in Tap Water from China and Several Other Countries. Environmental Science & Technology 43(13), 4824-4829.

Murakami, M., Kuroda, K., Sato, N., Fukushi, T., Takizawa, S. and Takada, H. 2009a. Groundwater Pollution by Perfluorinated Surfactants in Tokyo. Environmental Science & Technology 43(10), 3480-3486.

Murakami, M., Shinohara, H. and Takada, H. 2009b. Evaluation of wastewater and street runoff as sources of perfluorinated surfactants (PFSs). Chemosphere 74(4), 487-493.

doi:10.6342/NTU202201196

Muruganandham, M. and Swaminathan, M. 2004. Photochemical oxidation of reactive azo dye with UV–H_2O_2 process. Dyes and Pigments 62(3), 269-275.

Niu, J.F., Lin, H., Xu, J.L., Wu, H. and Li, Y.Y. 2012. Electrochemical Mineralization of Perfluorocarboxylic Acids (PFCAs) by Ce-Doped Modified Porous Nanocrystalline PbO_2 Film Electrode. Environmental Science & Technology 46(18), 10191-10198.

Novoselov, K.S., Geim, A.K., Morozov, S.V., Jiang, D., Zhang, Y., Dubonos, S.V., Grigorieva, I.V. and Firsov, A.A. 2004. Electric Field Effect in Atomically Thin Carbon Films. Science 306(5696), 666-669.

O'Regan, B. and Grätzel, M. 1991. A low-cost, high-efficiency solar cell based on dye-sensitized colloidal TiO_2 films. Nature 353(6346), 737-740.

Olvera-Rodríguez, I., Hernández, R., Medel, A., Guzmán, C., Escobar-Alarcón, L., Brillas, E., Sirés, I. and Esquivel, K. 2019. TiO_2/Au/TiO_2 multilayer thin-film photoanodes synthesized by pulsed laser deposition for photoelectrochemical degradation of organic pollutants. Sep. Purif. Technol. 224, 189-198.

Palominos, R.A., Mondaca, M.A., Giraldo, A., Peñuela, G., Pérez-Moya, M. and Mansilla, H.D. 2009. Photocatalytic oxidation of the antibiotic tetracycline on TiO_2 and ZnO suspensions. Catalysis Today 144(1), 100-105.

Panchangam, S.C., Lin, A.Y.-C., Shaik, K.L. and Lin, C.-F. 2009. Decomposition of perfluorocarboxylic acids (PFCAs) by heterogeneous photocatalysis in acidic aqueous medium. Chemosphere 77(2), 242-248.

Panchangam, S.C., Yellatur, C.S., Yang, J.S., Loka, S.S., Lin, A.Y.C. and Vemula, V. 2018. Facile fabrication of TiO_2-graphene nanocomposites (TGNCs) for the efficient photocatalytic oxidation of perfluorooctanoic acid (PFOA). Journal of Environmental Chemical Engineering 6(5), 6359-6369.

Park, K., Ali, I. and Kim, J.-O. 2018. Photodegradation of perfluorooctanoic acid by graphene oxide-deposited TiO_2 nanotube arrays in aqueous phase. Journal of Environmental Management 218, 333-339.

Peng, Y.P., Chen, H.L. and Huang, C.P. 2017. The Synergistic Effect of Photoelectrochemical (PEC) Reactions Exemplified by Concurrent Perfluorooctanoic acid (PFOA) Degradation and Hydrogen Generation over Carbon and Nitrogen codoped TiO_2 Nanotube Arrays (C-N-TNTAs) photoelectrode. Applied Catalysis B-Environmental 209, 437-446.

Post, G.B., Cohn, P.D. and Cooper, K.R. 2012. Perfluorooctanoic acid (PFOA), an emerging drinking water contaminant: A critical review of recent literature. Environmental Research 116, 93-117.

doi:10.6342/NTU202201196

Qi, H.-P., Wang, H.-L., Zhao, D.-Y. and Jiang, W.-F. 2019. Preparation and photocatalytic activity of Ag-modified GO-TiO_2 mesocrystals under visible light irradiation. Applied Surface Science 480, 105-114.

Qian, Y., Guo, X., Zhang, Y., Peng, Y., Sun, P., Huang, C.-H., Niu, J., Zhou, X. and Crittenden, J.C. 2016. Perfluorooctanoic Acid Degradation Using UV–Persulfate Process: Modeling of the Degradation and Chlorate Formation. Environmental Science & Technology 50(2), 772-781.

Ribao, P., Rivero, M.J. and Ortiz, I. 2018. Enhanced photocatalytic activity using GO/TiO_2 catalyst for the removal of DCA solutions. Environmental Science and Pollution Research 25(35), 34893-34902.

Richardson, S.D. and Ternes, T.A. 2018. Water Analysis: Emerging Contaminants and Current Issues. Analytical Chemistry 90(1), 398-428.

Rostkowski, P., Taniyasu, S., Yamashita, N. and Falandysz, J. 2008. Perfluorinated compounds in potable water. Roczniki Panstwowego Zakladu Higieny 59(3), 283-292.

Rubí-Juárez, H., Cotillas, S., Sáez, C., Cañizares, P., Barrera-Díaz, C. and Rodrigo, M.A. 2016. Use of conductive diamond photo-electrochemical oxidation for the removal of pesticide glyphosate. Sep. Purif. Technol. 167, 127-135.

Rusanova, M.Y., Polášková, P., Muzikař, M. and Fawcett, W.R. 2006. Electrochemical reduction of perchlorate ions on platinum-activated nickel. Electrochimica Acta 51(15), 3097-3101.

Sansotera, M., Persico, F., Pirola, C., Navarrini, W., Di Michele, A. and Bianchi, C.L. 2014. Decomposition of perfluorooctanoic acid photocatalyzed by titanium dioxide: Chemical modification of the catalyst surface induced by fluoride ions. Applied Catalysis B: Environmental 148-149, 29-35.

Santos, A., Rodríguez, S., Pardo, F. and Romero, A. 2016. Use of Fenton reagent combined with humic acids for the removal of PFOA from contaminated water. Science of The Total Environment 563-564, 657-663.

Saxena, S., Tyson, T.A., Shukla, S., Negusse, E., Chen, H. and Bai, J. 2011. Investigation of structural and electronic properties of graphene oxide. Applied Physics Letters 99(1), 013104.

Schaefer, C.E., Andaya, C., Urtiaga, A., McKenzie, E.R. and Higgins, C.P. 2015. Electrochemical treatment of perfluorooctanoic acid (PFOA) and perfluorooctane sulfonic acid (PFOS) in groundwater impacted by aqueous film forming foams (AFFFs). Journal of Hazardous Materials 295, 170-175.

Shao, T., Zhang, P., Jin, L. and Li, Z. 2013. Photocatalytic decomposition of perfluorooctanoic acid in pure water and sewage water by nanostructured gallium oxide. Applied Catalysis B: Environmental 142-143, 654-661.

doi:10.6342/NTU202201196

Shi, H., Wang, Y., Li, C., Pierce, R., Gao, S. and Huang, Q. 2019. Degradation of Perfluorooctanesulfonate by Reactive Electrochemical Membrane Composed of Magnéli Phase Titanium Suboxide. Environmental Science & Technology 53(24), 14528-14537.

Song, S., Fan, J., He, Z., Zhan, L., Liu, Z., Chen, J. and Xu, X. 2010. Electrochemical degradation of azo dye C.I. Reactive Red 195 by anodic oxidation on Ti/SnO_2–Sb/PbO_2 electrodes. Electrochimica Acta 55(11), 3606-3613.

Tan, C., Gao, N., Deng, Y., Zhang, Y., Sui, M., Deng, J. and Zhou, S. 2013. Degradation of antipyrine by UV, UV/H_2O_2 and UV/PS. Journal of Hazardous Materials 260, 1008-1016.

Tian, J., Sang, Y., Yu, G., Jiang, H., Mu, X. and Liu, H. 2013. A Bi_2WO_6-Based Hybrid Photocatalyst with Broad Spectrum Photocatalytic Properties under UV, Visible, and Near-Infrared Irradiation. Advanced Materials 25(36), 5075-5080.

U.S.EPA. 2016a U.S. Environmental Protection Agency. Office of Water. Drinking Water Health Advisory for Perfluorooctane Sulfonate (PFOS), EPA 822-R-16-004.

U.S.EPA. 2016b U.S. Environmental Protection Agency. Office of Water. Occurence Data for the Unregulated Contaminant Monitoring Rule: UCMR3 (2013–2015). https://www.epa.gov/dwucmr/occurrence-data-unregulated-contaminant-monitoring-rule.

U.S.EPA. 2016c U.S. Environmental Protection Agency.Office of Water. Drinking Water Health Advisory for Perfluorooctanoic Acid (PFOA), EPA 822-R-16-005. https://www.epa.gov/sites/production/files/2016-05/documents/pfoa_health_advisory_final-plain.pdf.

UNEP. 2004 Stockholm Convention on Persistent Organic Pollutants. http://chm.pops.int/.

Urtiaga, A., Fernández-González, C., Gómez-Lavín, S. and Ortiz, I. 2015. Kinetics of the electrochemical mineralization of perfluorooctanoic acid on ultrananocrystalline boron doped conductive diamond electrodes. Chemosphere 129, 20-26.

Wang, T., Wang, Y., Liao, C., Cai, Y. and Jiang, G. 2009. Perspectives on the Inclusion of Perfluorooctane Sulfonate into the Stockholm Convention on Persistent Organic Pollutants. Environmental Science & Technology 43(14), 5171-5175.

Wang, Y., Pierce, R.D., Shi, H., Li, C. and Huang, Q. 2020. Electrochemical degradation of perfluoroalkyl acids by titanium suboxide anodes. Environmental Science: Water Research & Technology 6(1), 144-152.

doi:10.6342/NTU202201196

Wang, Y. and Zhang, P. 2011. Photocatalytic decomposition of perfluorooctanoic acid (PFOA) by TiO_2 in the presence of oxalic acid. Journal of Hazardous Materials 192(3), 1869-1875.

Watts, M.J. and Linden, K.G. 2007. Chlorine photolysis and subsequent OH radical production during UV treatment of chlorinated water. Water Research 41(13), 2871-2878.

Wooh, S., Kim, T.-Y., Song, D., Lee, Y.-G., Lee, T.K., Bergmann, V.W., Weber, S.A.L., Bisquert, J., Kang, Y.S. and Char, K. 2015. Surface Modification of TiO_2 Photoanodes with Fluorinated Self-Assembled Monolayers for Highly Efficient Dye-Sensitized Solar Cells. ACS Applied Materials & Interfaces 7(46), 25741-25747.

Xiao, F., Simcik, M.F., Halbach, T.R. and Gulliver, J.S. 2015. Perfluorooctane sulfonate (PFOS) and perfluorooctanoate (PFOA) in soils and groundwater of a U.S. metropolitan area: Migration and implications for human exposure. Water Research 72, 64-74.

Xie, G., Chang, X., Adhikari, B.R., Thind, S.S. and Chen, A. 2016. Photoelectrochemical degradation of acetaminophen and valacyclovir using nanoporous titanium dioxide. Chinese Journal of Catalysis 37(7), 1062-1069.

Xu, X., Cai, J., Zhou, M., Du, X. and Zhang, Y. 2020. Photoelectrochemical degradation of 2,4-dichlorophenoxyacetic acid using electrochemically self-doped Blue TiO_2 nanotube arrays with formic acid as electrolyte. Journal of Hazardous Materials 382, 121096.

Yamamoto, T., Noma, Y., Sakai, S.-i. and Shibata, Y. 2007. Photodegradation of Perfluorooctane Sulfonate by UV Irradiation in Water and Alkaline 2-Propanol. Environmental Science & Technology 41(16), 5660-5665.

Yang, L., He, L., Xue, J., Ma, Y., Xie, Z., Wu, L., Huang, M. and Zhang, Z. 2020. Persulfate-based degradation of perfluorooctanoic acid (PFOA) and perfluorooctane sulfonate (PFOS) in aqueous solution: Review on influences, mechanisms and prospective. Journal of Hazardous Materials 393, 122405.

Yao, Y., Zhu, H., Li, B., Hu, H., Zhang, T., Yamazaki, E., Taniyasu, S., Yamashita, N. and Sun, H. 2014. Distribution and primary source analysis of per- and poly-fluoroalkyl substances with different chain lengths in surface and groundwater in two cities, North China. Ecotoxicology and Environmental Safety 108, 318-328.

Yeung, L.W.Y., Yamashita, N., Taniyasu, S., Lam, P.K.S., Sinha, R.K., Borole, D.V. and Kannan, K. 2009. A survey of perfluorinated compounds in surface water and biota including dolphins from the Ganges River and in other waterbodies in India. Chemosphere 76(1), 55-62.

doi:10.6342/NTU202201196

Yin, K., Deng, Y., Liu, C., He, Q., Wei, Y., Chen, S., Liu, T. and Luo, S. 2018. Kinetics, pathways and toxicity evaluation of neonicotinoid insecticides degradation via UV/chlorine process. Chemical Engineering Journal 346, 298-306.

Yin, P., Hu, Z., Song, X., Liu, J. and Lin, N. 2016. Activated Persulfate Oxidation of Perfluorooctanoic Acid (PFOA) in Groundwater under Acidic Conditions. Int J Environ Res Public Health 13(6), 602.

Zhang, J.-x., Liu, S., Yan, C., Wang, X.-j., Wang, L., Yu, Y.-m. and Li, S.-y. 2017. Abrasion properties of self-suspended hairy titanium dioxide nanomaterials. Applied Nanoscience 7(8), 691-700.

Zhang, K., Huang, J., Yu, G., Zhang, Q., Deng, S. and Wang, B. 2013. Destruction of Perfluorooctane Sulfonate (PFOS) and Perfluorooctanoic Acid (PFOA) by Ball Milling. Environmental Science & Technology 47(12), 6471-6477.

Zhang, L., Li, X., Chang, Z. and Li, D. 2011. Preparation, characterization and photoactivity of hollow N, Co co-doped TiO_2/SiO_2 microspheres. Materials Science in Semiconductor Processing 14(1), 52-57.

Zhang, W., Zhou, S., Sun, J., Meng, X., Luo, J., Zhou, D. and Crittenden, J. 2018. Impact of Chloride Ions on UV/H_2O_2 and UV/Persulfate Advanced Oxidation Processes. Environmental Science & Technology 52(13), 7380-7389.

Zhao, J., Nguyen, D.C.T., Areerob, Y. and Oh, W.-C. 2019. Novel synthesis of nano needle-like Cu_2O-GO-TiO_2 and CuO-GO-TiO_2 for the high photocatalytic performance of anionic and cationic pollutants. Solid State Sciences 91, 77-88.

Zhao, X., Qu, J., Liu, H., Qiang, Z., Liu, R. and Hu, C. 2009. Photoelectrochemical degradation of anti-inflammatory pharmaceuticals at Bi_2MoO_6–boron-doped diamond hybrid electrode under visible light irradiation. Applied Catalysis B: Environmental 91(1), 539-545.

Zhao, X. and Zhu, Y. 2006. Synergetic Degradation of Rhodamine B at a Porous ZnWO4 Film Electrode by Combined Electro-Oxidation and Photocatalysis. Environmental Science & Technology 40(10), 3367-3372.

Zhu, Y., Murali, S., Cai, W., Li, X., Suk, J.W., Potts, J.R. and Ruoff, R.S. 2010. Graphene and graphene oxide: synthesis, properties, and applications. Advanced materials 22(35), 3906-3924.

Zhuo, Q., Wang, J., Niu, J., Yang, B. and Yang, Y. 2020. Electrochemical oxidation of perfluorooctane sulfonate (PFOS) substitute by modified boron doped diamond (BDD) anodes. Chemical Engineering Journal 379, 122280.

Zhuo, Q.F., Deng, S.B., Yang, B., Huang, J. and Yu, G. 2011. Efficient Electrochemical Oxidation of Perfluorooctanoate Using a Ti/SnO_2-Sb-Bi Anode. Environmental Science & Technology 45(7), 2973-2979.

doi:10.6342/NTU202201196

Zrinyi, N. and Pham, A.L.-T. 2017. Oxidation of benzoic acid by heat-activated persulfate: Effect of temperature on transformation pathway and product distribution. Water Research 120, 43-51.

Zushi, Y., Ye, F., Motegi, M., Nojiri, K., Hosono, S., Suzuki, T., Kosugi, Y., Yaguchi, K. and Masunaga, S. 2011. Spatially Detailed Survey on Pollution by Multiple Perfluorinated Compounds in the Tokyo Bay Basin of Japan. Environmental Science & Technology 45(7), 2887-2893.

doi:10.6342/NTU202201196